1-1-1968

An experimental investigation of the influence of the surface grain size of the metal on the value of C(sf) in the Rohsenow equation for boiling heat transfer.

Ramanathan Nagarajan
University of Windsor

AN EXPERIMENTAL INVESTIGATION OF THE INFLUENCE OF THE SURFACE GRAIN SIZE OF THE METAL ON THE VALUE OF C_{sf} IN THE ROHSENOW EQUATION FOR BOILING HEAT TRANSFER.

A Dissertation
Submitted to the Faculty of Graduate Studies through the
Department of Chemical Engineering in Partial Fulfilment
of the Requirements for the Degree of
Doctor of Philosophy at the
University of Windsor

by

Ramanathan Nagarajan

Windsor, Ontario, Canada

1968

UMI Number:DC52624

ProQuest Information and Learning Company
789 East Eisenhower Parkway
P.O. Box 1346
Ann Arbor, MI 48106-1346

ABx 6508

APPROVED BY:

Maurice Feldman

Alex Gruft

by P. Mathur

Carl St. Pierre

H. Lidman

213753

TO MY PARENTS

BHAGIRATHI & RAMANATHAN

ABSTRACT

An experimental study was undertaken to investigate the influence of the surface grain size of the metal on the value of the coefficient C_{sf} in the Rohsenow Equation for boiling heat transfer.

The apparatus consisted of a copper heat transfer surface 6 inches in diameter from which heat was transferred to a pool of boiling water contained inside a glass boiler. Heat was supplied to the surface through a copper block 9 inches in diameter and 10 inches long. Heat flux was computed from accurate measurements of electric power supplied and the heat losses. Thermocouples located at precisely known points on the geometric axis of the heat transfer plate were used to measure the surface temperatures.

The technique of varying the grain size of the test surface consisted of electroplating a layer of a metal onto the original surface at different current densities. Grain size was determined according to standard metallographic methods. Surface roughness was maintained between 2 to 3 micro inches rms as measured by a profilometer. Four different metallic deposits namely copper, nickel, chromium and brass were studied but only the copper plated surfaces were extensively investigated.

Boiling data obtained at atmospheric pressure on surfaces with various grain sizes were plotted on log-log scales as heat flux Q/A vs ΔT_m, the difference between the mean surface temperature and the

saturation temperature of the liquid. These plots showed a definite effect of the grain size on boiling heat transfer. Application of the Rohsenow Correlation to the boiling data showed that the coefficient C_{sf} and the exponent r of the equation did not remain constant for a particular metal-fluid combination but were influenced by the grain size of the heat transfer surface. C_{sf} and r decreased as the grain size of the surface increased.

A slightly modified form of the Rohsenow equation as given below is proposed, which takes into account the influence of grain size of the surface for predicting boiling heat transfer:

$$\frac{C_{\ell}\Delta T}{h_{fg}} \times \frac{1}{N_{Pr}} = (0.0018G + 0.0125)\left(\frac{Q/A}{\mu_{\ell} h_{fg}}\sqrt{\frac{g_o \sigma}{g(\rho_{\ell} - \rho_v)}}\right)^{(0.044G + 0.228)}$$

where G is defined as grains per linear inch of a surface divided by a constant which for copper was chosen as 600.

ACKNOWLEDGEMENTS

The author wishes to express his deep gratitude and sincere thanks to Dr. Maurice Adelman, Head of the Department of Chemical Engineering, for suggesting the problem and for his able guidance, help and encouragement during the course of the present investigation.

Grateful acknowledgement is made to Mr. Otto Brudy, Superintendent of Central Machine Shop for his invaluable help in the construction of the equipment. Thanks are due also to Mr. Halil Parlar of the Chemical Engineering Work Shop, Mr. Dieter Liebsch of the Central Machine Shop, Mr. Wolfgang Eberhart, the glass blower, and Mr. Leonard Thomas, the author's friend for their help and cooperation.

Thanks are extended to the Noranda Copper and Brass Company of Canada and Dr. W.H. Gauvin of the above company for the generous gift of Copper billets which were used to construct the heater unit and the heat transfer plate.

Acknowledgement is made to the National Research Council of Canada for providing financial support.

TABLE OF CONTENTS

LIST OF TABLES

LIST OF FIGURES

NOMENCLATURE

Latin Letters

A	Area of heat transfer surface, sq. ft.
Br	Brass surface
Cr	Chromium surface
Cu	Copper surface
$C_d, C_{fd}, C_q, C_R, C_n$	Coefficients in Eq.8,14,16,18 and 19 respectively.
C_{sf}	Coefficient characteristic of liquid - heating surface combination in Rohsenow correlation, dimensionless
C_ℓ, C_p	Specific Heat of saturated liquid, $Btu/(lb_m)(^oF)$
D_b	Diameter of bubble when breaking off from heating surface, ft.
f	Frequency of bubble formation, sec^{-1}
G	Grain ratio defined as the number of grains per linear inch of a sample to the grains of a surface having 600 grains per linear inch.(Eq.(49))
G	Gibb's free energy as defined in Eq. 38, ft lb_f
GI	Number of grains per linear inch, 1/inch
G_b	Mass velocity of bubbles at their departure from heating surface, $lb_m/hr.ft.^2$
g	Acceleration of gravity, $ft/hr.^2$
g_o	Conversion factor, $4.17 \times \frac{10^8(lb_m)(ft)}{(lb_f)(hr^2)}$
h	Coefficient of heat transfer, $Btu/(hr)(ft^2)(^oF)$
h_m	Mean coefficient of heat transfer, $Btu/(hr)(ft^2)(^oF)$
h_{fg}	Latent heat of evaporation, Btu/lb_m
$I_p(x)$	Modified Bessel function of the first kind and order p, $= \sum_{s=0}^{s=\infty} \frac{(x/2)^{p+2s}}{s!\,\Gamma(p+s+1)}$
J	Conversion factor, ft lb_f/Btu

k	Thermal conductivity of stainless steel, Btu/(hr)(ft)(^{o}F)
k_{ℓ}	Thermal conductivity of saturated liquid, Btu/(hr)(ft)(^{o}F)
$K_p(x)$	Modified Bessel function of the second kind and order p, $= \frac{\pi\{I_{-p}(x)-I_p(x)\}}{2\sin(p\pi)}$
Ni	Nickel surface
n	Number of points of origin of bubble columns per sq.ft. of heating surface, 1/sq. ft.
N_{Nu}	Nusselt Number
N_{Nu_b}	Bubble Nusselt Number
N_{Gr}	Grashof Number
N_{Pr}	Prandtl number
N_{Re}	Reynolds number
N_{Re_b}	Bubble Reynolds Number
Δp	Pressure difference (p_v-p_∞), lb/ft^2. or psi
p_v	Pressure on vapor side of interface, lb_f/sq.ft.
p_{ℓ}, p_∞	Pressure on liquid side of interface, lb_f/sq.ft.
Q	Heat transfer rate, Btu/hr.
Q/A	Heat transfer rate per unit area of heating surface, Btu/(hr)(ft^2)
R	Bubble radius, ft.
R	Outer radius of the stainless steel fin, ft.
R_v	Gas constant, ft lb_f/lb_m.^{o}F
r	Exponent of the Rohsenow Correlation
r_o	Inner radius of the stainless steel fin, ft.

s	Exponent of the Rohsenow Correlation
T	Temperature, ^{o}F.
T_v	Vapor temperature, ^{o}F.
T_ℓ, T_{sat}	Saturation temperature of the liquid, ^{o}F
T_s, T_w	Surface temperature of the heating surface, ^{o}F
ΔT	Heating surface temperature minus saturation temperature of the liquid, ^{o}F
ΔT_m	Mean temperature difference driving force, ^{o}F
t	Time as defined in Eq. 25, hr.
t_1, t_2, etc.	Temperature from the thermocouple readings, ^{o}F
y	Half the thickness of the stainless steel fin, ft.

Greek Letters

α	Thermal diffusivity, $\frac{k}{\rho C_p}$, $ft.^2/Hr.$
β	Bubble contact angle, defined in Eq. (50).
θ	Temperature at any point on the fin, ^{o}F.
θ_o	Temperature at the inner edge of the fin, ^{o}F.
θ_1	Temperature at the outer edge of the fin, ^{o}F.
μ	Micron size
$M\mu$	Milli micron
μ_ℓ	Viscosity of saturated liquid, $lb_m/ft.hr.$
ρ_ℓ	Density of saturated liquid, $lb_m/ft.^3$
ρ_v	Density of saturated vapour, $lb_m/ft.^3$
$\sigma, \sigma_{\ell v}$	Surface tension of liquid-vapour interface, $lb_f/ft.$
σ_{sv}	Surface tension of vapour-solid interface, $lb_f/ft.$
σ_{ls}	Surface tension of liquid-solid interface, $lb_f/ft.$
σ_{bv}	Surface tension of boundary-vapour interface, $lb_f/ft.$
β_f	Volume coefficient of expansion in Eq.56 and Eq.59, $1/^{o}R.$

Subscripts

f	Subscript indicating that the property is evaluated at a film temperature halfway between the mean temperature of the surface and the temperature of the ambient fluid.
1,2,3	Subscripts used to describe the values of r and C_{sf} of the Rohsenow Correlation.

CHAPTER 1

INTRODUCTION

Modern research in the field of boiling heat transfer has received increasing attention during the past two decades. This great attention bestowed by researchers to boiling phenomena is mainly due to its widespread application in problems associated with nuclear reactors and other sophisticated equipment of the space age. With the advent of space travel and the ready availability of boiling liquids to cool various components of space vehicles, much effort has been expended in order to obtain a thorough understanding of the various aspects of the boiling mechanism. In addition to the above usages boiling has manifold applications in heat transfer equipment employed in a multitude of chemical industries.

One type of boiling which is of most interest to us from the utilitarian point of view is nucleate boiling also referred to as surface boiling. This type of boiling transfers large amounts of heat per unit time and area over moderate temperature differences between the heat transfer surface and the boiling liquid.

In nucleate boiling of liquids, bubbles form and rise in columns from preferred locations which are known as nucleation centers on the heater surface. Previous investigators (J_1,B_6,C_3,G_1,K_4) have established that factors such as the material of the heating

surface, the condition of the surface; its roughness or smoothness and the length of time of its usage influence the boiling behaviour by way of affecting the number of sites available for bubble formation. Research workers (C_2,G_3) have speculated that pits, scratches or other surface imperfections provide most of the nucleation sites.

However disagreement is reported between investigators (C_2,H_3) as to whether metallic grains and associated grain boundaries of the heating surface would act as nucleation sites. Clark, H.B. et al.(C_2) employed two methods to determine whether grain boundaries could act as nucleation sites. One way was to compare boiling curves for a polycrystalline zinc and single zinc crystal. The second approach consisted of a search with the microscope during actual boiling. Through their investigation, they concluded that grain boundaries have little or no effect on boiling nucleation. These conclusions do not agree with those of Harrison and Levine (H_3) who boiled stearic acid from two different faces of a single crystal copper and found that their best boiling curves for the above two cases were separate lines. The former research group tried to explain this observed discrepancy between the two conclusions by pointing out that a possibility existed that oxides might have formed, due to exposure to air, on the heat transfer surfaces used by Harrison and Levine. Actually very little work has been done in this area outside the above mentioned two investigations.

The grain boundaries are known to be regions of misfit or strained regions which yield to chemical and physical reactions (S_4). It is also common knowledge to the metallurgists that the presence of

grain boundaries in polycrystalline metals modify their mechanical properties considerably and the thermal and electrical properties to a lesser extent as compared to the properties of single crystals of the same metals. It is therefore conceivable that the grain boundaries which are regions of higher energy might provide favourable nucleation sites for bubbles to grow.

In the absence of supporting experimental evidence for the above inference and owing to the contradictory results reported in the literature, it was felt that a thorough experimental investigation of this problem was needed. Such an investigation should be able to cover wide range of grain sizes and hence widely varying grain boundaries of the boiling surface. With this aim in mind, the following study was undertaken to obtain an understanding of the effect of the grain boundaries of the metallic heat transfer surface on nucleate boiling behaviour. A solution to this problem is not only of academic interest but also desirable from the point of view of designing heat transfer equipment. As Westwater remarks (W_2) the scientific progress in this field should reach a level at which engineers will be able to decide what shape of nucleate boiling curve is desired for a particular application and then fabricate heat transfer equipment to produce the result. Until such a stage is reached it is imperative that research activities in the field of boiling be extended. It is hoped that the results of the present study will contribute to some extent towards the aforesaid goal by way of providing a better understanding of boiling from metal surfaces.

CHAPTER II

LITERATURE REVIEW

A. General

The field of boiling heat transfer is adequately covered by recent books on heat transfer and in several other monographs dealing especially with the various aspects of boiling. Books by McAdams (M_1), Jakob (J_1), Rohsenow and Choi (R_5) and by Kutateladze (K_5) and more recently by Tong (T_1) deal extensively with boiling. Excellent review articles by Westwater (W_3) Leppert and Pitts (L_2) and by Rohsenow (R_6) are devoted exclusively to this field and contain details of theoretical analysis and experimental results obtained by numerous investigators over the past several years.

The first available literature on boiling as a topic of scientific interest is by J.G. Leidenfrost (L_1), a German medical doctor who in 1756 reported the curious behaviour of 'repulsion' between a liquid and a very hot solid. There was a lapse of almost two centuries before scientific attention was again bestowed on boiling. Nukiyama (N_1) in 1934 reported an interesting observation which resulted in the rapid advancement of the science of boiling in modern times. Nukiyama conducted a simple experiment by submerging a platinum wire in water at 212°F and heating it electrically to produce boiling. Based on his observations, Nukiyama predicted the existence of several regimes of boiling which was later confirmed by Farber and Scorah (F_1) and

McAdams et al. (M_2). The progress of boiling heat transfer research within the time interval between Nukiyama's discovery and the present day is characterized by an almost exponential growth rate. Mention has to be made of the pioneering research works by Jakob, McAdams, Westwater, Rohsenow, Bonilla, Bankoff, Kutataladze, Griffith, Forster, Zuber, Myers and scores of other investigators who have greatly contributed to an understanding of boiling phenomena during the intervening years since Nukiyama's observations. For the sake of clarity, in the following discussion the theoretical approaches are dealt with briefly whereas the experimental results are only mentioned.

B. Nucleation for Bubbles

The primary requirements for nucleate boiling to occur are essentially two. First is the initiation of new bubbles which is referred to as the nucleation process since it suggests the presence of some kind of nuclei at the points where the bubbles are formed. Second is the growth of these bubbles by absorbing heat from the surrounding super heated liquid. Generally the theoretical treatment of this problem consisted of attempts to analyze the above two aspects separately in order to derive suitable correlations for prediction.

A nucleation process occurring in a pool of liquid can be classified into two categories namely the homogeneous case and the heterogeneous case.

1. Homogeneous Nucleation

In homogeneous nucleation, bubble nuclei are formed within the body of a pure liquid. Nuclei formation may be due to a high

energy molecular group resulting from the thermal fluctuations of liquid molecules or a cavity resulting from a local pressure reduction such as occurs in accelerated flow

(a) The Classical Rate Theory. The classical rate theory of nuclei formation advocated by Volmer (V_6) and others considers nucleation as a thermodynamic equilibrium state followed by a rate process. This model assumes that some molecules in a liquid have excess energy over others. This is called activation energy. These molecules combine with other molecules and activate them and gradually build up several activated cluster of molecules. These superheated liquid molecular clusters overcome resistance from forces such as surface tension and viscosity to form vapour bubbles.

Volmer developed a relation for the nucleation rate in a superheated liquid which agreed surprisingly well with Wismer's data for superheated ether at atmospheric pressure (W_3). This indicated the soundness of approach based on the rate theory of nucleation to describe homogeneous boiling phenomena. However assumptions of thermodynamic equilibrium between the liquid phase and the vapor phase and that the boundary between the two phases is a plane of zero thickness which are incorporated in the Volmer equation are open to question (W_3).

(b) Statistical Fluctuation Theory.

Among the proponents of a statistical fluctuation theory of nucleation, mention has to be made of Reiss (R_2,R_3). His approach has the advantage that it does not require the assumptions of equilibrium

and sharply defined boundary between phases which are incorporated into the classical rate theory. Even though light scattering measurements support the assumed fluctuations of energy, density and temperature in this theoretical approach, it has been found less useful because of the difficulty involved in evaluating certain terms (W_3).

Common to the above two theoretical approaches is the requirement that the liquid must be superheated and the superheat must be great enough to overcome surface tension effects tending to collapse tiny bubbles.

2. Heterogeneous Nucleation

The second type of nuclei formation which is called heterogeneous nucleation refers to the formation of nuclei on foreign objects which may include a solid surface, suspended impurities, cavities or grooves within the surface or other preferred locations. In practice one almost always encounters heterogeneous nucleation because of the presence of container walls and heat transfer surfaces, and the liquid is rarely free from dust particles, adsorbed gas, absorbed gas, and foreign ions. Heterogeneous nucleation differs from the homogeneous nucleation in that the number of nucleation sites and the work of forming a nucleus may be altered due to the presence of these foreign objects.

(a) Theory. The mechanism behind the formation of nuclei for the bubbles in heterogeneous boiling systems is complex. The commonly accepted theory (R_5,H_5) is as follows: Let us consider a

free spherical vapor bubble at equilibrium in a superheated liquid. Taking a force balance,

$$\pi R^2(p_v - p_\ell) = 2\pi R\sigma \tag{1}$$

or

$$\Delta p = p_v - p_\ell = \frac{2\sigma}{R} \tag{2}$$

By means of the Clausius-Clapeyron equation with the prefect gas approximation, the pressure difference may be replaced with the temperature difference as follows:

$$\frac{dp}{dT} = \frac{h_{fg}\rho_v}{T_v} = \frac{h_{fg}p_v}{R_v T_v^2} \tag{3}$$

where R_v is the gas constant of the vapor. Since

$$p_v - p_\ell = (T_v - T_{sat})\left(\frac{dp}{dT}\right) \tag{4}$$

equations (2) and (3) can be combined to give

$$T_v - T_{sat} = \frac{2R_v(T_{sat})^2\sigma}{h_{fg}p_\ell R_c} \tag{5}$$

In equation (5), R_c is the critical radius. A bubble will grow if the size of the nuclei is greater than R_c; if smaller the bubble will collapse.

In addition to the vapor at p_v if an inert gas at partial pressure p_g is present in a bubble at equilibrium, expressions (2) and (5) have to be modified as follows:

$$p_v - p_\ell = \frac{2\sigma}{R} - p_g \tag{6}$$

$$T_v - T_{sat} = \frac{R(T_{sat})^2}{h_{fg}p_\ell}\left(\frac{2\sigma}{R} - p_g\right) \tag{7}$$

(b) Postulations and Experimental Data on Bubble Nucleation. Investigate generally (R_6,G_1,C_2,G_3,N_2,P_4) believe that bubbles originate at small cone-like cavities in the heating surface which contain a trapped gas. A growing bubble on a heating surface as illustrated in Fig. 1 is under the influence of the buoyancy force and the force due to surface tension. The bubble grows until its buoyant force is greater than the force due to surface tension when it usually breaks off at the opening of the cavity and rises through the liquid. Usually a bubble encompasses many cavities before it detaches; thus, this vapor trapping process induces adjoining inactive cavities into activity. After a long period of continuous nucleation a cavity will be completely depleted of trapped gas and replaced with vapor which will condense when the surface temperature is reduced. A conical pit can not be filled with liquid without the expenditure of a great amount of work, because the surface tension forces will oppose the movement of liquid into the tip. On the other hand, in a pit with rounded bottom, nucleation will cease when the inert gas is gone and the pit is filled with liquid. The above postulations of heterogeneous nucleation from surface cavities have been substantiated by the experiments of Corty and Foust (C_3), Gaertner and Westwater (G_1) Griffith and Wallis (G_3) and Kurihara and Myers (K_4) in addition to the high speed photographic observations of Westwater and his coworkers (C_2,W_5). In their experiments Corty and Foust (C_3) removed all possible gases and vapor from the heating surface and found that a much higher degree of superheat is required to cause boiling under the same heat flux which indicated

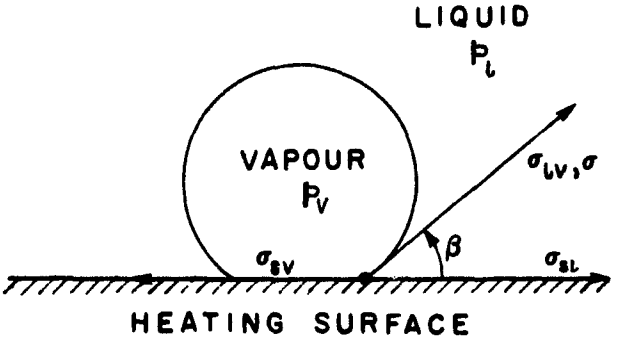

FIG. 1 BUBBLE ON A HEATING SURFACE

that activities of nucleation sites were much reduced due to the reduced amount of trapped gas in the cavities. Gaertner and Westwater (G_1) devised a technique for determining active nucleation sites which consisted of plating a thin layer of nickel on the copper heat transfer surface during the boiling runs and subsequently counting the number of pin holes in the plate. They observed that the heat flux was approximately proportional to the square root of the number of sites. Griffith and Wallis (G_3), Preckshot and Coworkers (N_2,P_4) and Young and Hummel (Y_1) created artificial cavities on the heat transfer surface. Their experimental observations showed that preferred nucleation occurs from pre-existing gas filled cavities on the surface. Still photographs and motion pictures taken by Westwater et al. (C_2) showed that pits with diameters between 0.0003 and 0.003 inches were very active nucleation sites. Some scratches, a plastic-metal interface and a mobile speck of unidentified material were also found to act as active sites. Han and Griffith (H_2) found that the temperature of bubble initiation on a given surface is a function of the temperature conditions in the liquid surrounding the cavity as well as the surface properties themselves and developed a criterion for bubble initiation from a gas filled cavity. Some theoretical conditions for microscopic grooves or cavities to be effective vapor traps have been deduced by Bankoff (B_1,B_2,B_3). These are essentially of a geometrical nature, and depend upon the liquid contact angle, and assume quasi-static conditions. These give necessary, but not sufficient conditions for nucleation. A dynamic

theory of penetration of liquid into potential nucleation site remains largely to be developed, although some preliminary work has been done by Bankoff (B_4).

C. Bubble Growth and Motion

An elucidation of the mechanism of boiling is possible only if we obtain a thorough understanding of bubble formation, growth and motion in a superheated liquid. Previous sections of this chapter dealt with bubble formation. In this section research in bubble size, growth and motion are briefly discussed.

1. Bubble Size and Departure Frequency

At departure from a heated surface, the bubble size may be predicted from a dynamic force balance on the bubble. Fritz (F_4) and Wark (W_1) derived equations for predicting the bubble diameter at departure as

$$D_b = C_d\beta\left[\frac{2g_o\sigma}{g(\rho_l-\rho_v)}\right]^{1/2} \tag{8}$$

The above equation correlated nicely the data for hydrogen and water vapor by Kabanow and Frumkin and by Jakob and Kipeke (J_1).

When a bubble starts to grow on a heating surface a time interval t_d is required for it to depart from the surface and a time interval t_c is required to heat the cold liquid which rushes behind the bubble so that nucleation can occur again. The bubble frequency f is then defined as $1/(t_c+t_d)$.

Jakob (J_1) assumed that $t_d = t_c$ and observed that the product of frequency and the bubble diameter at departure is a constant for all liquids. In their experiments, Hsu and Graham (H_6), and Westwater and Kirby (W_4) noticed that t_d is not necessarily equal to t_c and also D_b is not constant at high heat fluxes. However on verification of the relations of Jakob and Fritz, Han and Griffith (H_2) found that they are applicable as long as the true (non equilibrium) bubble contact angle is used in the equations. Attention has also been focused on the effect of heat flux, pressure, surface orientation and other factors in determining the bubble shape and the waiting period (J_1,W_3).

2. Bubble Growth Rate

Reasonably successful attempts to obtain exact expressions for bubble growth were made by Plesset and Zwick (P_1,P_2) and Forster and Zuber (F_3). Besides the above mentioned works, the available theories include those of Scriven (S_1), Han and Griffith (H_2), Bankoff and coworkers (B_4,S_5), Hamburger (H_1), Dougherty and Rubin (D_2), and Van Wijk et al. (V_4). They claim agreement with the limited experimental measurements of Ellion (E_1), Gunther and Kreith (G_4), and Dergarabedian (D_1).

Successful use of high speed photography to obtain basic knowledge of bubble formation and bubble growth was carried out by Westwater and coworkers (S_6), Jakob (J_1) and Gunther and Kreith (G_4).

For a rather complex case of binary mixtures Scriven (S_2), Bruiyn (B_{10}) and Van Stralen et al. (V_4) have attempted to predict the bubble growth rates. Experimental data for binary mixtures are scarce. Practically no work has been done on the bubble growth

rates in multicomponent liquids. Much remains to be done experimentally and theoretically in all aspects of bubble behaviour at solid surfaces such as nucleation, coalescence, departure and interaction (B_4).

D. Factors Affecting Nucleate Pool Boiling

The complex boiling phenomena of liquids is affected by a large number of variables as discussed below in addition to the physical properties of the boiling liquid.

1. Nature of Liquid

(a) Water. Data for water boiling at atmospheric pressure was first reported by Nukiyama (N_1) followed by an extensive list of investigators as listed in the review articles (W_3,L_2,R_6) and books (M_1,T_1). The burn-out heat flux obtained in experiments for various heating bodies which included wires, tubes and flat surfaces at different positions such as horizontal, vertical, downward facing or upward facing range from about 0.482 to 2.69 $\frac{K.Cal}{M.hr}$ as tabulated by Ishigai et al.(I_1). The reported values for the critical temperature difference range from about 40°F to 90°F with most values around 50°F (W_3). The value is dependent on the condition of the heating surface and other factors discussed below.

(b) Other Liquids. Experimental investigation of the nucleate boiling behavior of many ordinary liquids have been reported (W_3). The shape of boiling curves of single component liquids resemble that of water closely, however with the critical heat flux values considerably lower than that of water. The critical temperature difference

seems to be essentially the same as for water.

(c) Liquid Metals. Liquid metals have desirable characteristics as heat transfer media for use in atomic reactors and space vehicles where it is necessary to remove heat from a surface at a very high rate with the lowest possible surface temperature. Under these conditions liquid metals have certain advantages over water at high pressure because they are stable as liquids over a wide temperature range and have high heat transfer coefficients. A summary of liquid metal pool boiling data is given in the book by Tong (T_1). The wettability of the surface and the surface roughness seemed to increase greatly the boiling heat transfer in the case of mercury (T_1).

2. Effect of Pressure

Pressure is a vital factor in nucleate boiling. At a given ΔT an increase in pressure causes an increase in heat transfer (A_1). The maximum heat flux and the critical temperature difference are functions of pressure also. The maximum heat flux increased with pressure till the critical pressure was reached and then decreased with pressure as shown by the experiments of Cichelli and Bonilla (C_1), Farber and Scorah (F_1), Kazakova (K_1) and McAdams (M_1). Rohsenow and Clark (R_7) and Kreith and Sommerfield (K_3) have studied boiling inside nickel and stainless steel tubes at higher pressures and observed similar results.

3. Material of the Heating Surface

The material of the surface was found to affect heat transfer under boiling liquids in the experiments of Agarwal and Hsu (A_2),

Bonilla and Perry (B_8), Corty and Foust (C_3) and Mead et al. (M_4). Agarwal and Hsu conducted a series of experiments using boiling FC-75 liquid and steel wire plated with various metals, namely nickel, zinc, copper, and cadmium. They observed that the difference in the plating material resulted in a difference in heat transfer. For example copper-plated wire had a heat transfer coefficient of 3100 Btu/ft^2.hr.$^\circ$F, while for the same temperature difference the heat transfer coefficient for zinc-plated wire was only about 520. Similarly the h VsΔT curves obtained by Mead for boiling water were distinctly different for copper and stainless steel. The same trend was exhibited by boiling methanol on copper and nickel and ethanol on copper, gold and chromium (W_3). In all these cases copper gave a greater heat transfer coefficient at a fixed temperature difference than did the other metals.

Agarwal and Hsu contend that high thermal conductivity metals such as copper, aluminum and silver are not efficient mediums for boiling heat transfer. Metals and alloys having relatively very low values of thermal diffusivity seem to stand highest heat fluxes and hence are efficient mediums for boiling heat transfer.

4. Condition of the Heating Surface

The characteristic pool boiling curve is affected by the condition of the surface; its roughness or smoothness and the length of time it has been used. Rate of heat transfer for rough surfaces was found to be appreciably higher than smooth surfaces by several investigators (B_6,C_3,K_4). In Berenson's experiments (B_6) the nucleate boiling

heat transfer coefficient varied by 600% owing to variations in surface finish. The rougher surface with regard to boiling is that which has the greater number of cavities of appropriate size, regardless of the r.m.s. roughness. Surface roughness not only influences the intercept of the boiling curve, but also its slope. However, most of the correlations ignore the dependence of the slope of the boiling curve on the surface conditions. This is undoubtedly due, at least in part, to the difficulty of describing surface roughness mathematically. Kurihara and Myers (K_4) were the first to attempt to incorporate surface effects quantitatively into a correlation of nucleate pool boiling heat transfer.

5. Effect of Aging

Surfaces that have been in service for long periods of time often require higher ΔT for the same heat flux. During one of their experimental runs lasting about 12 hours with copper surface, Corty and Foust (C_3) noticed that the ΔT required to maintain constant coefficients increased approximately $3^{\circ}F$. This may be due partly to the decrease in the amount of trapped gas, partly to the fouling effect of the solids deposited on the surface during the time of use or possibly due to annealing of copper surface which might have changed the grain structure of the surface.

6. Mechanical Agitation

The data of Pramuk and Westwater (P_4) obtained for boiling methanol with agitation provided by a three inch triple-bladed propellor at speeds up to 1000 rpm. indicated that the rate of heat transfer may

be increased more than 100% by agitation.

7. Effect of Geometrical Arrangements

Neither shape, size, nor inclination seems to have much effect upon the rate of heat transfer to a liquid boiling on a submerged surface as proved in the experiments of Jakob and Linke (J_1), McAdams (M_1), and others. Recent work of the Japanese researchers Ishigai et al. (I_1) who studied pool boiling from a downward facing surface substantiated the above conclusions.

8. Effect of Gravity

The photographic evidence obtained by Siegel and Usiskin (S_3) showed that at zero gravity in free fall, nucleate boiling stopped and a large bubble of vapor surrounded a heating surface. As gravity was increased from 1 to 20 G's, Merte and Clark (M_5) observed very little change in the position of the nucleate boiling curve in the higher range. However in the convection region and in the beginning of nucleate boiling, an appreciable shift in the boiling curve was noticed by them. This was mainly due to increased natural convection as gravity was increased.

In conclusion of this chapter, it may be pointed out that in spite of the voluminous theoretical and experimental works reported in the literature in boiling heat transfer todate, there are several areas which need further investigation. One can only speculate that a complete and thorough understanding of all aspects of boiling will probably require intensive research for several years to come.

CHAPTER III

THEORETICAL CONSIDERATIONS

A. General

Boiling phenomena are characterized by the appearance of several regimes of boiling. In each of those regimes the controlling mechanism of heat transfer is so complex that it has defied the ingenuity of many investigators in their attempts to develop satisfactory theoretical models. However there exists agreement to a certain degree as to how heat is being transferred in the various regimes. Postulations have been made of the mechanisms and based on these, attempts have been made to develop theoretical and semi-theoretical expressions to predict the heat transfer behavior of boiling systems under a set of conditions. Preceeding a consideration of the existing correlations, it is indispensable to examine how the different regimes of boiling are encountered.

B. Types of Boiling

The existence of mainly three regimes of boiling called nucleate, transition and film boiling have been established conclusively (M_1, R_5, W_3).

Some of these regimes have been further subdivided by researchers for the convenience of description.

When a pool of liquid is heated gradually at atmospheric

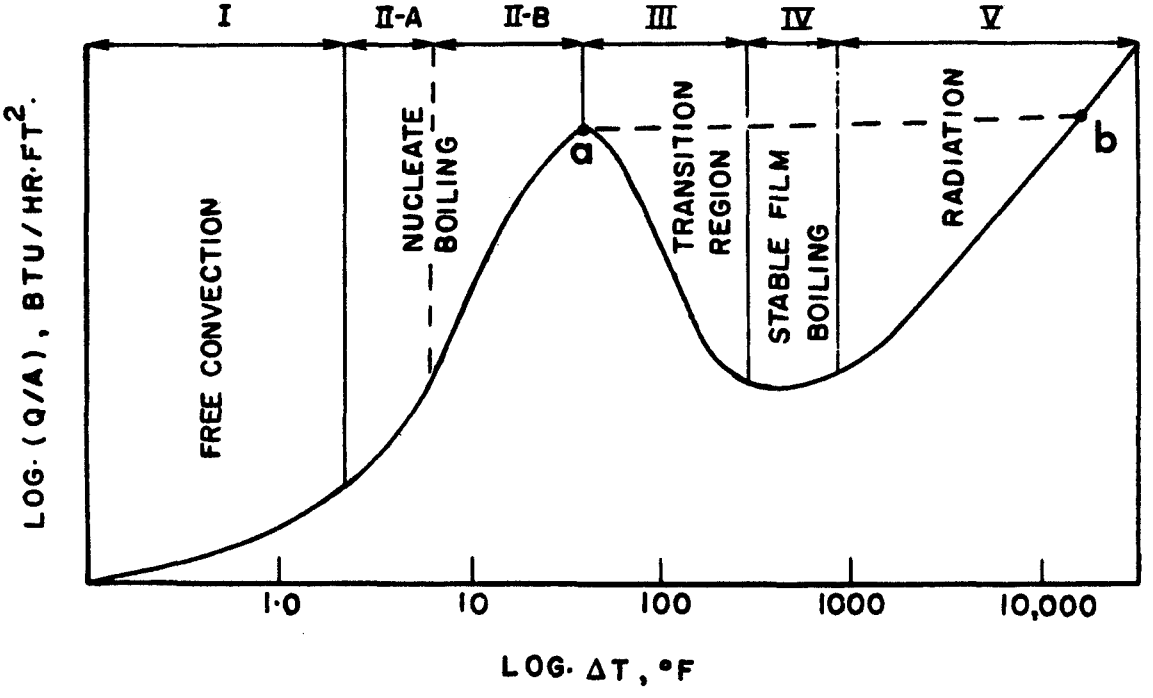

FIG. 2 TYPICAL PLOT OF POOL BOILING

pressure, the resulting boiling curve exhibits a characteristic shape as illustrated in Fig. 2. The boiling curve is usually a plot of the temperature difference between the heat-transfer surface and the bulk liquid on the x-axis and the heat flux on the y-axis drawn on log-log paper.

In region I heat is transferred to the liquid by natural convection and practically no boiling takes place. Regions II-A and II-B encompass the nucleate boiling regime which is of interest for the present study. In region II-A vapor bubbles form at favored spots on the heat transfer surface and are dissipated in the liquid after breaking away from the surface. On further increase of the temperature difference, larger and more numerous bubbles form and rise all the way to the free liquid surface. The heat flux reaches a maximum at the higher end of regime II-B, beyond which liquid no longer is able to reach the heater surface at sufficient rate to form the required amount of vapor. On account of this, either one of the following two things can happen depending upon the type of heating system being used.

When electrical heating is used, as the electric energy and hence the heat flux is increased beyond the peak value, the boiling process cannot remove heat equal to the electrical energy input. The difference between these two quantities causes a rise in internal energy and hence temperature of the resistance wire, which in turn is accompanied by a further decrease of heat flux. In short, the system is unstable and unless the electrical input is reduced, the system will proceed toward point 'b' in Fig. 2 where the temperature of the resistance wire

is very high. Generally this temperature is above the melting point for most metals, and the wire melts before reaching point 'b'. This type of behaviour was observed first by Nukiyama (N_1) with copper wires, but not with platinum wires which have a much higher melting point. Point 'a', the peak heat flux in nucleate boiling is variously called the burn-out point or critical heat flux point.

However when other than electrical heating is being used, the boiling curve goes through a transition region, as shown in Fig. 2. At the transition boiling region an unstable vapor film covers the heat transfer surface which under the action of circulation currents collapses and reforms rapidly. The thermal resistance of this vapor film causes a reduction in heat flux as observed in region III. Stable film boiling is encountered in region IV in which the heater surface is in contact with only the vapor phase which exists as a film between the heater and the liquid. The surface temperatures required to maintain stable film boiling are high and gradually thermal radiation becomes the controlling mechanism of heat transfer as indicated in region V.

C. Nucleate Boiling Mechanism and Correlations

1. General Considerations

To date several attempts have been made to derive a generalised correlation for the prediction of the boiling behavior of fluid-surface systems. These have not been very successful mainly because of the inability of the investigators to fit all the physical properties and variables involved in such systems into a single correlation.

However correlations have been developed which have limited applicability within a particular regime of boiling. In the following discussion some of the semitheoretical and empirical expressions available for nucleate boiling regime will be considered and their limitations will be analysed.

2. Postulations of the Mechanism of Boiling

In nucleate boiling, when the heating surface is in direct contact with the liquid, the highest temperature drop occurs through the thin liquid layer adjacent to the wall. Professor Jakob (J_1) first postulated that only a very small part of the heat produced in a heater is directly transferred to the interior of the bubbles adhering to the surface. The main part of the energy makes a detour through the liquid owing to the high rate of convection existing in the liquid near the heating surface. The above observations were incorporated by Rohsenow (R_8) in developing a correlation for nucleate boiling which will be considered in detail later.

Forster and Grief (F_2) proposed a vapor-liquid exchange mechanism in which the increased heat transfer in nucleate boiling was attributed to a 'pumping action' caused by the growth and collapse of vapor bubbles.

Recently Bankoff (B) has discounted the notion, propagated by Forster and Greif (F_2), Rohsenow and Clark (R_7), Levy (L_3) and others, that latent heat transport plays only a minor role in heat transfer at the heated surface. As a matter of fact latent heat transport seems to contribute very significantly to heat transfer near the critical heat

flux range. Bankoff hypothesised the microlayer vaporization mechanism and pointed out that thin liquid films would exist at the base of vapor bubbles in nucleate boiling. These films evaporate into the bubble removing heat very rapidly. Mesler and his associates (M_6,W_6) provided experimental evidence for Bankoff's prediction when they measured a temperature fluctuation of several degrees at the heat transfer surface directly beneath a number of growing bubbles.

3. Correlations of Nucleate Boiling Data

A rather large number of empirical and semi-empirical formulas have been proposed for nucleate boiling up to the present time. The most satisfactory description of experimental data is provided by formulas incorporating the dimensionless groups of the system, notable among them being the correlations of Rohsenow (R_8), Forster and Zuber (F_3), Forster and Grief (F_2) and Levy (L_3).

(a) Rohsenow's Correlation. Rohsenow assumes that a major portion of the heat in nucleate boiling is transferred directly from the surface to the liquid and the bubbles act as agitators. The size of the bubble at the point of break off is an important parameter because when a bubble breaks loose, the liquid flows behind and great agitation is achieved. Therefore Rohsenow postulates that there should exist a bubble Reynolds number which measures the effect of this increased agitation on heat transfer. A comparison is made of nucleate boiling with heat transfer in forced convection turbulent flow without boiling. In the latter case, the usual correlation is of the form

$$N_{Nu} = C(N_{Re}, N_{Pr}) \tag{9}$$

Therefore one can expect a correlation of similar nature to be satisfactory also for nucleate boiling.

The dimensionless groups are defined as follows:

$$N_{Nu_b} = \frac{(Q/A)_b D_b}{(T_w - T_{sat})k_\ell} \tag{10}$$

$$N_{Re_b} = \frac{G_b D_b}{\mu_\ell} \tag{11}$$

The definition of bubble Reynolds number is justified when we interpret it as the ratio of inertia to viscous forces; hence G_b associated with the inertia of the bubble and μ_ℓ associated with the friction force on the bubble are used. The N_{Re_b} term postulated above measures the amount of liquid agitation caused by the bubble motion.

D_b, the maximum bubble diameter at departure or just before collapse can be computed using Fritz's expression (F_4):

$$D_b = C_d \beta \sqrt{\frac{2g_o \sigma}{g(\rho_\ell - \rho_v)}} \tag{12}$$

The heat transfer to the bubbles while attached to the surface can be written with good approximation as

$$(Q/A)_b = h_{fg} \rho_v n \frac{\pi}{6} D_b^3 f \tag{13}$$

where the bubbles on the average may be assumed as spheres.

Jakob (J_1) has shown that for the case of water and carbon tetrachloride, the product of the frequency of bubble formation and the

diameter of the bubble when it leaves the surface is nearly a constant value.

$$\text{i.e.} \quad fD_b = C_{fd} \text{ , constant} \tag{14}$$

Since the total heat flux will be very nearly directly proportional to the number of columns of bubbles,

$$Q/A \sim (Q/A)_b \tag{15}$$

or

$$(Q/A) = C_q \, h_{fg} \, \rho_v \, n \, \frac{\pi}{6} \, D_b^3 \, f \tag{16}$$

where the constant C_q may be a function of pressure. The mass velocity of the vapor bubbles leaving the surface may be written as

$$G_b = \frac{\pi}{6} \, D_b^3 \, f \, \rho_v \, n \tag{17}$$

substituting equations (12),(16), and (17) into Eq. (11), we obtain an expression for the bubble Reynolds number as

$$N_{Re_b} = C_R \, \beta \, \frac{Q/A}{\mu_\ell h_{fg}} \sqrt{\frac{g_o \sigma}{g(\rho_\ell - \rho_v)}} \tag{18}$$

where the constant C_R incorporates the two constants C_d and C_q from Eq. (12) and (16) and is equal to $\sqrt{2}$ Cd/Cq. Eq. (12) for bubble diameter can be substituted in the expression (10) for bubble Nusselt number to obtain

$$N_{Nu_b} = C_n \, \beta \, \frac{h}{k_\ell} \sqrt{\frac{g_o \sigma}{g(\rho_\ell - \rho_v)}} \tag{19}$$

where constant $C_n = \sqrt{2} \; C_d$.

The final expression suggested by Rohsenow for boiling heat transfer is of the form:

$$N_{Nu_b} = \phi\,(N_{Re_b}, N_{Pr}) \tag{20}$$

where N_{Nu_b} and N_{Re_b} are defined by Eq. (19) and (18) respectively and the Prandtl number is evaluated as usual from liquid properties.

In applying the above expression for correlating the data of several experimenters, the terms C_R, C_n and β were all summed up into a single constant C_{sf} as shown below:

$$\frac{C_\ell \Delta T}{h_{fg}} = C_{sf}\left(\frac{Q/A}{\mu_\ell h_{fg}}\sqrt{\frac{g_o \sigma}{g(\rho_\ell - \rho_v)}}\right)^{0.33}\left(\frac{C_\ell \mu_\ell}{k_\ell}\right)^{1.7} \tag{21}$$

or

$$N_{Nu} = (\text{const})\,(N_{Re_b})^{2/3}\,(N_{pr})^{-0.7} \tag{22}$$

Expressions (21) and (22) are the final forms of Rohsenow's correlation. In these expressions the exponents 0.33 and 1.7 were really obtained by plotting the experimental data of several research groups. It should also be noted that there is nothing definite about the values of these exponents except that they were found to fit the limited amount of data available for clean heat transfer surfaces. Since its publication, Rohsenow's semiempirical expression (Eq. (21)) has been found to correlate the data of several single component fluids boiling on clean surfaces and in all cases the coefficient C_{sf} has been found to vary over wide range from 0.0025 to 0.015 depending upon the surface-fluid combination as seen from Table I of Appendix I. Rohsenow attributes these significant

variations observed by various experimenters mainly to a lack of information on β, the contact angle measurements for the systems considered. Part of the blame has also been attributed to the inaccuracy of the surface temperature measurements which magnify the errors in $(T_s - T_{sat})$ values used in the computations. Rohsenow argues that, owing to the above mentioned two factors, there is good reason to expect a different value of C_{sf} to result for every combination of kind of surface and kind of fluid. The author finally concludes that additional information regarding the values of β for various combinations of surfaces and fluids should clarify this matter and produce a valid correlation for all such combinations.

(b) Forster-Zuber Correlation. Forster and Zuber developed a correlation for nucleate boiling heat transfer which is similar to that of Rohsenow's correlation in that the former also included the dimensionless Nusselt, Prandtl and Reynolds numbers. However the exponents on the Reynolds and Prandtl numbers in Forster and Zuber equation are roughly the same as those used for ordinary forced convection heat transfer whereas Rohsenow's correlation contains the Prandtl number term with a negative exponent which has seemed 'illogical' to many scientists (W_3).

According to this approach the agitation caused by the movement of the bubble boundary while bubbles are still attached to the heating surface is the dominant mechanism in increasing the heat transfer. The authors develop analytical expressions for bubble radii and growth rates starting from Lord Rayleigh's classical equation for bubble dynamics of an incompressible and inviscid fluid.

$$R\ddot{R} + \frac{3}{2}\dot{R}^2 + \frac{2\sigma}{\rho_\ell R} = \frac{P_v - P_\infty}{\rho_\ell} \tag{23}$$

It was demonstrated by the authors that the equation for the growth of vapor bubble in a superheated liquid is given by

$$R = 2\sqrt{\frac{\pi}{4}}\ Ja\ \sqrt{\alpha_\ell t} \tag{24}$$

where Ja, the Jakob number is $\frac{C_\ell \rho_\ell \Delta T}{h_{fg}\rho_v}$ and α_ℓ, the liquid thermal diffusivity is defined as $k_\ell/\rho_\ell C_\ell$. The radial velocity of the bubble boundary is obtained by differentiating Eq. (24) with respect to time 't'.

$$\dot{R} = \frac{dR}{dt} = \sqrt{\frac{\pi}{4}}\ Ja \sqrt{\frac{\alpha_\ell}{t}} \tag{25}$$

The product of bubble radius and radial velocity is a constant, independent of the bubble radius as shown below:

$$R\dot{R} = \left(\frac{C_\ell \rho_\ell \Delta T\ \sqrt{\pi\ \alpha_\ell}}{h_{fg}\rho_v}\right)^2 \tag{26}$$

$$= \pi\ \alpha_\ell\ Ja^2 \tag{27}$$

The authors also assume that the final correlation will be similar to the forced convection heat transfer correlation of the form,

$$N_{Nu} = (\text{const})\ (N_{Re})^m (N_{pr})^n \tag{28}$$

The dimensionless groups in the above expression (28) have to be formulated.

The authors consider the state of liquid motion in the thin layer of fluid adjacent to the heating surface to be most important in

influencing the heat transfer. Therefore they substitute the bubble radii and the bubble growth velocities for the characteristic length and velocity term respectively of the Reynold's number. The Reynolds number is now written as

$$N_{Re_b} = \frac{R\,\dot{R}\,\rho_\ell}{\mu_\ell} = \frac{\rho_\ell}{\mu_\ell}\left(\frac{C_\ell \rho_\ell \Delta T \sqrt{\pi\alpha_\ell}}{h_{fg}\rho_v}\right)^2 \tag{29}$$

The Nusselt number for the system is defined as

$$N_{Nu} = \frac{\frac{Q}{A} R}{k_\ell \Delta T} \tag{30}$$

where the length R is obtained from considerations of bubble dynamics and is given by

$$R = \left(\frac{C_\ell \rho_\ell \Delta T \sqrt{\pi\alpha_\ell}}{h_{fg}\rho_v}\right)\left(\frac{2\sigma}{p_v - p_\infty}\right)^{\frac{1}{2}}\left(\frac{\rho_\ell}{p_v - p_\infty}\right)^{\frac{1}{4}} \tag{31}$$

Substitution of Eq. (29), (30) and (31) into (28) gives the final form of Forster-Zuber correlation:

$$\frac{(Q/A)\,C_\ell \rho_\ell \sqrt{\pi\alpha_\ell}}{k_\ell h_{fg}\rho_v}\left(\frac{2\sigma}{\Delta p}\right)^{\frac{1}{2}}\left(\frac{\rho_\ell}{\Delta p}\right)^{\frac{1}{4}} = 0.0015\, N_{Re_b}^{0.62}\, N_{pr}^{\frac{1}{3}} \tag{32}$$

or

$$N_{Nu} = 0.0015\,(N_{Re})^{0.62}\,(N_{pr})^{\frac{1}{3}} \tag{33}$$

The main criticism of the above correlation is that it predicts the same heat transfer coefficient for a liquid boiling on any hot surface (all heterogeneous cases) or boiling in the bulk (the homogeneous case). Such a prediction is open to serious question in view of the

ample experimental evidence available contradicting such a behaviour of homogeneous and heterogeneous boiling systems.

(c) Forster-Grief Correlation. Forster and Grief analysed various transfer mechanisms which have been proposed by previous researchers and reached a conclusion in favour of a vapor-liquid exchange mechanism. According to this mechanism, during boiling the bubbles in growth and collapse act as highly efficient piston pumps working at about 1000 cycles per second, which mechanically pump the hot liquid from the heating strip to the bulk and the cold liquid from the bulk to the heating surface. This is the reason attributed to the tremendous increase in heat flux observed after boiling starts. The authors use the experimental data of Gunther and Kreith (G_4) who measured the bubble radii and the temperature distribution near the heating surface during boiling and show quantitatively that the amount of heat transferred by the vapor-liquid exchange taking place every time a bubble grows and then collapses on, or detaches from the heating surface is by itself sufficient to account for the heat flux in nucleate boiling and claim that the proposed mechanism explains the observed insensitivity of boiling heat flux to the level of subcooling. They deduce a correlation for the pool boiling heat flux in water at 14.7 - 700 psia as

$$Q/A = 4.3 \times 10^{-5} \frac{k_\ell T_{sat} \Delta p^2}{\sigma^{1/2}(h_{fg}\rho_v)^{3/2}} \left[(C_\ell T_{sat} \alpha_\ell^2)^{\frac{1}{2}\frac{1}{4}} \left(\frac{\rho_\ell}{\mu_\ell}\right)^{\frac{5}{8}} \left(\frac{\mu C_\ell}{k_\ell}\right)^{\frac{1}{3}}\right] \quad (34)$$

However the above correlation has to be tested widely as experimental data become available before any opinion about its validity can be

expressed.

(d) Levi's Correlation. The generalized equation of Levi (L_3) to correlate the boiling data of all fluids independently of pressure and heating surface-fluid combination is of the form:

$$Q/A = \frac{k_\ell C_\ell \rho_\ell^2}{\sigma T_{sat}(\rho_\ell - \rho_v)} \quad \frac{1}{B_L} \quad (\Delta T)^3 \tag{35}$$

The above relation was obtained from a simplified model of bubble growth rate close to the heated surface and an empirical determination of the relation between heat-transfer rate at the heated surface and that at the bubble surface. Forster and Zuber's equation for bubble growth rate was made use of by the author to obtain the heat flux to the bubble as shown below.

$$\frac{Q_b}{A_b} = h_{fg}\rho_v \frac{dR}{dt} = \frac{(T-T_{sat})^2 C_\ell \rho_\ell \pi k_\ell}{R\, h_{fg}\, \rho_v} \tag{36}$$

The total heat flux Q/A was assumed to be equal to a constant times the heat flux to the bubbles,

$$\text{i.e.} \quad Q/A = \frac{1}{B_L} \frac{Q_b}{A_b} \tag{37}$$

The dimensionless constant B_L was found by empirical methods to be dependent upon the product $\rho_v h_{fg}^2$ and could be read directly from a plot of $\frac{1}{B_L} v_s \rho_v h_{fg}$ provided by the author. It was noticed (L_3) that good correlation between the proposed equation and several test results of other experimenters was achieved.

D. Grains and Grain Boundaries in Metals and Their Influence on Physical and Chemical Phenomena

1. Introductory Remarks

The important role played by crystals or grains and associated grain boundaries in influencing the engineering properties of a metal can only be understood by recognizing the importance of crystal structure first. What is a crystalline solid? One way to answer this is to state that a crystalline solid is one that diffracts x-rays. In order that diffraction occurs there must be a three dimensional scheme of repetition of the atoms or molecules comprising the crystals. Because of the bonding in metals in which there is no directed linkage, each metal atom tries to surround itself by as many other atoms as possible. This leads to structures which are face-centered cubic (fcc), hexagonal close-packed (hcp), or body-centered cubic (bcc). About seventy percent of the metallic elements crystallize in these structures. The balance of the metallic elements are either hexagonal, rhombohedral, or orthorhombic in structure.

Engineering materials are polycrystalline. The presence of internal surface (or grain boundaries as they are called) and external surfaces can greatly affect the various properties of a solid (S_4)

2. Grain Boundaries

It would be logical to define a grain boundary and then to describe its properties. McLean (M_3) defines the grain boundary in a piece of metal as the boundary separating two crystals (or 'grains')

that differ either in crystallographic orientation, composition, or dimensions of the crystal lattice, or in two or all of these properties.

Boundaries can form on crystallization from a liquid, on the recrystallization of a solid, on the allotropic transformation of a solid, on the precipitation of one solid from solution in another solid as in the case of electroplating, or by the sintering or the interdiffusion of small particles to form an aggregate. Although grain boundaries can be formed in many ways, this does not necessarily mean that there are any differences between the boundaries so generated. In all cases they are the regions of misfit between adjacent crystalline phases. The grain boundary is characteristic of polycrystalline solids and is not found in amorphous materials.

3. Grain Boundary Properties

It can be said that grain boundaries modify the properties of the adjacent crystals rather than show separate properties (S_4). The presence of grain boundaries greatly modifies mechanical properties. As compared to the properties of a single crystal, it will be found that yield and tensile strengths of polycrystalline materials are increased. The plasticity, as measured by the ductility and reduction in area is markedly decreased. The cleavage or fracture strength is increased, as is the fatigue strength and creep strength. All of these changes are dependent upon the number of grain boundaries present, or as it is more commonly stated, are grain-size dependent.

A comparison of the thermal and electrical properties of

single crystals versus polycrystals will show differences in behaviour but usually never more than 50-100% changes. Generally, properties that are a function of electronic energies will be affected by the presence of a boundary in the sense that this region is like a lattice imperfection. As such it represents an interruption or discontinuity in the potential field in which the electrons move, but it is not a barrier that completely blocks electronic interchange. The mechanical properties, on the other hand, depend on actual mass movements and the grain boundary barriers for these processes are sufficiently great so as to modify the behaviour of the solid as a whole.

The grain boundary represents a region of misfit between two of more crystalline lattices. The atoms in such a boundary are shared by the adjacent crystals, but the force field in which the atom finds itself is not uniform, since it is not a regular part of either of the lattices it adjoins. This viewpoint represents the grain boundary as being a problem of crystallographic disorientation, and, as indicated by experimental evidence, this is true for certain types of boundaries. Since it is a region of misfit, one can anticipate that it is a strained region, and there are several experimental facts to confirm this.

The hardness of the material adjacent to a boundary is different than in the matrix. Studies of melting points indicate that grain boundaries melt before the matrix material. Diffusion studies show that atoms move through grain boundaries at a rate many orders of magnitude greater than through the crystal lattice. Chemical effects at boundaries are quite pronounced. The effect of acids and alkalies, for

example, when applied to a polished polycrystalline surface is invariably to attack the grain boundaries more rapidly than the crystals. Electrical measurements show that there is an emf set up between boundaries and the matrix material with the boundary at the higher energy level. The impurity content of grain boundaries is higher than the matrix material. Precipitation, transformation, and recrystallizations occur first at grain boundaries. The presence of grain boundaries has an important bearing on transformations from one allotropic form to another, since the transformation is nucleated first at the boundaries. Similarly, precipitation processes in which a phase, compound, or element is rejected from a solid solution are quite sensitive to grain boundary conditions, since nucleation almost invariably starts in these regions. The foregoing are a few of the more important effects produced by the presence of boundaries (S_4).

4. The General Theory of Interfaces

If we consider a planar interface between two pure phases, from thermodynamic considerations it can be shown (S_7) that the Gibbs free energy 'G' is related to the interfacial tension 'σ' between the two phases as follow:

$$G = \sigma A \tag{38}$$

or

$$\sigma = G/A , \tag{39}$$

if σ is independent of interfacial area A. In applying the above general deduction to solid phases considerable caution must be exerted because with a crystalline solid σ is not independent of crystal

orientation but is strongly dependent upon the types of crystallographic planes forming the interface. Also in deriving the above relation, it was assumed that σ, equal to the free energy per unit area, is not a function of area, an assumption which is not valid generally for many solids. This reservation is not important if the interface is atomically disordered or if the temperature is sufficiently elevated as in the case of high angle crystal boundaries (S_7).

5. Grain Boundary Triangle of Forces: Dihedral Angle

An important feature which is made use of to determine grain boundary tension is the equilibrium arrangement where grain boundaries meet. Grain boundaries nearly always meet three at a time. Let us consider a triple junction as shown in Figure 2a below. The dihedral angles α, β and γ will tend to adjust themselves into the lowest energy

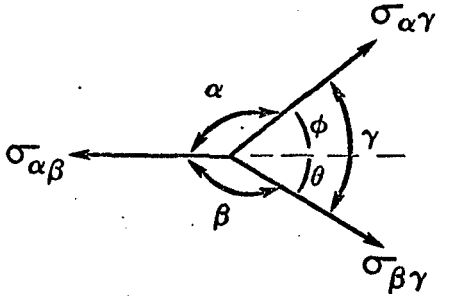

Fig. 2a

configuration possible. At equilibrium we have from trigonometry,

$$\frac{\sigma_{\alpha\beta}}{\sin\gamma} = \frac{\sigma_{\alpha\gamma}}{\sin\beta} = \frac{\sigma_{\beta\gamma}}{\sin\alpha} \tag{40}$$

or

$$\sigma_{\alpha\beta} - \sigma_{\alpha\gamma}\cos\phi - \sigma_{\beta\gamma}\cos\theta = 0 \tag{41}$$

The above equations are valid for liquid phases. For solids consideration has to be given to the fact that σ is a function of crystallographic orientation of the boundary. As a result there will exist forces trying to shorten the boundaries; in addition there may be angular forces attempting to cause the boundary to turn into a crystallographic orientation having lower energy. For such a case Herring (S_7) derived the following relationship:

$$\sigma_{\alpha\beta} - \sigma_{\alpha\gamma}\cos\theta - \sigma_{\beta\gamma}\cos\theta + \frac{\partial\sigma_{\alpha\gamma}}{\partial\phi}\sin\phi + \frac{\partial\sigma_{\beta\gamma}}{\partial\theta}\sin\theta = 0 \quad (42)$$

For most inernal boundaries in solids, the change of interfacial tension with angle $(\frac{\partial\sigma}{\partial\alpha})$ is small. So Eq. (41) is a good approximation in these cases.

6. Boundary Energies

Whatever the precise structure of grain boundaries the fact that the atoms at the boundary between two crystals must be displaced from the positions which they would occupy in a crystal and due to this there is departure from the perfect crystal structure means that each boundary atom on the average has more total energy than a grain interior atom (M_3). It does not immediately follow that each boundary atom on the average also has more free energy. However, calculations done by Read and Stockley (R_1) suggest that this is so and experiment confirms it (M_3). When metals are heated to a temperature high enough for adjustments to take place at the boundaries, except in special cases, those adjustments take place that reduce the total boundary area, there being

therefore a net transfer of atoms from positions in boundaries to positions in grain interiors. Grain boundaries also possess an interfacial tension, the existence of which can be demonstrated experimentally by the phenomenon of thermal etching in which grain boundary tension is balanced against surface tension.

Just as the atoms along boundary interfaces are in positions of higher free energy than are those inside the grain, so the atoms at grain boundary junctions, being under the influence of three instead of two competing forces, are in positions of still higher free energy. The free energy per atom along a triple junction is higher than that per atom in a grain boundary by about one-third of the free energy per atom in the surface row of boundary atoms.

7. Methods of Measuring Boundary Energies

Methods exist (M_3) that are potentially capable of determining the absolute magnitude of boundary energies directly, but so far with uncertain accuracy. As yet it has not been possible to make a direct measurement of the energy of a boundary and all the determinations have been indirect in the sense that in each case the energy of a boundary has been compared with that of an external surface, of which the surface energy is measured by some other method.

In the triangle of forces method, the angles α,β,γ in the figure (Fig. 2a)are measured on a section, from which the ratios between the tensions can be determined with the aid of equation (40). The absolute values of tensions can be determined by relating the boundary

tension to a tension which has been measured or can be measured with fair accuracy in some other interface.

The thermal etching method has been used to relate grain boundary to surface tensions, and also to determine the variation of grain boundary tension with orientation difference between the two crystals which the boundary separates. When metals are heated in a vacuum or suitable atmosphere, grooves form where the grain boundaries meet the surface. The angle at the bottom of the groove can be measured by suitable experimental techniques and related to the grain boundary energy (M_3). The two foregoing methods give only relative values of grain boundary tensions.

The grain boundary energy might be determined directly from the energy released during grain growth, assuming the energy evolved to come from the reduction in grain boundary areas. Such measurements might be possible, and the method would be very direct. (H_4)

8. Influence of Orientation on Interfacial Free Energy

Both the orientation difference between the two crystals separated by the boundary and the direction of the boundary will affect the energy of the boundary. Neither effect has been explored thoroughly but enough measurements or observations have been made to show that both effects are small except over certain ranges of orientation and direction (M_3). The grain boundary energy as compared to the surface energy has been shown to vary continuously from a very small value at small angles through a range of increasing angles to a fairly steady maximum that

persists over a considerable range of angles and so for practical purposes the boundary energy may be considered to be independent of orientation angle for a high angle boundary (S_7).

9. Summary of the Above Discussion on Grain Boundaries

Grain boundaries exist in metals as physically distinct regions from the grains on either side. Many properties of metals are affected by grain boundaries. Some are affected more or less directly, while others are affected indirectly.

It is fairly clear that the grain boundaries are in a higher energy state than the adjoining grains themselves. This excess energy apparently acts as the driving force for the many physical and chemical reactions occurring at the boundaries. It is probable that in boiling too, the grain boundaries present in the heat-transfer surface might readily provide favourable sites for the bubble nuclei to initiate and grow. In that case the existence of a relationship between the boiling rate and the extent of grains and grain boundaries in the surface is quite conceivable.

CHAPTER IV

APPARATUS AND EXPERIMENTAL PROCEDURE

A. Heat Transfer Equipment

To design an apparatus to carry out an investigation of this nature, consideration has to be given to several factors. The principle aim of this study was to find out the relation between microscopic grain boundaries of the metallic surface and its boiling characteristics. In order to observe any appreciable effects of grain boundaries on boiling it was considered desirable to conduct boiling studies from a surface area as large as feasible so as to minimize the edge effects. Such a boiling surface will be a true representative of actual industrial boiling equipment. In addition, due to the numerous metallic grains and grain boundaries present in larger surfaces, a quantitative estimation of the influence of grain boundaries on boiling heat transfer might be more reliable.

There was a practical limitation to the size of the boiling surface used here due to the available power supply. A large experimental surface under nucleate boiling conditions at atmospheric pressure requires enormous amounts of heat. A computation showed that with the available heat source of approximately 20 kilo-watts, a surface of 6 inch diameter could be used and operated conveniently in the nucleate boiling region.

It was decided to have the horizontal surface immersed in a pool of boiling water owing to the simplicity and experimental convenience of this type of system. Electric power was chosen to provide heat not only because of its cleanliness but also because it is accurately controllable and easily measureable.

Fig. 3 is a schematic diagram of the boiling apparatus assembly. Fig. 4 shows the details of the heater unit and heat transfer surface.

1. Heat Transfer Surface

The heat-transfer surface was provided by a copper plate of 6 inch diameter by 2.5 inch thickness. One face of this plate served as the surface from which boiling was conducted; on the other face helical grooves of about 0.5 inch depth by 0.5 inch width to match the corresponding grooves of the heater unit were milled. When mounted on top of the heater unit, the copper plate fitted smoothly into the grooves ensuring good thermal contact at the junction. This arrangement, at the same time facilitated the easy separation of the copper plate from the heavy heater to enable mechanical treatment and electroplating operations to be carried out conveniently on the boiling surface as will be described later in the experimental procedure. In order to provide a continuous non-boiling surface, a 10 inch O.D. and 0.25 inch thick stainless steel fin was fitted over the top surface of the copper plate using a 'parker' viton high temperature 'o' ring seal. The boiling surface and the fin were then machined to a smooth finish so that any preferential boiling at the edge of the copper surface was eliminated. Earlier an attempt was made

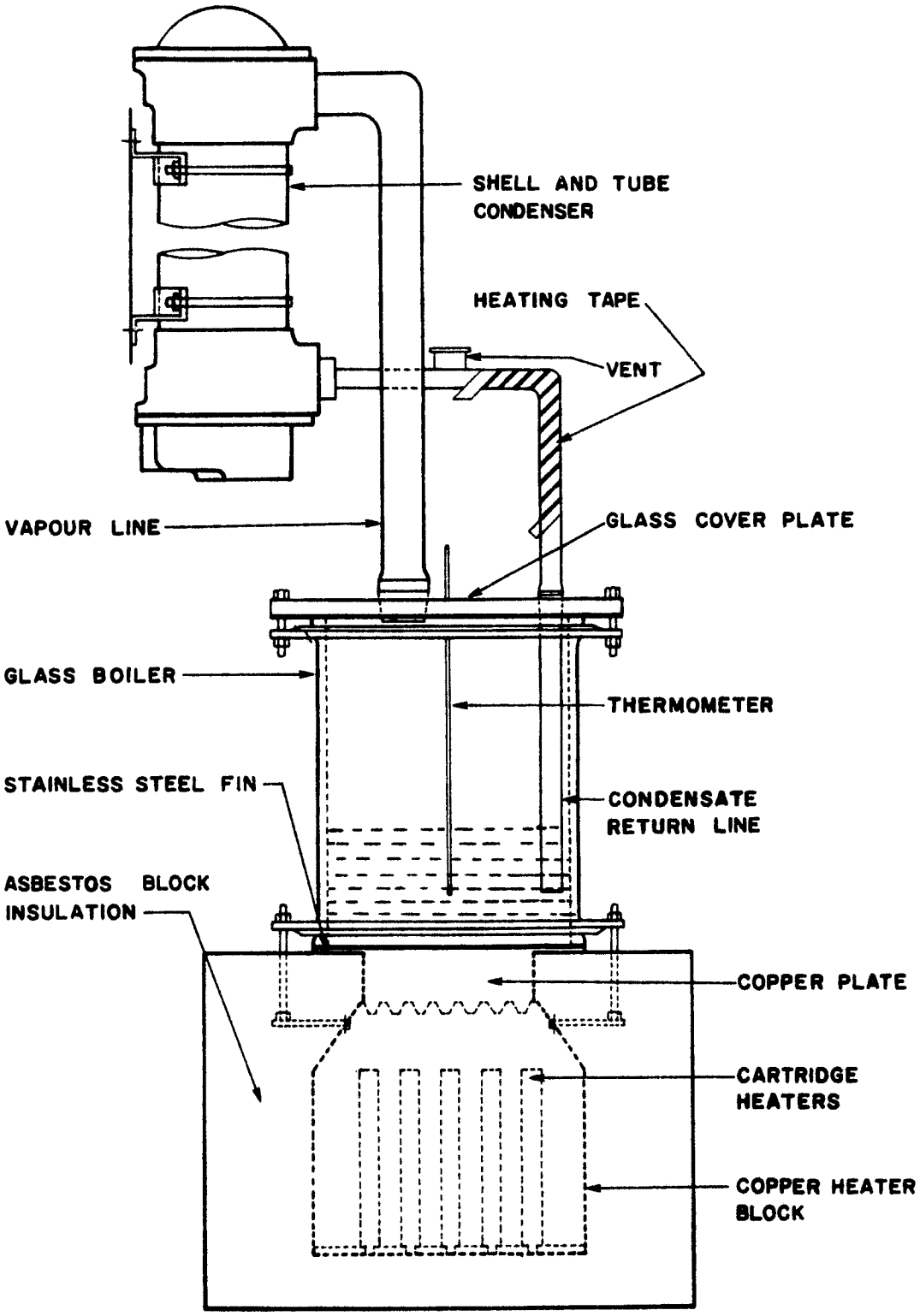

FIG· 3 SCHEMATIC ARRANGEMENT OF APPARATUS

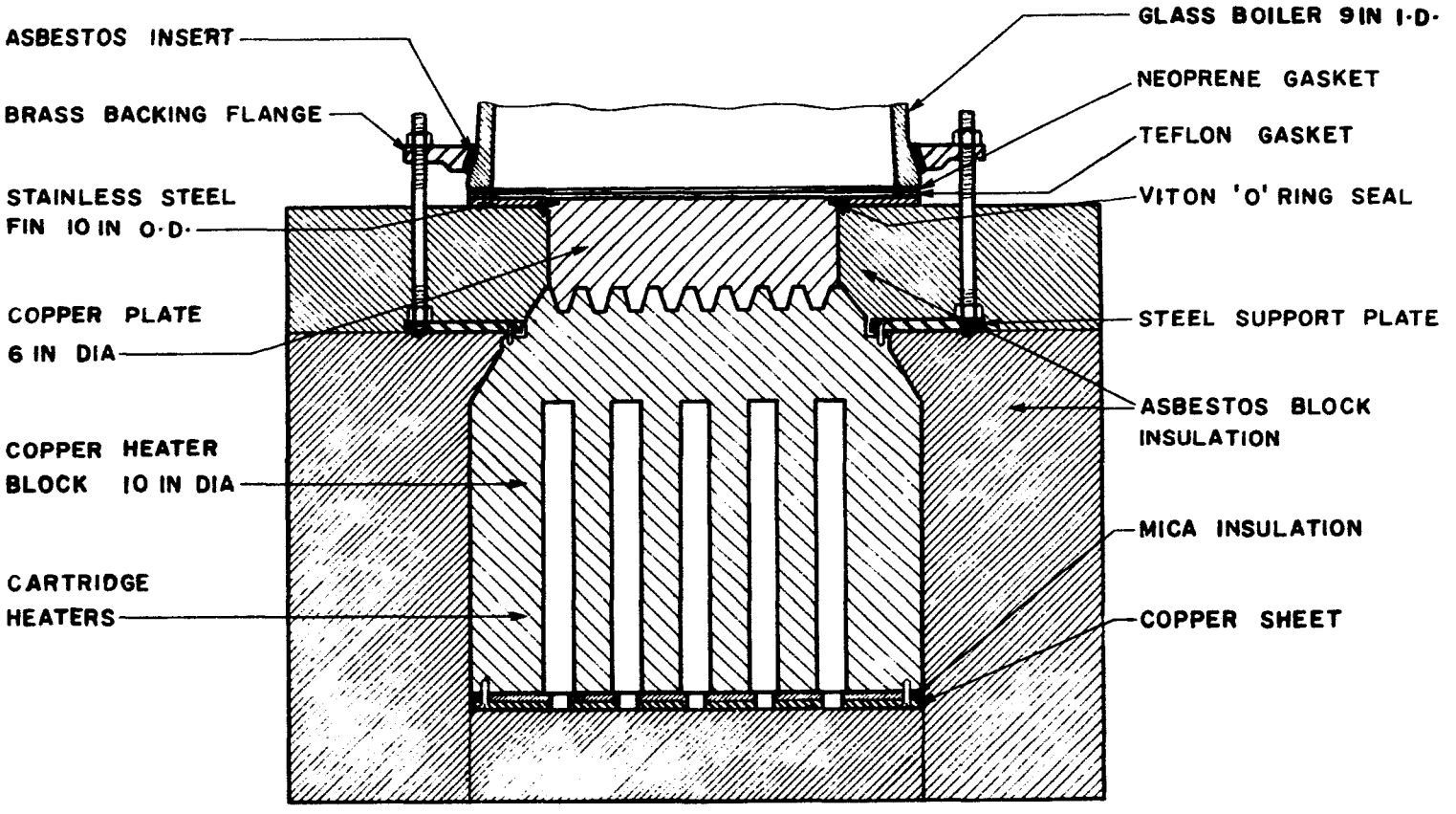

FIG· 4 DETAILS OF THE HEATER UNIT AND HEAT TRANSFER SURFACE

to silver solder the fin to the copper surface, but due to the occurance of uneven warping this technique was discarded.

2. Heater Unit

The heater unit was made from a solid copper cylinder 10 in. diameter and 9 in. high. Twenty five high temperature chromalox cartridge heaters, each 5/8 in. in diameter by $6\frac{1}{2}$ inches long and having a capacity of 990 watts at 240 volts were embedded into suitable holes drilled vertically into the copper cylinder as shown in Figs. 4 and 5. The heaters were supported on several layers of thin mica and a layer of 1/8 inch copper sheet at the bottom of the copper cylinder. The top surface of the cylinder was tapered and reduced to a diameter of $6\frac{1}{2}$ inches. Longitudinal, tropezoidal grooves of 0.5 inch depth, 0.5 inch widthat the bottom and 0.25 inch width at the top were milled into the surface so that they matched the corresponding grooves at the bottom of the heating surface, thereby ensuring good thermal contact. These grooves also prevented seizing of the contacting surfaces and hence permitted their easy separation whenever needed.

3. Power Supply

A schematic diagram of the electrical circuit is given in Fig. 6. Electric power for the heaters was obtained from a three phase 220 volt a.c. source. Power input was controlled by a 3ϕ, 50 Amp.(W50G3M) variac autotransformer made by General Radio Company. The voltage and current in each phase was checked with a 300 V voltmeter and 50 ampere ammeter. Equal loading of the power lines of the 3ϕ system was ensured

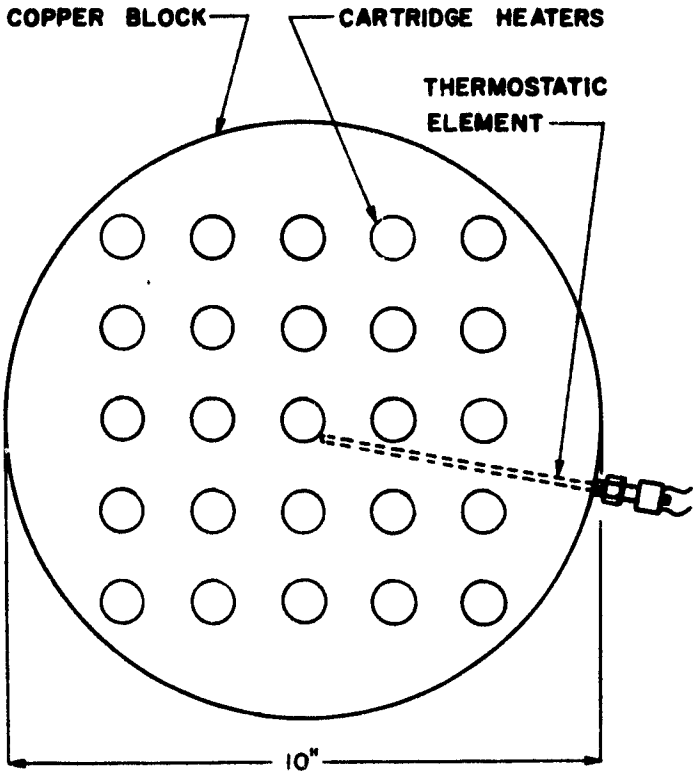

FIG. 5 ARRANGEMENT OF HEATERS

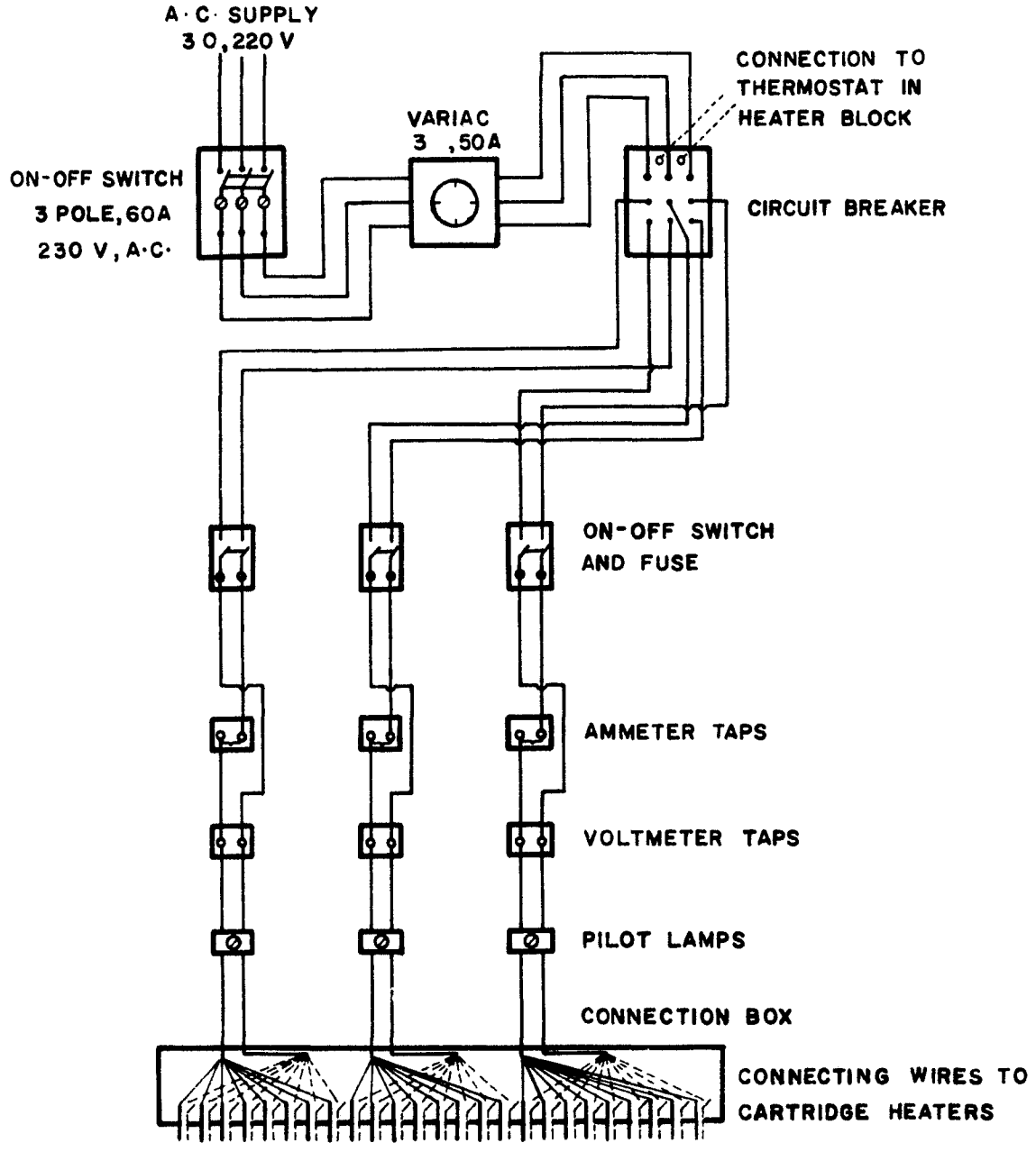

FIG·6 SCHEMATIC DIAGRAM OF ELECTRICAL CIRCUIT

by connecting 8 heaters to each of them. The heaters were protected against burn-out due to accidental overloading by individual fuses. In addition, the copper heater unit was provided with an adjustable thermostatic control and relay arrangement to automatically cut off the power supply to the heaters. The thermostatic control could be set at a predetermined value to ensure that the copper heater unit would never attain a temperature above the safe operating temperature recommended for the heaters. The heater unit was placed on top of a 2 inch thick block of Johns-Manville thermobestos insulation and covered with two layers of 2 inch thick thermobestos pipe insulation on the sides.

4. Boiler and Other Accessories

Boiling took place inside a 9 inch I.D. and 12 inch long Q.V.F. glass flanged pipe section. The glass section could be fitted to the top of the boiling surface by means of four bolts whose tail ends were screwed into a steel plate which was in turn supported at four corners by the copper heater unit. A twin gasket consisting of one layer of 1/16 inch thick neoprene rubber and a second layer of teflon sheet of the same thickness was used between the glass boiler and the heat-transfer surface to prevent leaking.

The top of the glass boiler was closed with a 1 inch thick pyrex glass plate into which two large tapered openings were ground to accommodate vapour outlet and return water inlet lines. The inlet line extended below the liquid level in the boiler so that any disturbance to the boiling due to convection currents from the returning liquid was

avoided. An additional opening in the glass cover plate facilitated suspension of a calibrated thermometer to measure the boiling liquid temperature. The vapor was condensed in a 'perfex' 4 pass shell and tube heat exchanger consisting in each pass of twenty-four 1/4 inch copper tubes each 15 inches long. The cooling water to the heat exchanger was supplied from an overhead tank. A heating tape was wound around the condensate return line to keep the condensate as close to the saturation temperature as possible.

B. Temperature Measurements

Nine thermocouple wells which consisted of three sets of three thermocouples each were drilled in the heat-transfer plate as shown in Fig. 7. One set containing three thermocouples was located at the centre of the 6 inch diameter plate. The second set of three thermocouples was positioned at 2/3 rd. of the radius of the copper plate and the third set was positioned at 1/3 rd the radius. All three thermocouples of one set were located directly beneath one another at exactly measured distances from the boiling surface. The nearest three thermocouples belonging to all three sets were situated at a distance of 3/16 inch below the boiling surface. The other two thermocouples of each set were located at a distance of about 0.76 inch and 1.30 inch respectively from the heat-transfer surface. The exact location of these thermocouples is given in Table 2 of Appendix I. The thermocouples were made from 24 gauge teflon taped glass braided copper-constantan wire and were sealed inside thin copper tubing before insertion

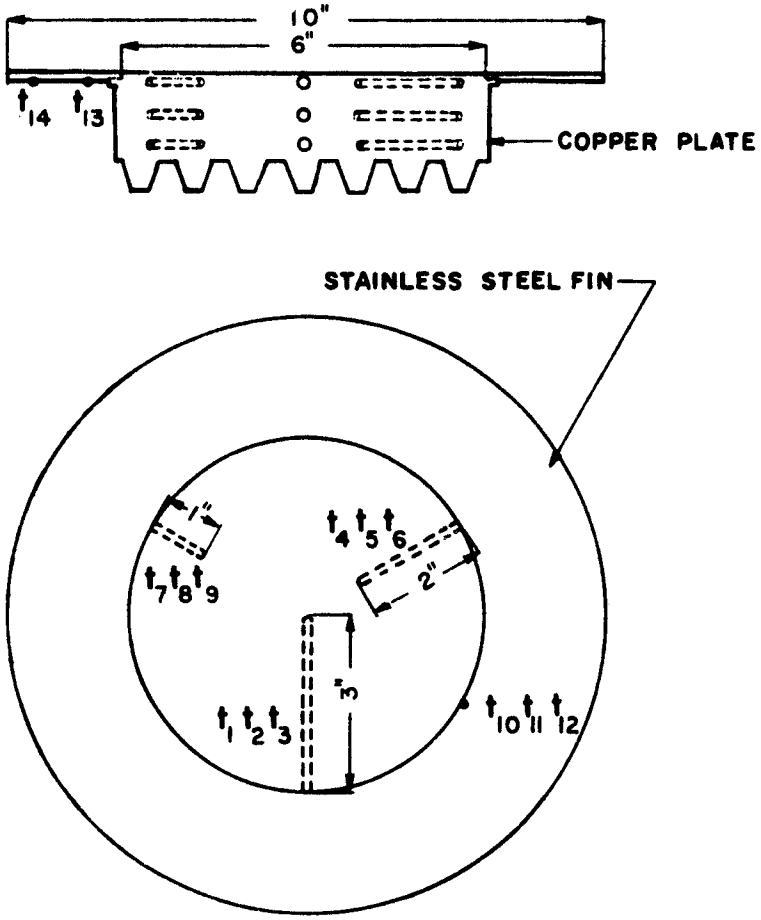

FIG. 7 LOCATION OF THERMOCOUPLES

into the thermocouple wells.

Three additional thermocouples were welded to the side edge of the copper plate and covered with a layer of 'Thermon' heat transfer cement in order to prevent their readings being affected by external convection currents. These thermocouples were useful to compute the temperature at the top edge of the copper plate where it was joined to the stainless steel skirt. Two more thermocouples spot-welded to the bottom of the stainless steel skirt aided the estimation of heat loss through the skirt. Temperature measurements were made on a Leeds-Northrup type K potentiometer and were also intermittently recorded using a Philips 12-channel temperature recorder. Details of computation using these measurements are illustrated in the later chapters.

C. Electroplating

1. Selection of the Method

To elucidate the role of surface grains on boiling heat transfer required a suitable technique of surface preparation in order to produce heat transfer surfaces of widely different grain sizes. Commercially available samples of electrolytic cooper and other non-ferrous metals usually encompass very limited range of grain sizes. A technique which seemed to have considerable merit for this purpose was electrodeposition. Previous investigations (B_7,L_4,B_{11}) made in the field of electrodeposition have shown that the structure of electrodeposits is influenced by various conditions which pertain to the electrolysis. As a result of these works there is enough evidence to indicate that the grain

size can be varied over a tenfold range for plated metals such as copper. The plated layers with various grain sizes could be obtained by changing one or more of the variables during electrolysis. The properties involved were current density, temperature, acidity or p_H, cathode potential, concentration of the metal ion, agitation, addition agents, presence of other ions, and condition of the surface of the base metal.

Current density seemed to have appreciable effect on grain size and yielded to easier manipulation (B_7,B_{11}). Therefore all the other quantities were kept constant and current density alone was varied for electrodeposition in order to get deposits of different grain size for each boiling run.

Two sets of experiments were conducted, the first set with copper plating on the heat transfer surface at different current densities and the second set with nickel plating. The second set of runs was not as exhaustive as the first set of runs. However, the trend of the experimental results were observed to be the same for both sets as illustrated in later chapters. A few additional experiments with chromium and brass plated surfaces were carried out; however in these cases the metal deposition was done by commercial electroplaters.

2. Arrangement of Plating Bath

The electrodeposition on the copper plate was conducted inside a tank of dimension 15 in. by 15 in. by 15 in. made of a 0.5 inch thick epoxy phenolite sheet. This material, in addition to its easy machinability, was found to be chemically resistant to the plating

solutions used and water tight joints were readily made by cementing the surfaces with an epoxy cement. The tank was filled with about 25 litres of plating solution.

The anode and the cathode were placed vertically into the square electrolytic tank and were supported by the two opposite side walls. These electrodes were connected to the electrical circuit by insulated lead wires with the help of copper clamps. An A.C. to D.C. rectifier unit with built in voltmeter and ammeter constituted the power source for electroplating. All surfaces of the cathode except the front boiling surface were prevented from coming into contact with the plating solution by a coating of masking paint or stop-off lacquer. After the plating was completed, the masking paint was stripped off the surfaces using a solvent 'microstrip A'.

The temperature of the electrolytic bath was controlled by circulating water from a constant temperature water bath through glass coils immersed in the plating tank. Proper mixing of the tank during electrolysis was ensured by a constant speed stirrer.

3. Preparation of the Cathode Surface

It was an essential requirement to obtain an adherent, fairly smooth, flat deposit of sufficient thickness on the cathode, which later formed the heat transfer surface for boiling experiments. To facilitate this, the treatment of the cathode surface was carried out systematically with great care. To ensure the reproducibility of the base surface, the cathode surface was polished successively with emery papers of No. 2,1,0

and 00 grades and then buffed. Further treatment of the electrode surface for electrolysis was similar to the procedure followed by Gauvin and Winkler (G_2) and is described below.

The electrode was degreased in benzene and washed with distilled water. Later it was etched for a few minutes in a solution containing 435 ml. per litre of concentrated sulfuric acid and 72 ml. per litre of concentrated nitric acid and washed again in distilled water before mounting in the plating bath. The thermocouple wires were not removed from their wells in the copper plate during deposition; however they were protected from the attack of the electrolyte by an additional layer of plastic tape wound over the portions of the wires which were submerged in the solution. The electroplating was usually carried out for several hours until the plated layer was of sufficient thickness. In the case of copper deposition, the thickness of the plated layer averaged about 0.003 inches. The nickel deposits were about 0.001 inches thick.

4. Control of the Bath

As long as a good deposition was obtained on the cathode surface, rigid control of the bath was considered unnecessary. However, care was taken to maintain the purity, composition and acidity of the plating solution. At intervals the electrolyte was filtered and the composition was measured by volumetric methods and adjusted. The pH values were determined at room temperature with an automatic pH meter and glass electrodes and adjusted frequently by the addition of small amounts of sulphuric acid to the electrolyte.

5. Copper Deposition

The anode for copper plating was a 0.5 inch thick by 9 inch diameter circular copper plate of 99.99% purity supplied by Noranda Copper and Brass Company.

The plating solution consisted of 125 gm. of reagent grade copper sulphate and 50 gm. of Analar concentrated sulphuric acid per litre. The acidity of the copper electrolyte remained practically constant during deposition. The electrolyte was discarded completely and replaced with fresh solution only once during the course of the present experiments.

The current density used for copper plating ranged from 5 amp/sq.ft. to about 40 amp/sq.ft. prior to final electroplating standard surface characteristics were imparted to the cathode as recommended by Gauvin and Winkler (G_2) by electroplating for about an hour at a current density of 2 amp/dm^2. The establishment of such a steady state cathode surface ensured that the surface structure of the base metal is not perpetuated or reproduced in the fresh deposit.

6. Nickel Deposition

The nickel anode was a thin sheet of nickel 200, 12 inch by 6 inch by 0.062 inch, supplied by the Huntington alloy products division of the International Nickel Company.

The nickel plating solution was of the Watt type containing 300 gms. of $NiSo_4 7H_2O$, 60 gms. of $NiCl_2 6H_2O$ and 38 gms. of H_3BO_4 per litre and was operated at a pH of about 5 at 35°C (B_7). After dissolution of

the chemicals, the nickel plating solution was treated with activated carbon and filtered before use. A cotton anode bag was found to be advantageous to hold back excessive amounts of loose anode particles generated during deposition. An addition, once a day of one part of 30% H_2O_2 per 2000 parts of electrolyte was helpful in preventing hydrogen pitting.

The current density for the electrodeposition of nickel varied from about 40 amp/sq.ft. to 65 amp/sq.ft.

7. Treatment after Electrodeposition

Following electrodeposition, the cathode copper plate was removed from the electrolyte, the masking paint layers were stripped off completely and the plate was washed in distilled water followed by a rinse of distilled water. In the next step, the electroplated heat transfer surface was polished with silicon carbide papers of 240, 320, 400, and 600 grits mounted on a power operated hand grinder and then buffed on a buffing wheel. Afterwards the surface was washed successively in hot distilled water and acetone and dried. The above treatment was found to protect the surface from atmospheric oxidation for extended periods.

8. Roughness Measurements

Surface roughness measurements were made on the heat transfer surface using a profilometer, an instrument commonly used for such measurements. The diamond tip of the instrument made a to and fro motion along a line on the surface which was interpreted and recorded by the instrument as the roughness in terms of root mean square (rms) value in micro inches.

For surfaces treated carefully as described previously, the average roughness, which was computed as the mean of five measurements in each direction of the surface, never exceeded 3 microinches rms, and in most cases it was around 2.5 microinches. Profilometer measurements made on the surface after boiling had taken place indicated an increase in roughness to a maximum of 5 microinches rms. This increase could be attributed to a slight scaling of the surface which occurred during boiling.

D. Experimental Procedure for Boiling Runs

Before a boiling run was started, the helical contacting grooves of both the heater proper and the heat transfer plate were ground with emery papers to remove all metallic oxides left from previous runs. This procedure was carried out to ensure good thermal contact between the two contacting faces. The glass boiler was then bolted to the top of the heat transfer surface and connections to the steam condenser were made. The distilled water used in the boiling runs was degassed by heating it to the boiling temperature in a separate still and then filtered through a micropore filter of size 10 Mμ. Four litres of this water was transferred to the boiler. Power to the heaters were switched on and increased gradually to the upper value below which the boiling was to be conducted. The boiling was allowed to take place for an initial period of three hours until steady state is reached before the first set of readings were taken. One set of readings consisted of measuring all the thermocouple readings, voltmeter and ammeter readings, boiling

temperature and manometer pressure readings, the coolant inlet and outlet temperature readings and its flow rate. The power input to the heaters was decreased in steps at intervals of 45 minutes and readings were taken. Preliminary runs showed that an interval of 45 minutes between power changes was sufficient for the boiling to stabilize and for the thermocouples to reach thermal equilibrium. Once readings had been taken at the lowest heat flux, the boiling run terminated, the top portion of the apparatus was dismantled and the heat transfer plate was removed to facilitate further treatment.

E. Estimation of Grain Size Distribution

1. Selection of Method

The next step consisted of estimating the grain size distribution of the boiling surface. Developing a suitable procedure for determining and expressing the grain size of the deposited metal on the heat transfer surface presented several problems. The large size of the plate presented itself as a distinct barrier to the adoption of the usual metallographic tools for the grain size determination. In the usual metallographic practice (K_2), a small metal specimen of size 3/4 to 1 inch in cross section is embedded in a circular bakelite mold to facilitate easier handling during polishing and etching procedure. In addition such a small specimen can be easily placed on the viewing stage of the laboratory microscopes, thus eliminating any vibration during observation through the microscope. The size of the plate in the present experiments precluded the adoption of any such convenient technique. However

the timely availability on the market of a portable polishing unit 'portamet' and a portable 'unitron' depth measuring Rollscope reduced the difficulties to a great extent.

The 'portamet' polisher consisted of a vertically mounted motor supported on adjustable tripod legs. A rubber disk holder whose shaft was rotated from above by the motor moved in a horizontal plane. Smaller circular abrasive disks of varying grit sizes, pasted to the bottom surface of the rubber disk holder produced the desired abrasive action on the surface. The resultant effectively polished area was approximately 1 inch in diameter. The three legs of the portamet could be positioned directly on the heat transfer surface and polishing could be done at the desired spot.

During observation of the grain structure, the microscope could be placed directly above the polished spot on the heat transfer surface, being supported on its two feet. As long as the copper heat transfer plate was held firmly on a table, the microscope remained free from the deleterious effects of vibration during visual observation and photomicrography. The microscope contained a built-in mechanism for photomicrography. A camera coupling tube with attached projection lens was received as standard equipment. A 35 mm. 'Cannon' camera back loaded with a film cartridge was screwed on to the coupling tube and photographs of the grain structure of the metal surface was taken whenever desired.

To obtain clear vision of the grain structure for counting, a polishing and etching technique was developed after considerable practice and with continual observation of a number of important precautions.

2. Grinding and Polishing Procedure

The purpose of the grinding and polishing operations was to secure a small area of flat, mirror-like spot on the heat transfer surface and at the same time to leave the metal under that spot as nearly as possible in its original, undisturbed condition. The following procedure was followed to obtain the above objective (B_{12}).

The portable polishing unit was positioned on the surface and its tripod legs were adjusted so that the unit was perfectly level. Fine grinding of a spot on the surface was carried out by using successive abrasive disks of 320, 400 and 600 grits attached to the rubber portion of the abrasive pad holder with water as lubricant. When grinding with one abrasive disk was completed and before proceeding with another disk, the polished spot was thoroughly washed in running water. The orbital path of the abrasive disks produced a polished area of about 1 inch in diameter.

The final polishing operations were done for the purpose of removing any scratches introduced during previous grinding and to ultimately produce a uniformly polished scratch-free surface. In this operation, a gamal polishing cloth disk was fixed to a sponge rubber disk holder and used with two grades of alumina as polishing medium. Water suspensions of alpha alumina with an average particle size of about 0.3 micron and the gamma modification of alumina of uniform particle size of less than 0.1 micron were used.

When the final polishing operations were completed, the

COPPER PLATED SURFACES

Etched and Viewed through Microscope

Sample 1: Magnification 200x

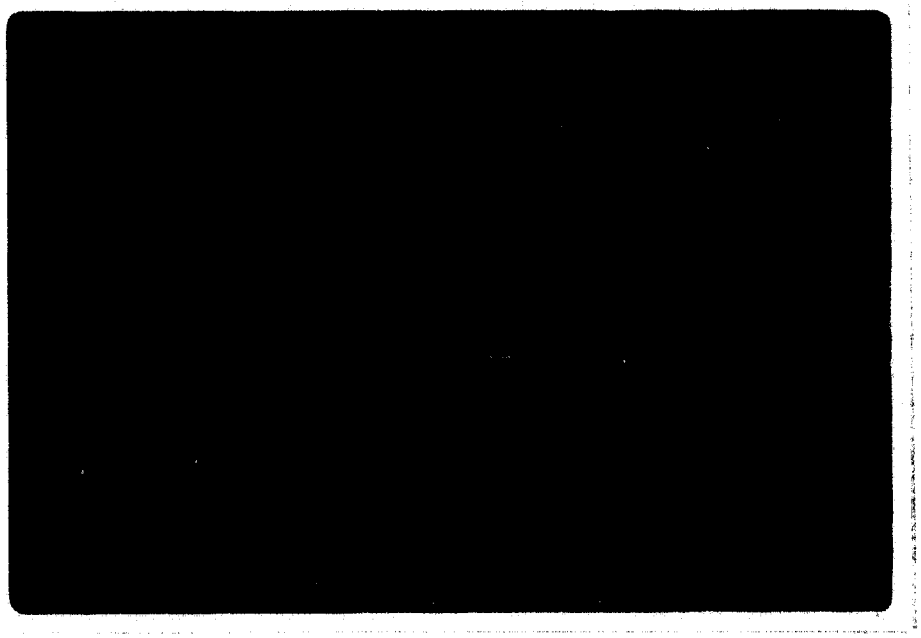

Sample 2: Magnification 400x

FIGURE 7a

specimen was thoroughly washed in running water, swabbed with water-wet cotton to remove the last traces of clinging abrasive and finally rubbed with trichloroethylene and dried in a warm stream of air.

3. Etching Technique (K_2)

The purpose of etching was to bring about contrast between the grain structure of the plated surface by suitable chemical attack of the polished spot. For deposited copper metal, several etchants were tried before selecting a satisfactory reagent which was composed of 5 parts of ammonium hydroxide, 5 parts of distilled water and 3 parts of 3 per cent hydrogen peroxide. An etchant was made up and used immediately because of its tendency to deteriorate rapidly. The etchant consisting of 50 ml. of concentrated nitric acid and 50 ml. of glacial acetic acid was found to be suitable for nickel plated surfaces.

During etching, the reagent was swabbed on the surface of the polished spot with a tuft of cotton. Etching time varied anywhere between 10 seconds and 60 seconds. At times the etching procedure had to be repeated on the same spot a few times before a high quality etched structure characterized by a certain brilliance could be obtained. This exhibited delicate contrasts between the grains when viewed under the microcope as seen in the photomicrographs (Fig. 7a).

After treating the surface with the etching solution for the required length of time, the etched spot was immediately washed with tap water and then with distilled water. Finally it was rinsed with alcohol and dried carefully in a stream of hot air from a hair dryer.

The specimen was then ready for microscopic examination.

4. Determination of Grain Size

To quantitatively characterize the grain size of the deposited metal, a method was selected, which due to its simplicity had been found particularly useful by investigators (B_{11}, K_2) for alloys and non-ferrous metals. The method referred to as the Intercept method consisted of determining by count, at some appropriate magnification, the number of grains intercepted by a line engraved on the eyepiece of the microscope. The arithmetic average of five or six counts of grains were taken by rotating the eyepiece and positioning the line along the bisectors. Knowing the actual length of the line and the magnification, the grain size could be expressed as the average number of grains per linear unit i.e., grains per inch or grains per millimeter. In the present experiments the grain determinations were made at three or more different polished spots for each run and an overall average value of grains per linear length was computed.

CHAPTER V

EXPERIMENTAL RESULTS

The experimental data taken on electrodeposited surfaces of copper, nickel, chromium and brass in this boiling investigation were tablulated as shown in Table 3, of Appendix I. The temperatures indicated by the three sets of thermocouples are t_1, t_2, etc. up to t_9. The locations of these thermocouples were measured accurately from the sides and the top surface of the copper plate and recorded in Table 2. Appropriate corrections were made during every run to include the thickness of the electrodeposited metal layers.

The temperature at the top edge of the copper heat transfer surface was computed from the readings of three thermocouples t_{10}, t_{11}, t_{12} which were welded to the side edge of the copper plate. For the same power input these thermocouples were found to show virtually constant readings in the experiments as verified by several repeated measurements. During electrodeposition these thermocouples when left in place, were liable to constant attack by the plating solutions. Their locations were also a source of inconvenience during machining on the lathe for the removal of plated layers between runs and therefore these thermocouples were removed during later runs. The readings of t_{10} to t_{12} are tabulated in Table 4 along with the corresponding power inputs. The temperatures of the stainless steel fin were measured by means of two additional thermocouples t_{13} and t_{14} welded to its bottom and are recorded in

Table 6. The exact locations of all the thermocouples are given in Table 2.

To calculate the net heat input Q to the boiling liquid the following procedure was adopted. First the total heat loss was computed. This involved the radial heat loss through the heavy 4 inch thick thermal insulation around the heater block and the loss through the stainless steel fin. In order to estimate the heat loss through the insulation, the method described by Kurihara (K_4) was followed as below: cold water at tap temperature was fed to the glass boiler at a known rate and drained out at the same rate. The heaters were switched on and raised to the maximum heat input. Even after three hours of heating, the temperature rise of the outer insulation was found to be negligible. However, when water in the boiler was heated by an immersion heater, within a short time there was an appreciable temperature rise of the heater enclosure indicating that it was being heated chiefly by transfer of heat from the boiling liquid through the fin and not by radial conduction from the heater block.

After having thus determined that a significant portion of the heat loss was through the stainless steel skirt, the problem was approximated to that of heat dissipation through an annular fin of uniform thickness when heat is received through one of its edges whose temperature is known and transmitted on one side to water at boiling temperature and on the other to air at room temperature. The above problem has been solved previously mathematically (M_7). The details of computation for the heat loss from the fin using this solution have

been given in Appendix II. The net heat input 'Q' to the boiling liquid through the heat transfer surface was then equal to the total heat input to the heater minus the heat loss through the fin. The heat loss ranged from about 3 per cent at high heating rates to slightly more than 30 per cent at very low values of heat flux as shown in Table 7.

The temperatures at the surface of the copper plate were calculated by simple linear extrapolation of the four sets of temperature obtained from thermocouple readings. Fig. 8 shows the surface temperature distribution of a typical run from which one can observe the variations in the surface temperatures which are higher in magnitude at high heat fluxes and much lower at low heat fluxes. This variation was unavoidable in the experiments due to the large size of the copper plate used and the design features of the heater employed. However efforts were made to reduce the variation as far as possible and increase the reproducibility of thermocouple measurements by thoroughly cleaning both the meshing faces of the copper plate and the heater block between runs and fixing the plate in the same position on the heater in every run.

The equation for heat transfer in boiling can be expressed as

$$Q = hA\Delta T \tag{43}$$

A single value for ΔT cannot be used in Eq. (43) because of the variations observed in the surface temperature. Expressing in terms of a small differential element dA, Eq. (43) becomes

$$dQ = h\Delta T\, dA \tag{44}$$

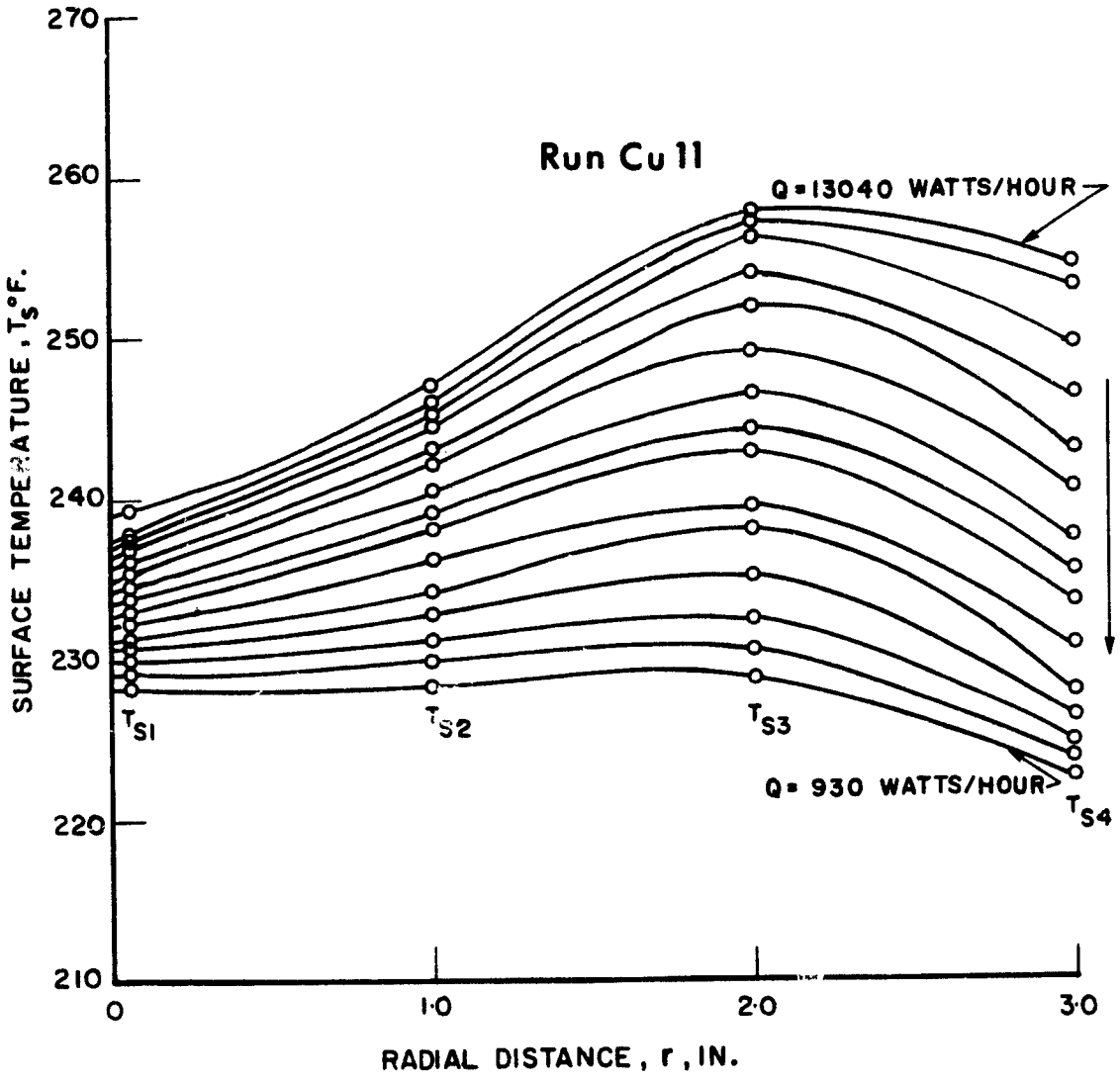

FIG. 8 SURFACE TEMPERATURE DISTRIBUTION

Integrating Eq. (44) over the whole area of the heat transfer surface,

$$Q = h_m \int_o^A \Delta T \, dA \tag{45}$$

where h_m is the mean boiling coefficient. If the mean temperature difference ΔT_m is defined as

$$\Delta T_m = \frac{\int_o^A \Delta T \, dA}{A} = \int_o^1 \Delta T d\left(\frac{r}{r_o}\right)^2 \tag{46}$$

then

$$Q = h_m A \Delta T_m \tag{47}$$

To obtain ΔT_m, values of ΔT vs $\left(\frac{r}{r_o}\right)^2$ have to be plotted as in Fig. 9 for every set of readings and graphically integrated. This procedure was rather time consuming whereas a numerical integration method using the digital computer yielded results of good accuracy and was found to be much simpler. Hence by the use of a numerical integration method, values of ΔT_m were calculated as illustrated in Appendix I and the results obtained were tabulated in Table 5 and 7. An error analysis carried out on the experimental measurements is reported in Appendix III. This yielded an estimate of errors as follows:

	Q/A	ΔT_m	Grain Count
High heat flux (250000 Btu/hr.ft^2)	$\pm$1 %	$\pm$2%	$\pm$5 %
Low heat flux (11000 Btu/hr.ft^2)	$\pm$ 5%	$\pm$5%	$\pm$5 %

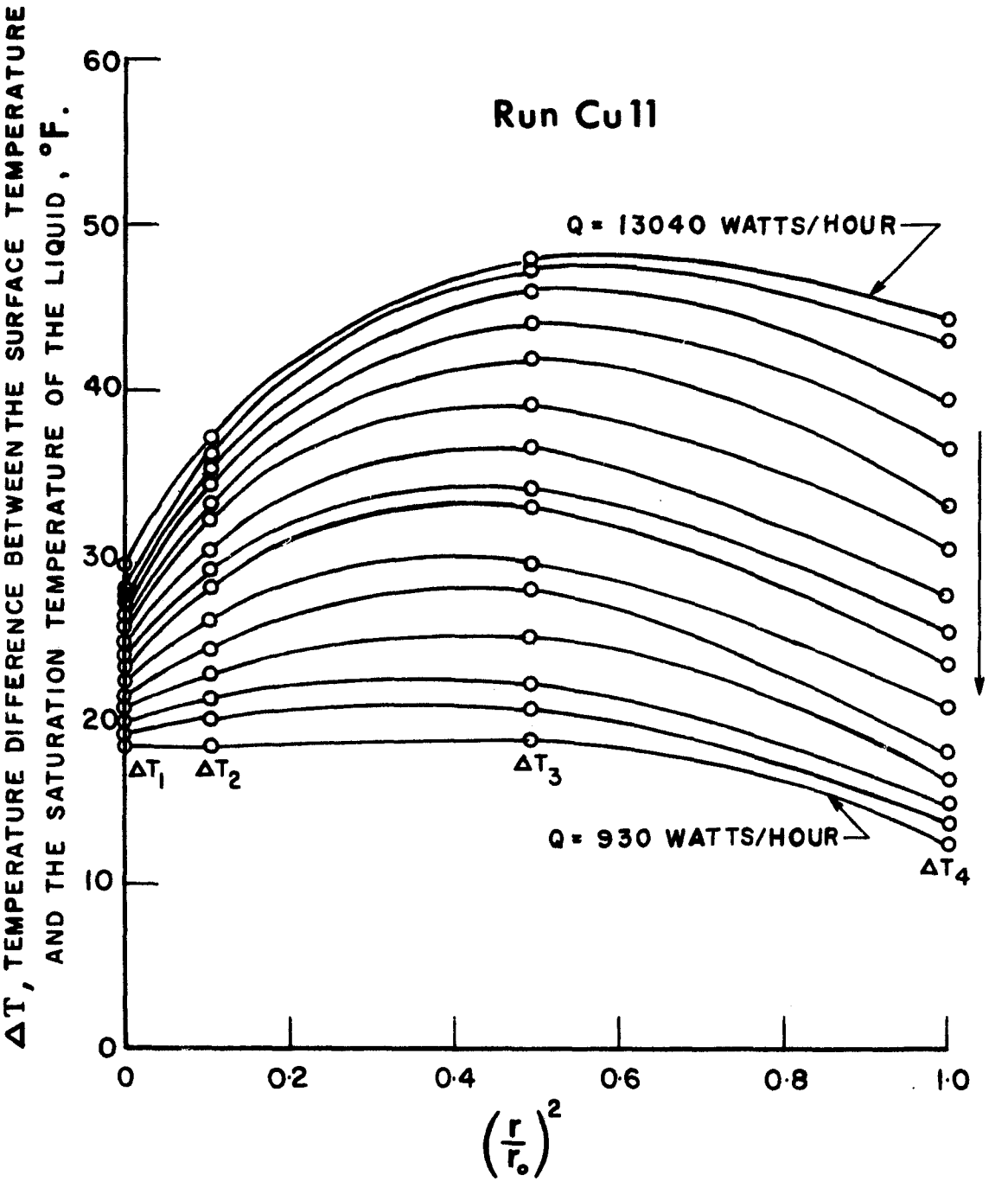

FIG·9 TEMPERATURE DIFFERENCE DRIVING FORCE
VS·
SQUARE OF RADIAL DISTANCE RATIO

CHAPTER VI

DISCUSSION AND CORRELATION

A. Discussion of Results

The experimental results obtained here were plotted on log-log paper as Q/A, the heat flux against ΔT_m, the difference between the mean surface temperature and the saturation temperature corresponding to the local pressure. These plots are shown in Figs. 10 to 22 for copper plated surfaces, 23 for nickel plated surfaces, and 24 and 25 for surfaces of brass and chromium.

The results of Runs Cu1 and Cu2 on copper surfaces are considered separately from those of the later runs because of the following reasons:

(i) In run Cu1, the freshly machine worked copper plate was used and subjected to heat transfer at high heat flux for the first time. Some unknown factors which are probably due to the internal realignment and reorientation of grains of the fresh copper metal when subjected to heat may have contributed to the observed shift in the Q/A vs. ΔT curve which is actually shifted downwards as compared to the second run on the same surface as seen from Fig. 10. The run carried out on the initial copper surface gave a comparatively higher value for the Rohsenow constant C_{sf} than the second run as can be seen from Table 9.

(ii) During runs Cu1 and Cu2, the power input to the heater was decreased stepwise and following an interval of half an hour the temperatures

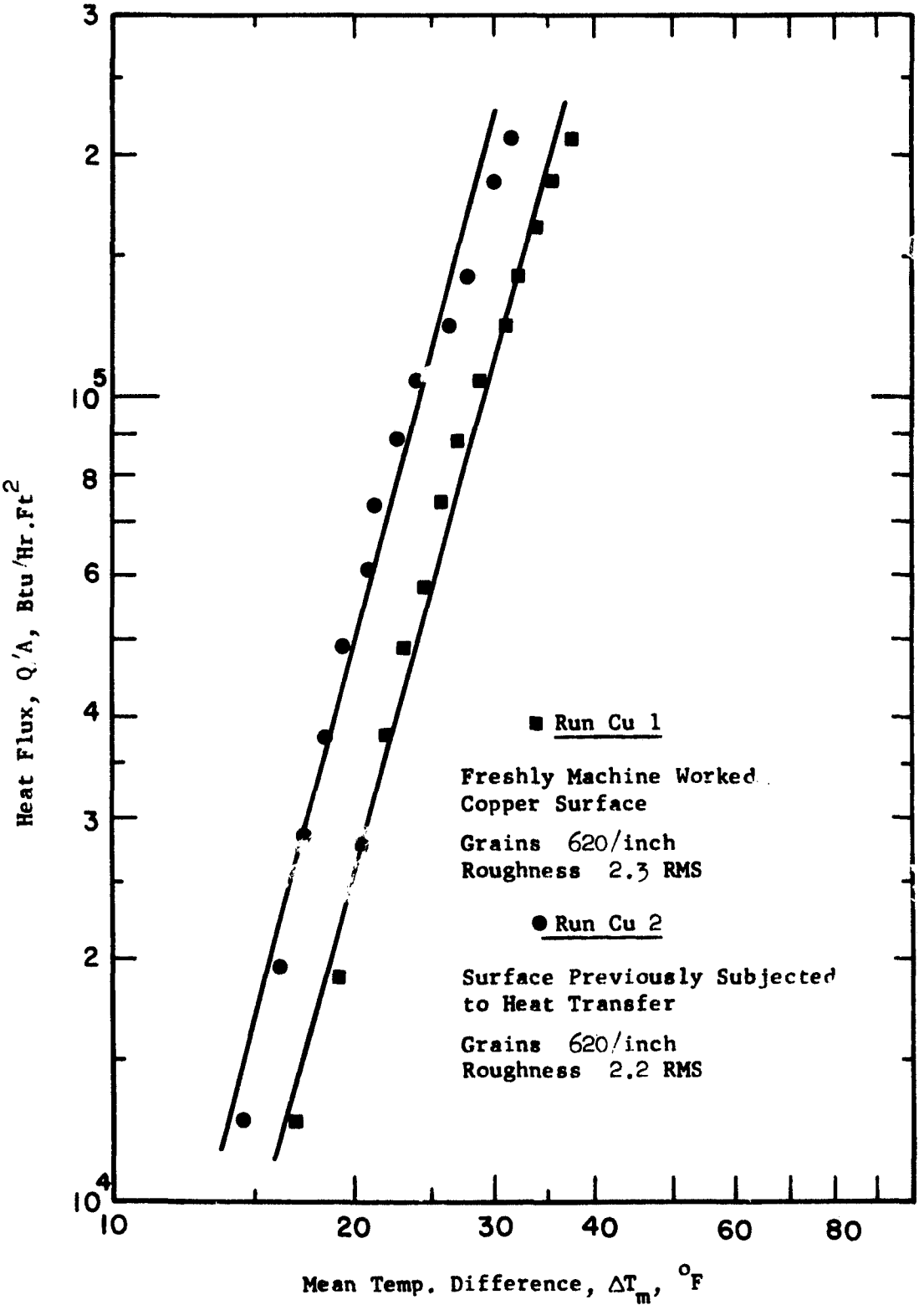

Fig. 10 Boiling Data for Water on Copper Surface.

were measured. This time interval was not quite sufficient for the thermocouple readings to stabilize. Therefore in later runs the interval between power changes was increased to 45 minutes and was adequate for the thermocouples to attain steady state temperatures.

After the two initial runs, subsequent runs were conducted on the heat transfer plate which had already undergone a few cycles of heating and cooling. The data for these later runs were found to be more consistent and reproducible.

Runs Cu 3 and Cu 5 were intended to determine the minimum roughness below which this parameter ceases to appreciably influence boiling from heat transfer surfaces. Once the minimum rms roughness was available the experimental surfaces could be treated and brought as close as possible to that roughness. This procedure would eliminate roughness as a parameter and ensure smooth surfaces of comparable roughness for use in the experimental runs. The rms roughness range studied was very limited and varied from about 2.6 micro inches to about 7 micro inches only. Repeated polishing and buffing operations carried out on the surface as described in the earlier chapter failed to produce surfaces smoother than about 2 to 3 micro inches rms so that no minimum roughness was established.

The results of runs Cu 3 to Cu 5 plotted together in Fig. 11 seem to follow the general observation of previous workers (B_6,C_3,K_4) namely a higher value of the slope of the curve of Q/A vs ΔT with increasing roughness. In other words an increase in heat transfer was observed with increasing rms roughness for the same temperature

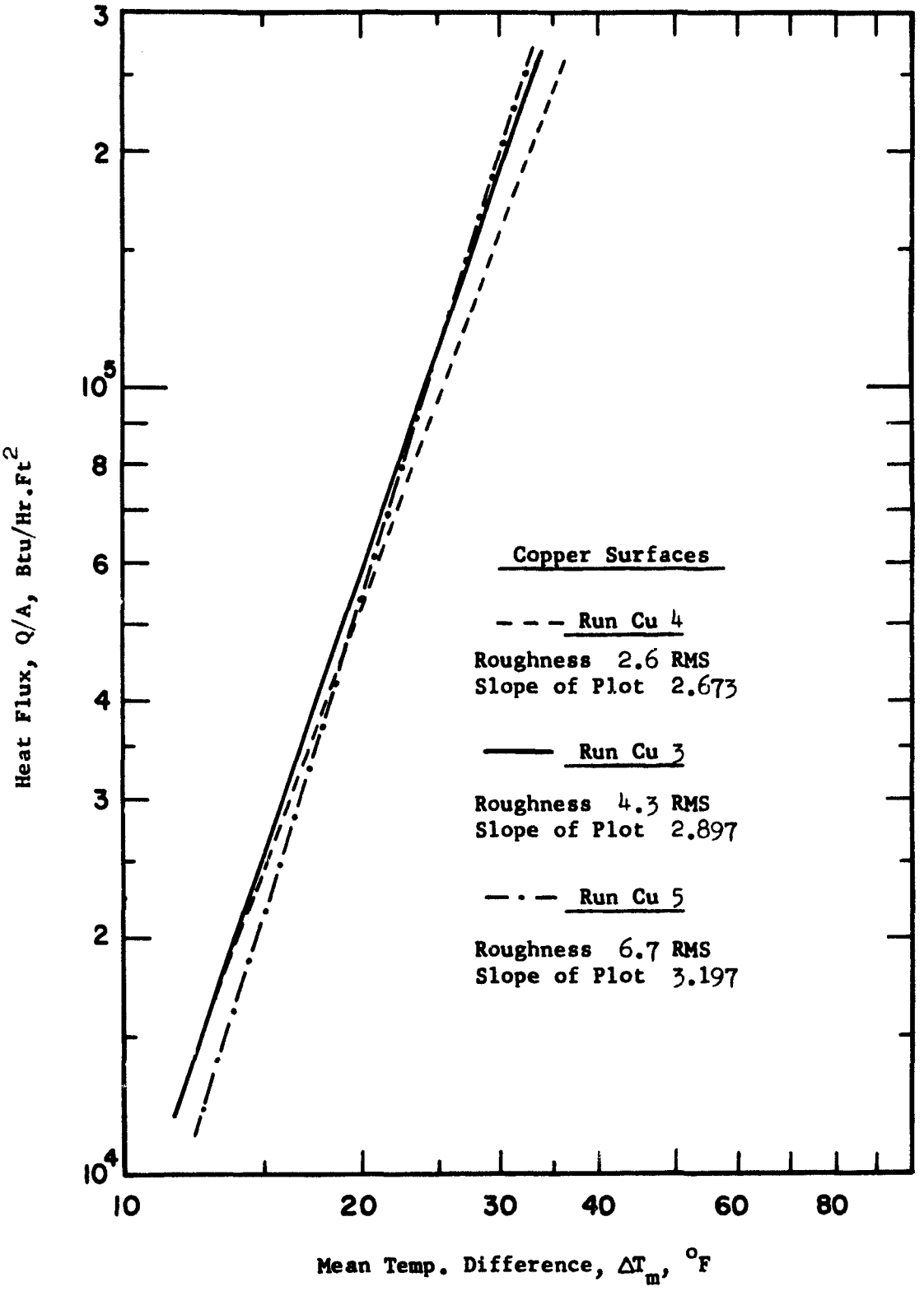

Fig.11 Boiling Data for Water on Copper Surfaces of Varying Roughness.

difference within the confined range of observation. It should be noted here that some research groups (B_6,V_1) have found the heat transfer to increase and subsequent y to decrease as the rms roughness is further increased. These changes in heat transfer have been attributed not only to the varying rms roughness but also to the surface preparation technique employed (V_1). It has also been suggested (B_6) that rms roughness is not the significant parameter in boiling because the 'rougher' surface with regard to boiling is that which has the greater number of cavities of appropriate size, regardless of the rms roughness. Since the present work was not particularly concerned with studying the effect of these factors on boiling, further investigation along this line to cover wider range of roughness was not carried out. Succeeding experimental runs were confined to exploring the role of surface g ains on boiling heat transfer with the notable exception of run Cu 10B which was devoted to finding the effect of aging. During these experiments the surface roughness was always brought to a value within 2 to 3 micro inches rms before starting a boiling run.

Four different metals namely copper, nickel, chromium and brass were studied for boiling heat transfer. As mentioned earlier, during each run one particular metal was electrodeposited on top of the copper surface. This constituted the actual heat transfer surface. During electroplating from conventional plating baths, the important variables, namely the composition of the plating solution, its pH value and its temperature were maintained at fixed values except for the current density which was varied for each run over the recommended

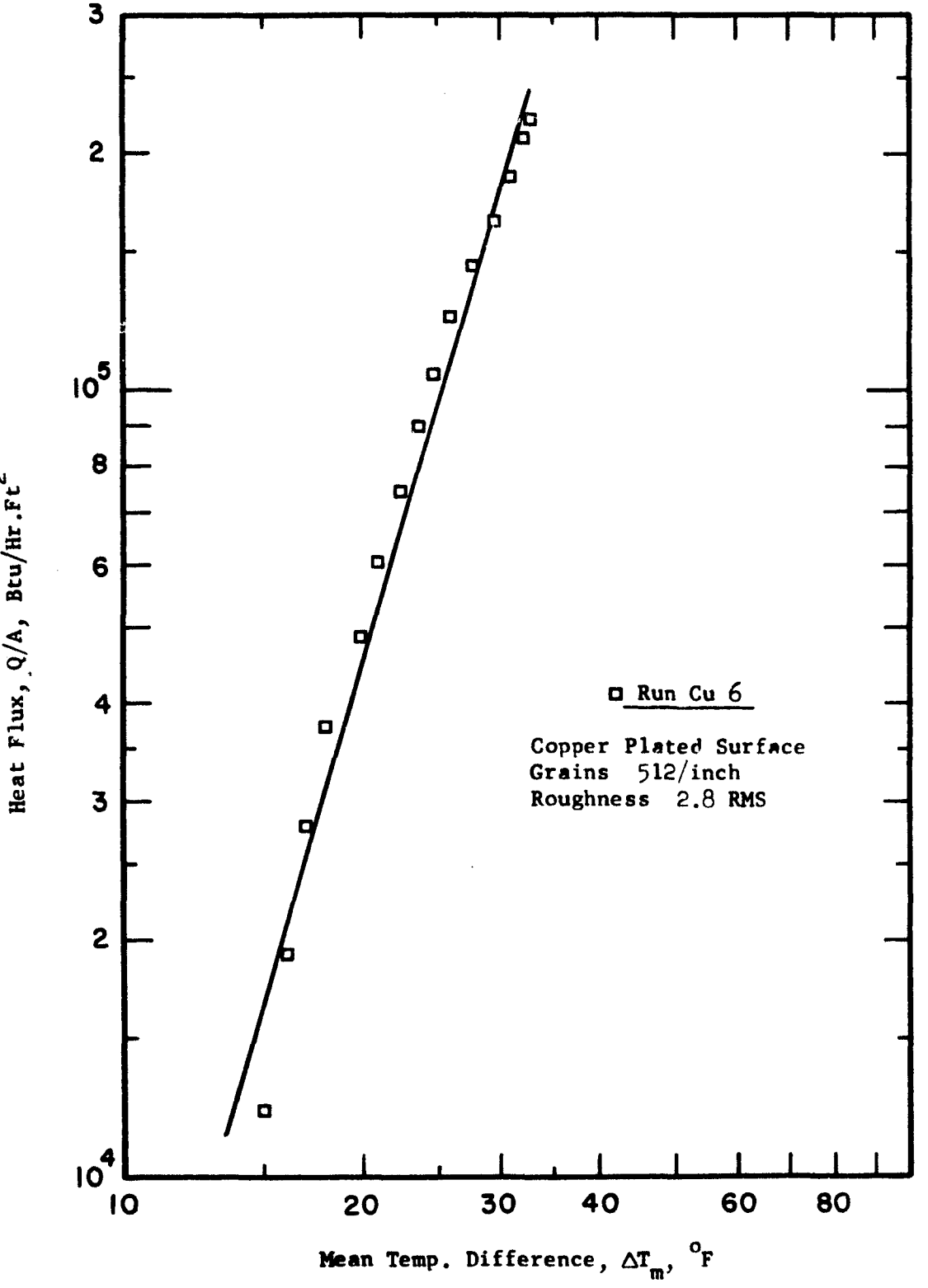

Fig.12 Boiling Data for Water on Copper Plated Surface.

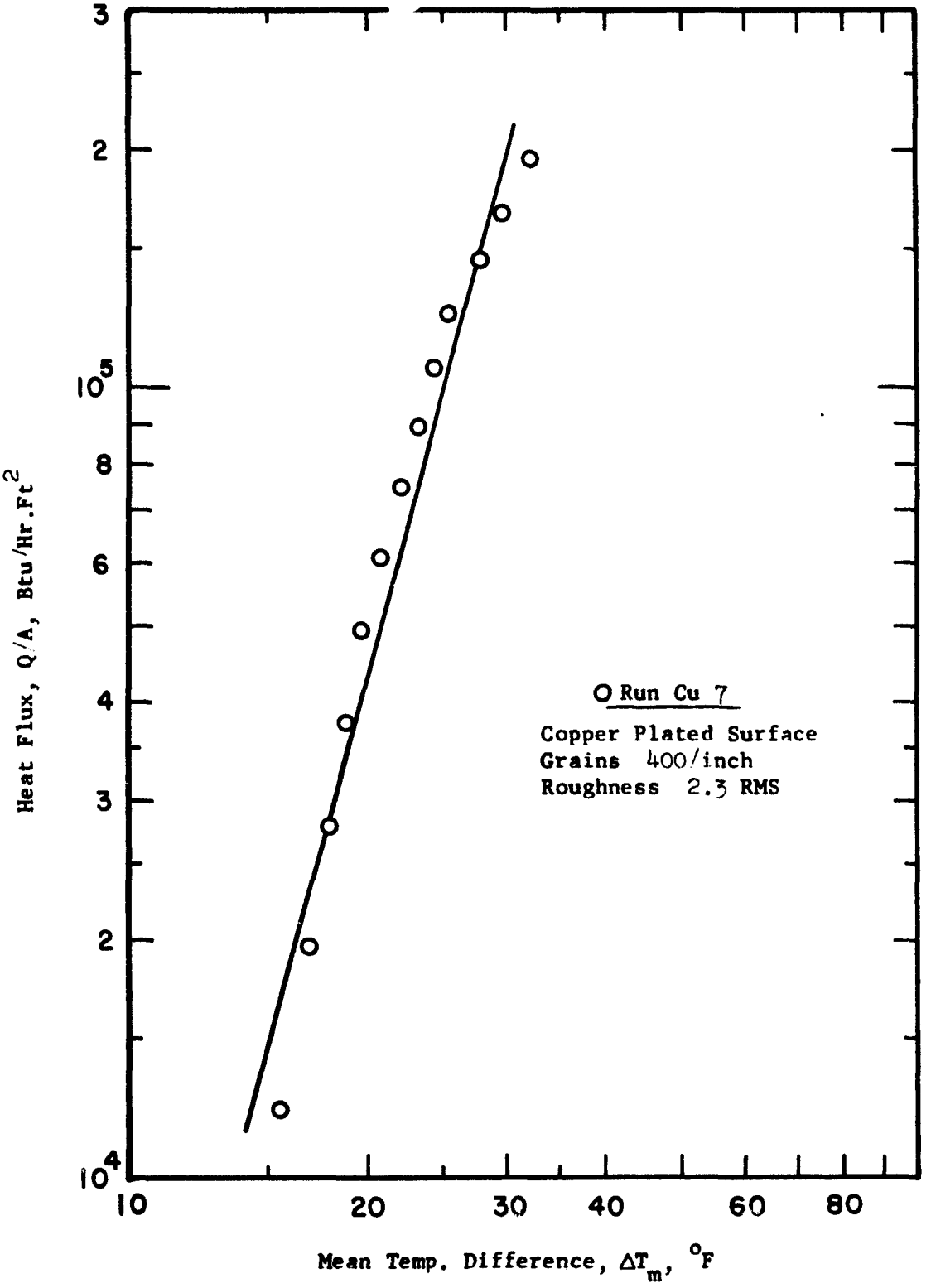

Fig.13 Boiling Data for Water on Copper Plated Surface.

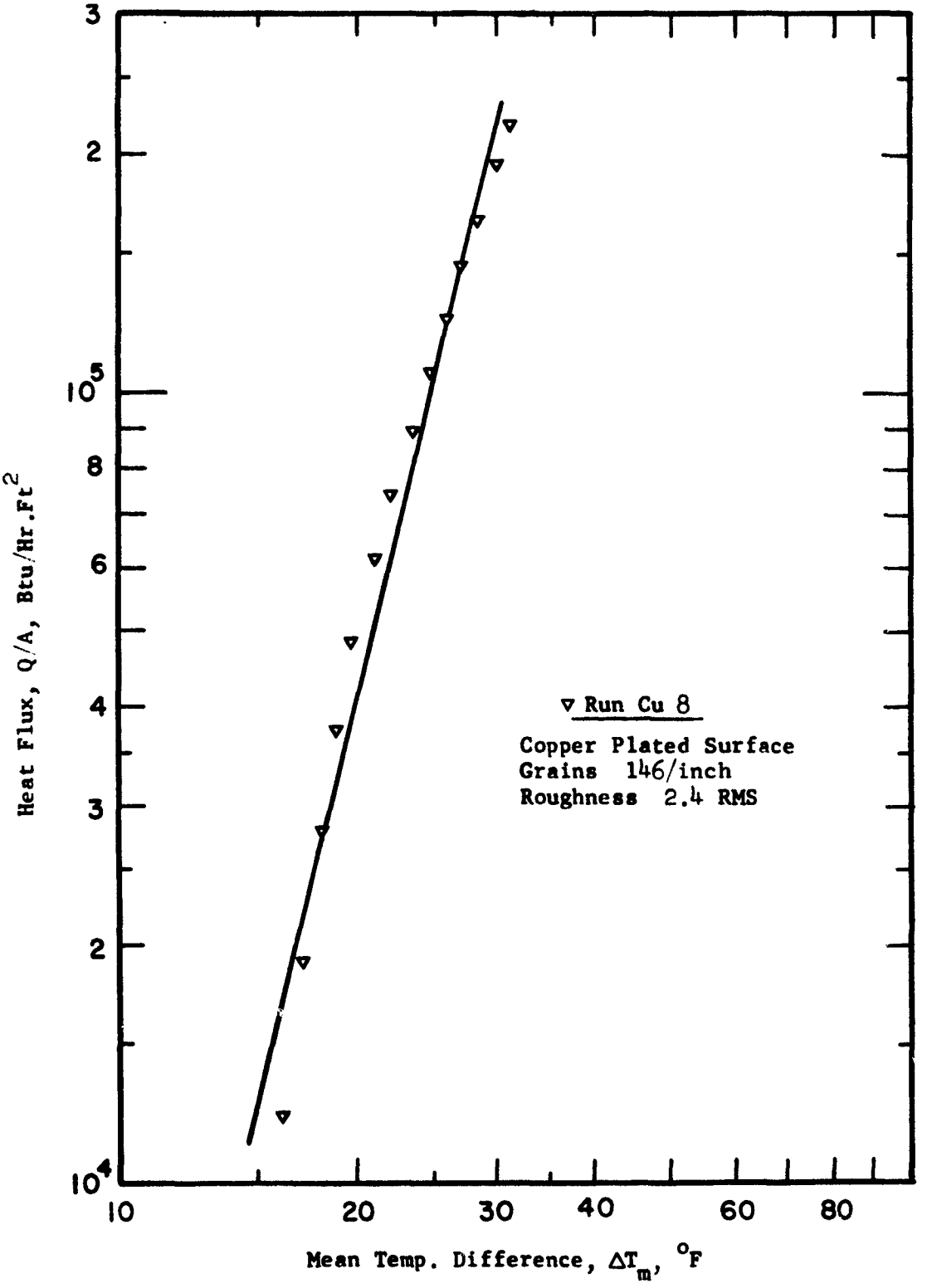

Fig. 14 Boiling Data for Water on Copper Plated Surface.

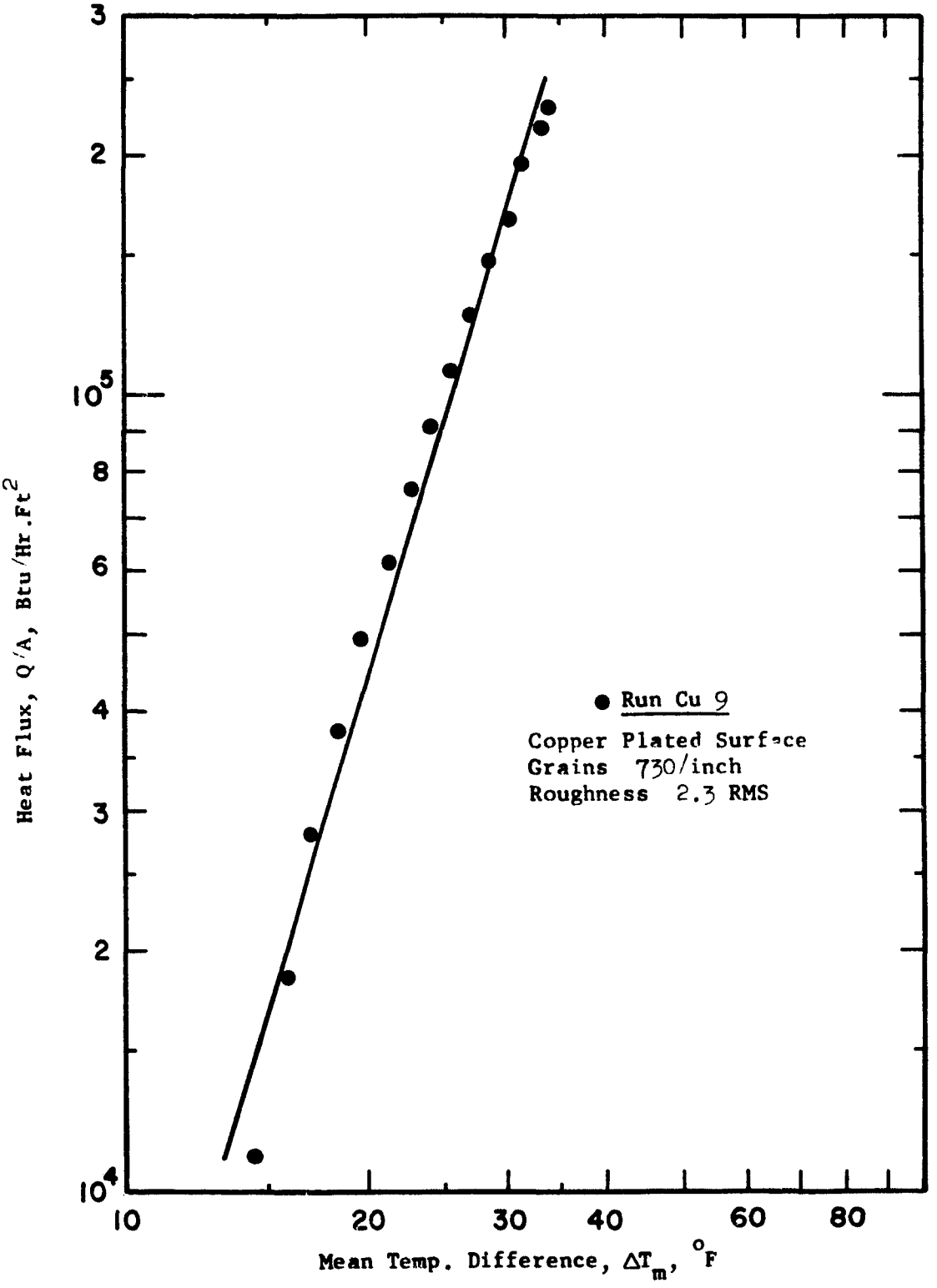

Fig.15 Boiling Data for Water on Copper Plated Surface.

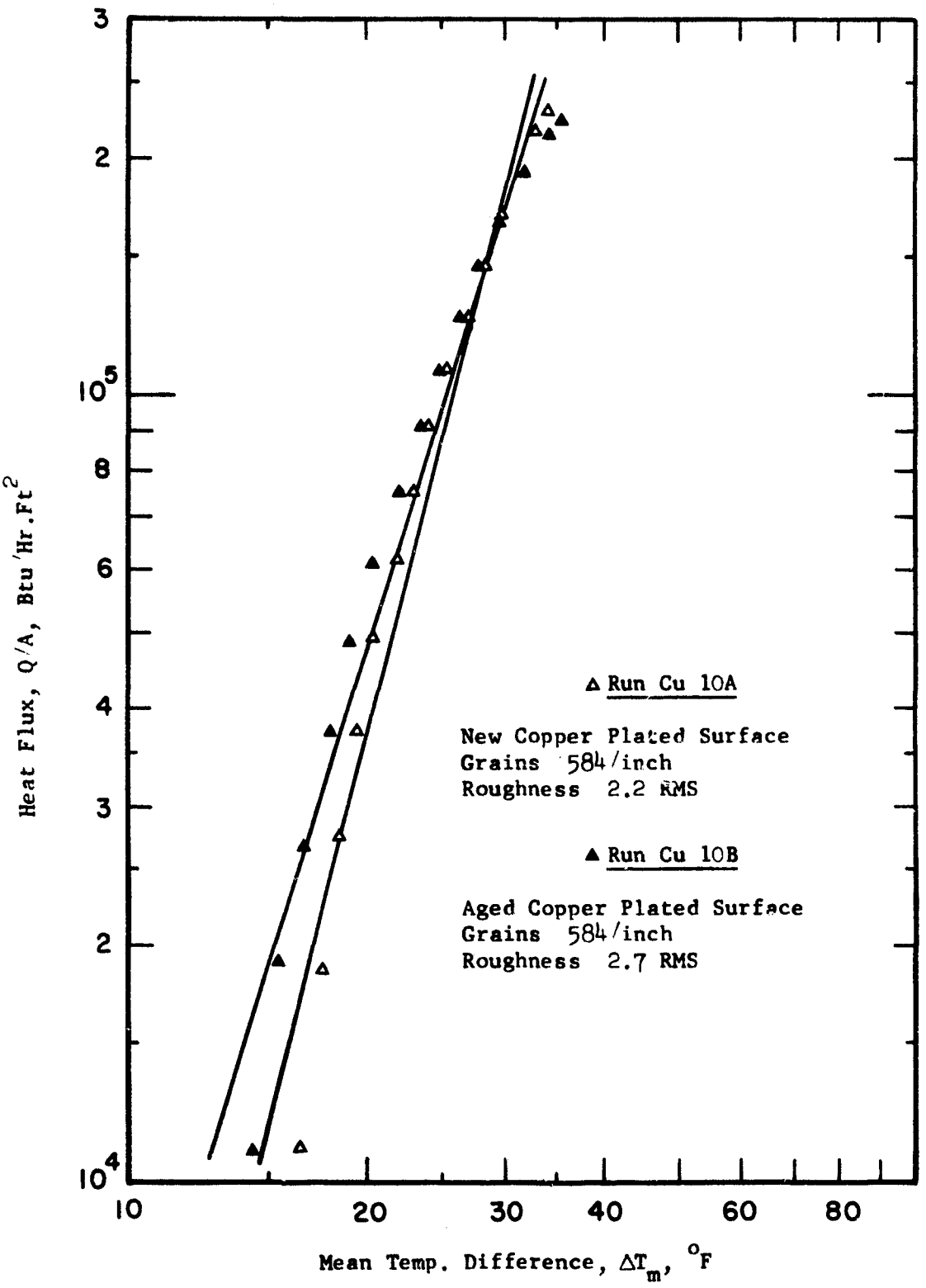

Fig.16 Boiling Data for Water on Copper Plated Surface.

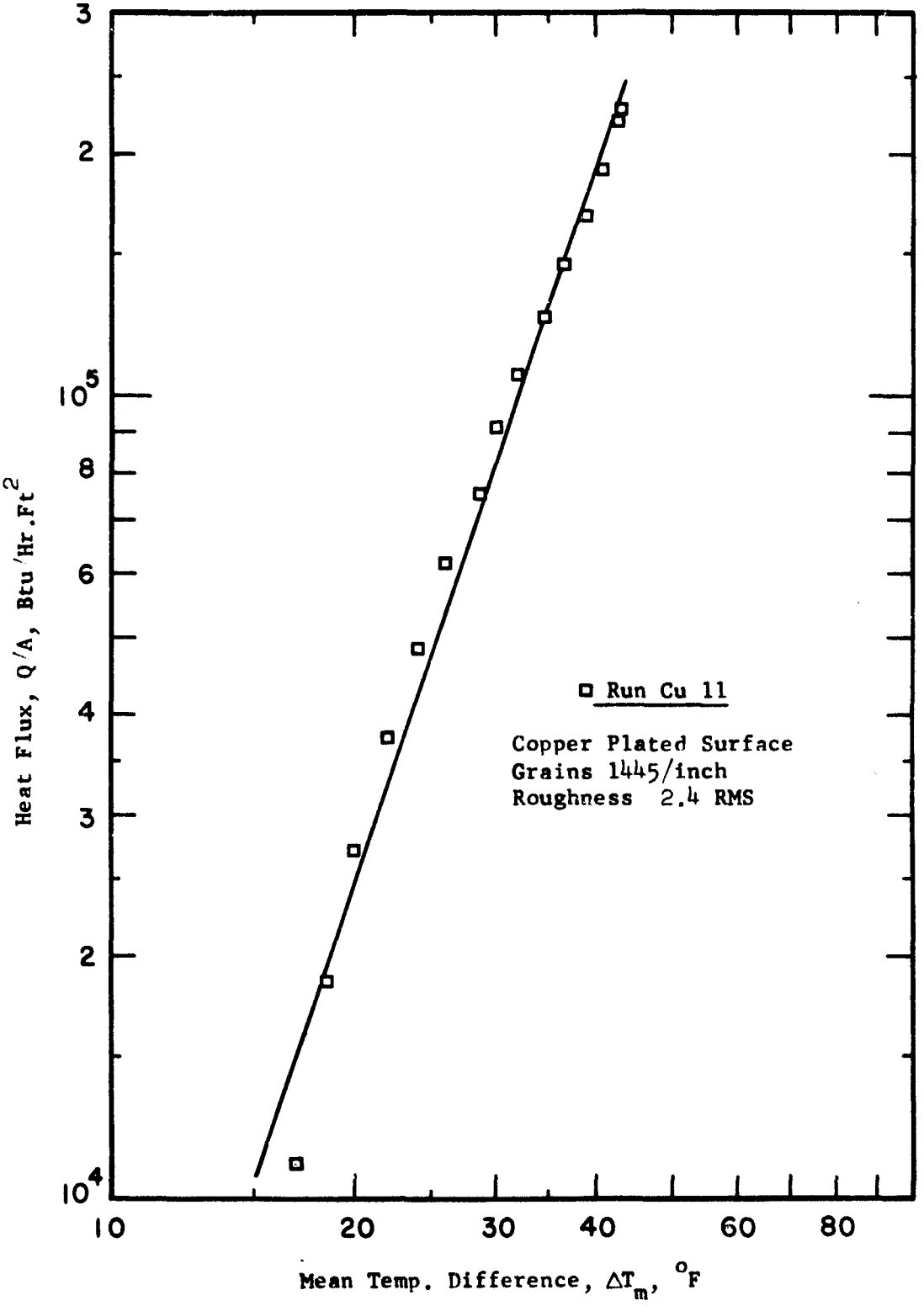

Fig.17 Boiling Data for Water on Copper Plated Surface.

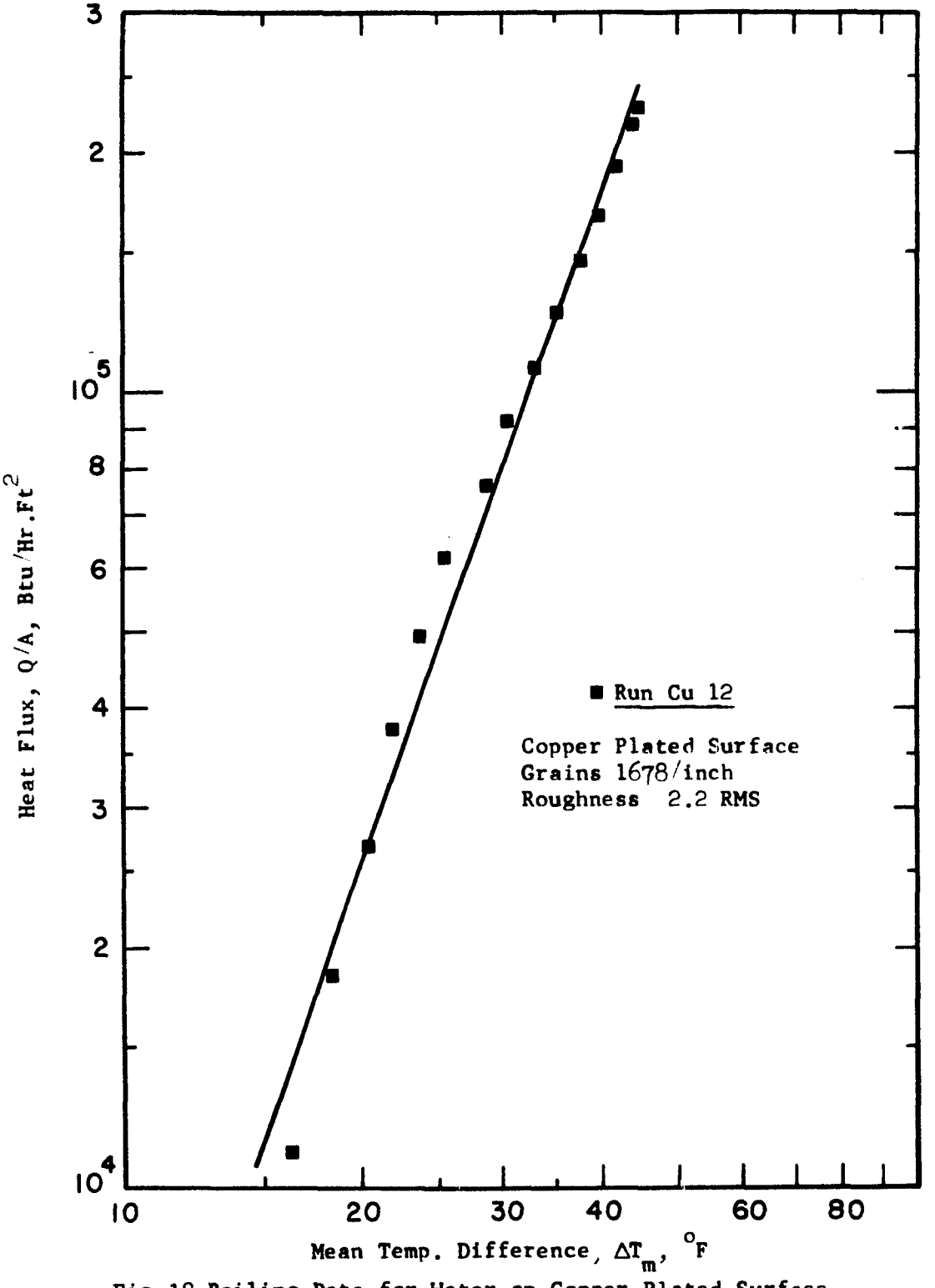

Fig.18 Boiling Data for Water on Copper Plated Surface.

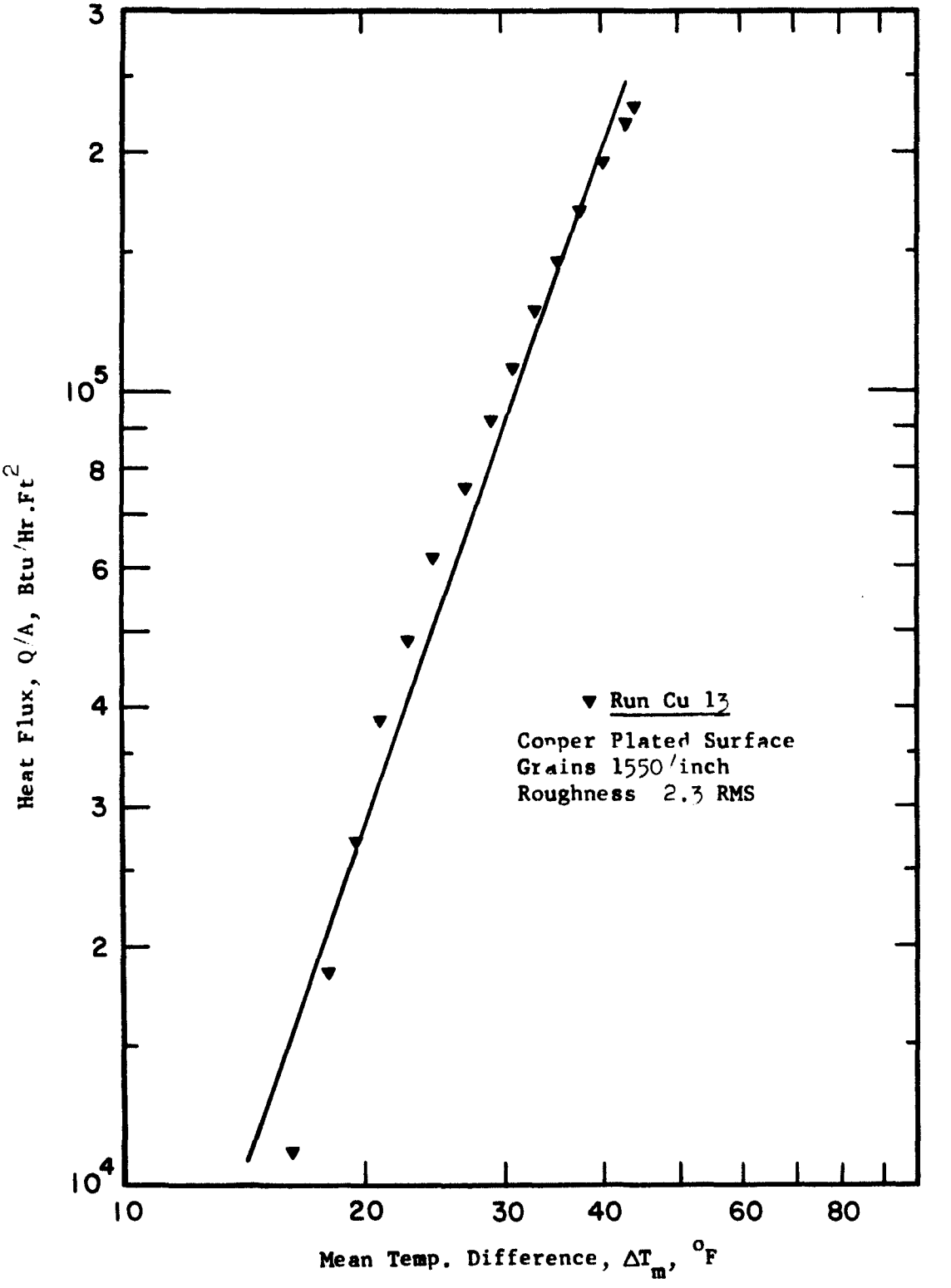

Fig.19 Boiling Data for Water on Copper Plated Surface.

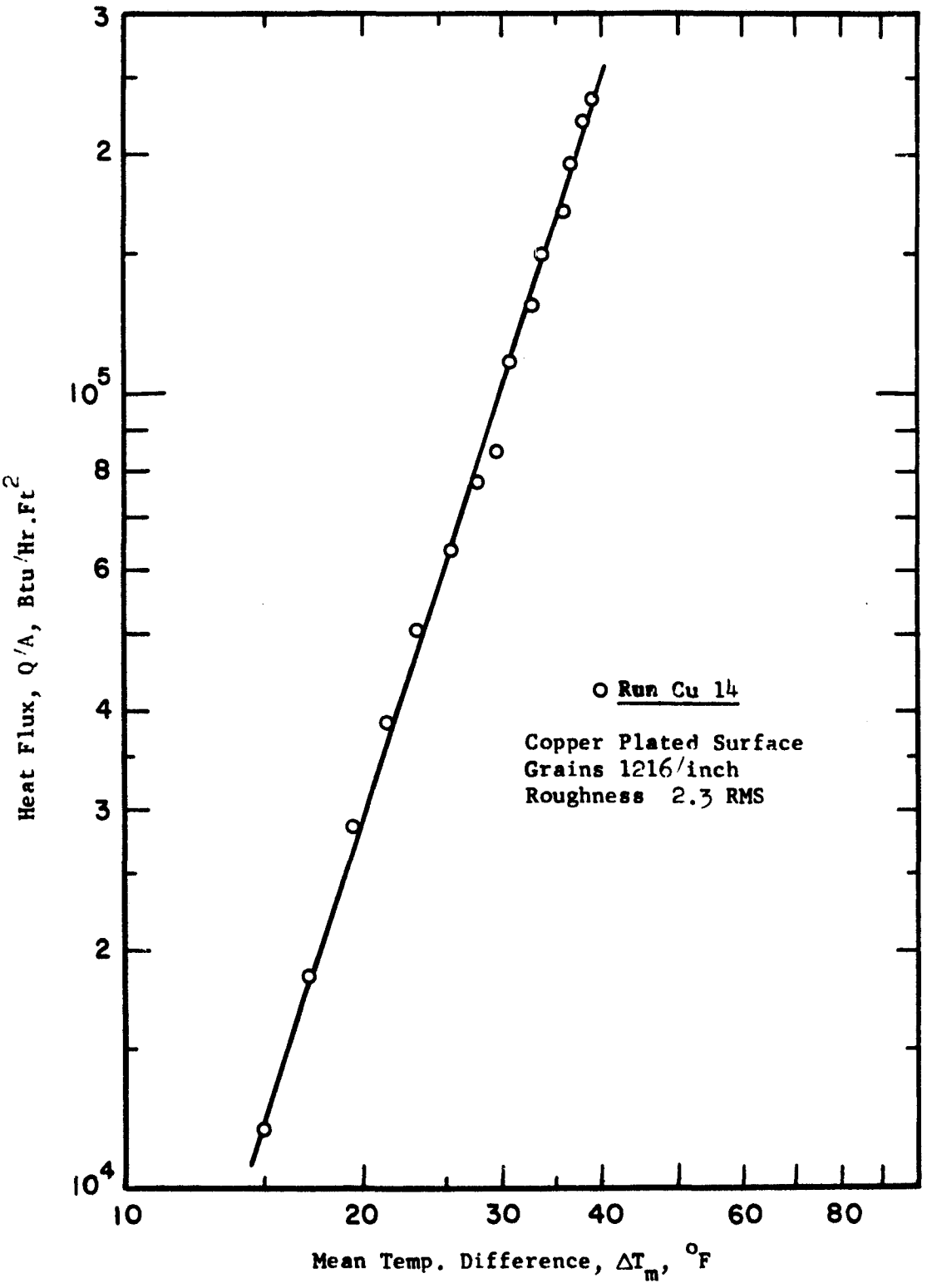

Fig.20 Boiling Data for Water on Copper Plated Surface.

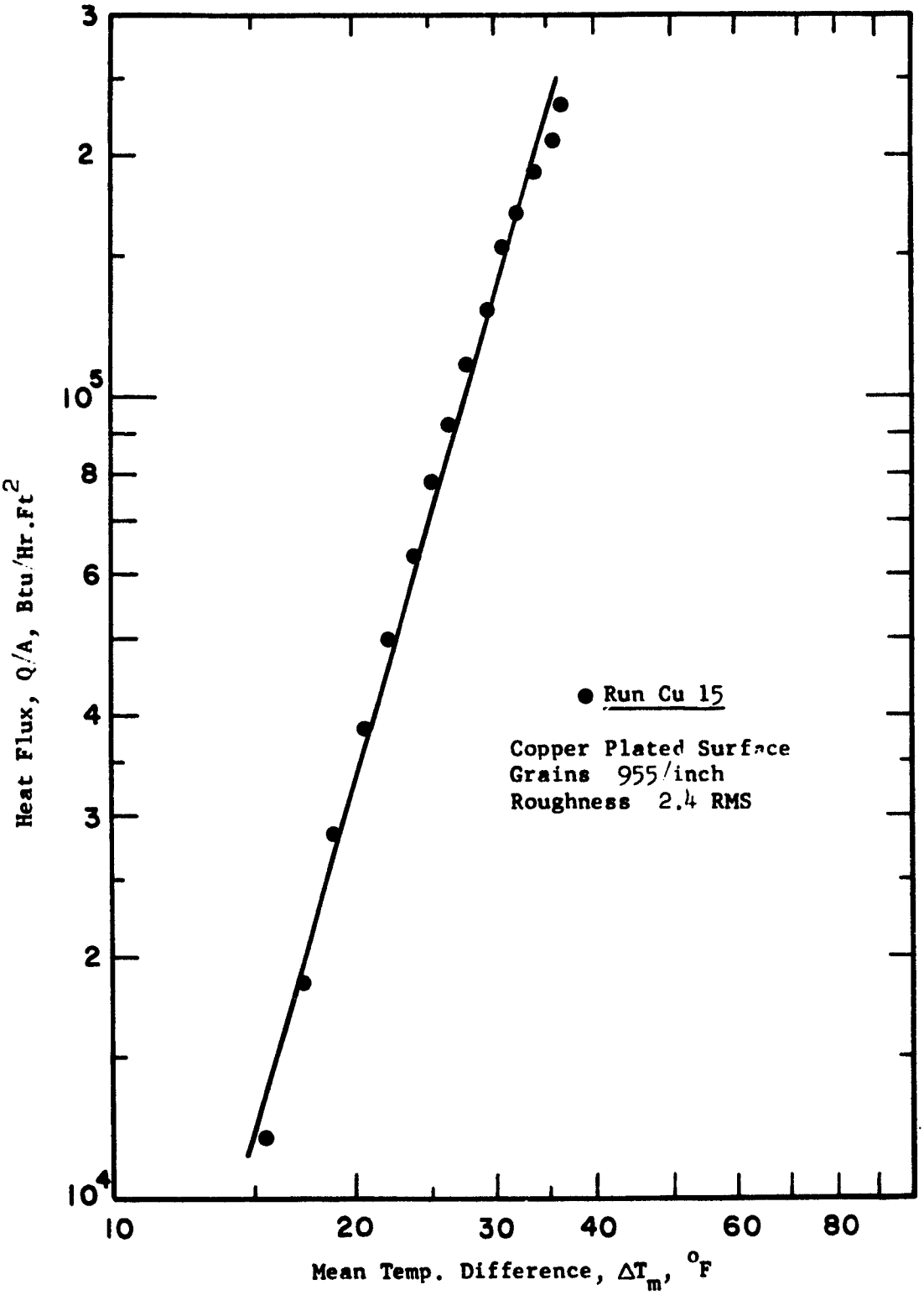

Fig.21 Boiling Data for Water on Copper Plated Surface.

plating range in order to obtain different grain sizes of the deposited metal. Before starting the boiling run on the plated surface, it was polished with a power machine sander and then buffed in order to eliminate any directional variations in rms roughness values as commonly exhibited by mechanically polished samples (V_1) and to reduce the roughness to a value between 2 and 3 micro inches.

Runs Cu 6 to Cu 16 were carried out on copper plated surfaces whose grains ranged from about 150 to 1700 per linear inch. Figs. 12 to 21 represent the data obtained in these runs. For run Cu 10B, the experimental set-up of the previous run namely Cu 10A was allowed to remain intact for three days without disturbing the pool of water over the surface and the run was repeated. The data of runs Cu 10A and Cu 10B plotted together in Fig. 16 show that the slope of Q/A vs ΔT for the aged surface is slightly less steep than that of the freshly polished surface. Also at high heat fluxes the aged surface seems to require a higher ΔT to maintain a particular heat flux whereas at low heat fluxes it requires lower ΔT than the fresh surface to sustain the same amount of heat flux. If fouling and depletion of trapped gas are the only factors, then the aged surface would have exhibited higher temperature differences consistently to sustain the heat fluxes as reported by Corty and Foust (C_3). The present observations suggest that possibly another factor, namely the annealing of the copper surface could have occurred to alter the stored energy of the plated surface during run Cu 10A which in turn may have contributed to the observed anamoly in heat transfer during run Cu 10B.

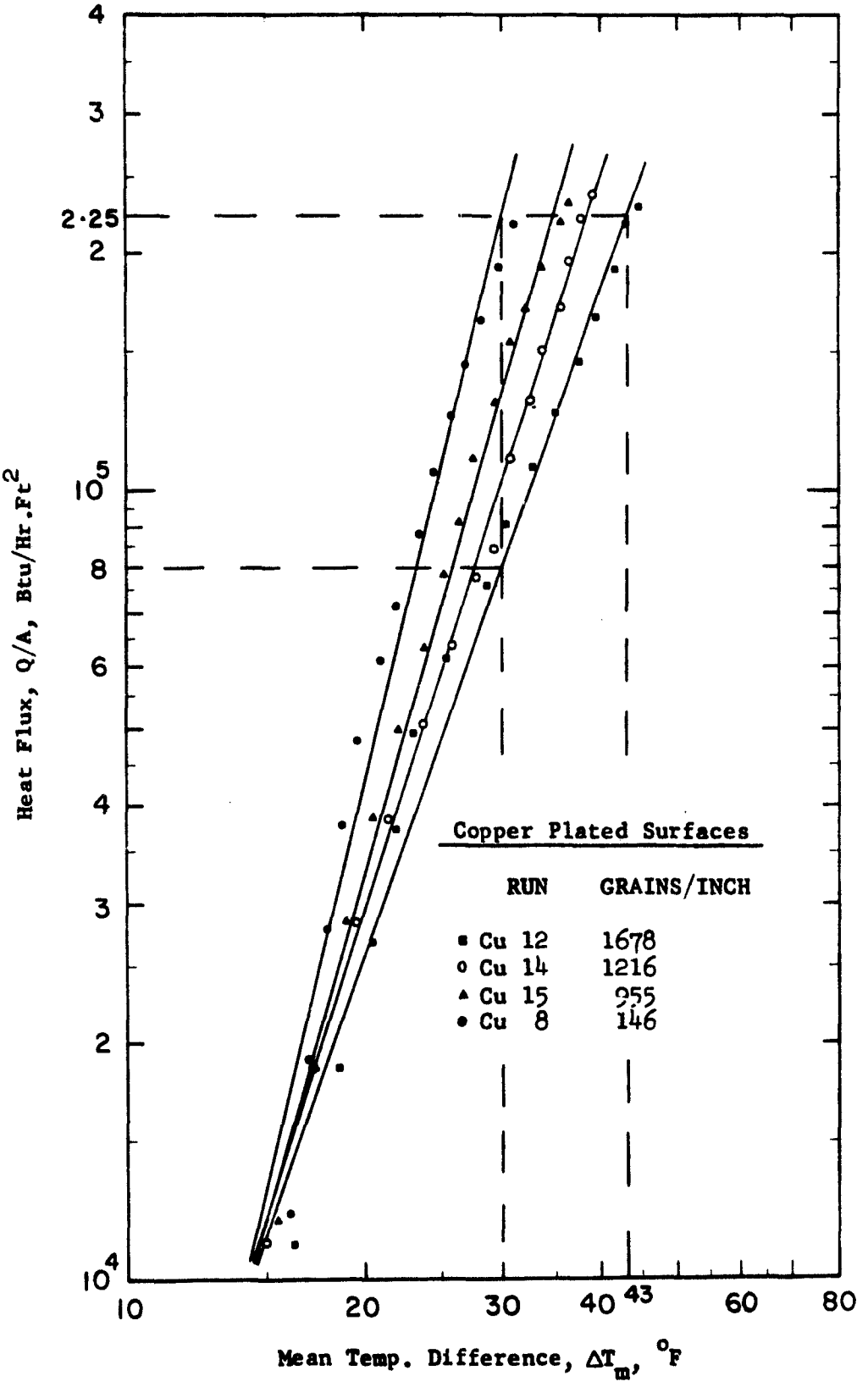

Fig.22 Comparison of Boiling Data for Water on Copper Plated Surfaces of Different Grain Sizes.

In general all the plots representing runs on copper surfaces exhibit decreasing slopes for the Q/A vs ΔT curve with increasing number of grains as seen from Table 8. Alternately an increase in heat transfer is observed with an increase in grain size or a decrease in the number of grains per unit area of the surface even though the rms roughness was maintained at more or less the same value in all the experimental runs. Figure 22 shows a combined plot of Q/A vs ΔT_m for four typical runs on copper plated surfaces. It will be useful to compare the two runs Cu 12 and Cu 8 which had the maximum difference in surface grain sizes.

From Fig. 22, at a ΔT_m of $30^{\circ}F$:

RUN	GRAINS/INCH	Q/A, Btu/Hr.Ft^2
Cu 12	1678	8×10^4
Cu 8	146	2.25×10^5

Ratio of heat fluxes is approximately equal to 2.8.

A comparison can also be made of the temperature difference ΔT_m at a particular heat flux for the above two runs as follows:

At a heat flux of about 2.25×10^5 Btu/hr.Ft^2,

RUN	GRAINS/INCH	ΔT_m, $^{\circ}F$
Cu 12	1678	43
Cu 8	146	30

It is seen that there is a difference of about $13^{\circ}F$ between the ΔT_m values for the two runs considered at an arbitrarily chosen heat flux.

It can also be observed from Fig. 22 that the plots for individual runs tend to separate further at higher values of heat flux

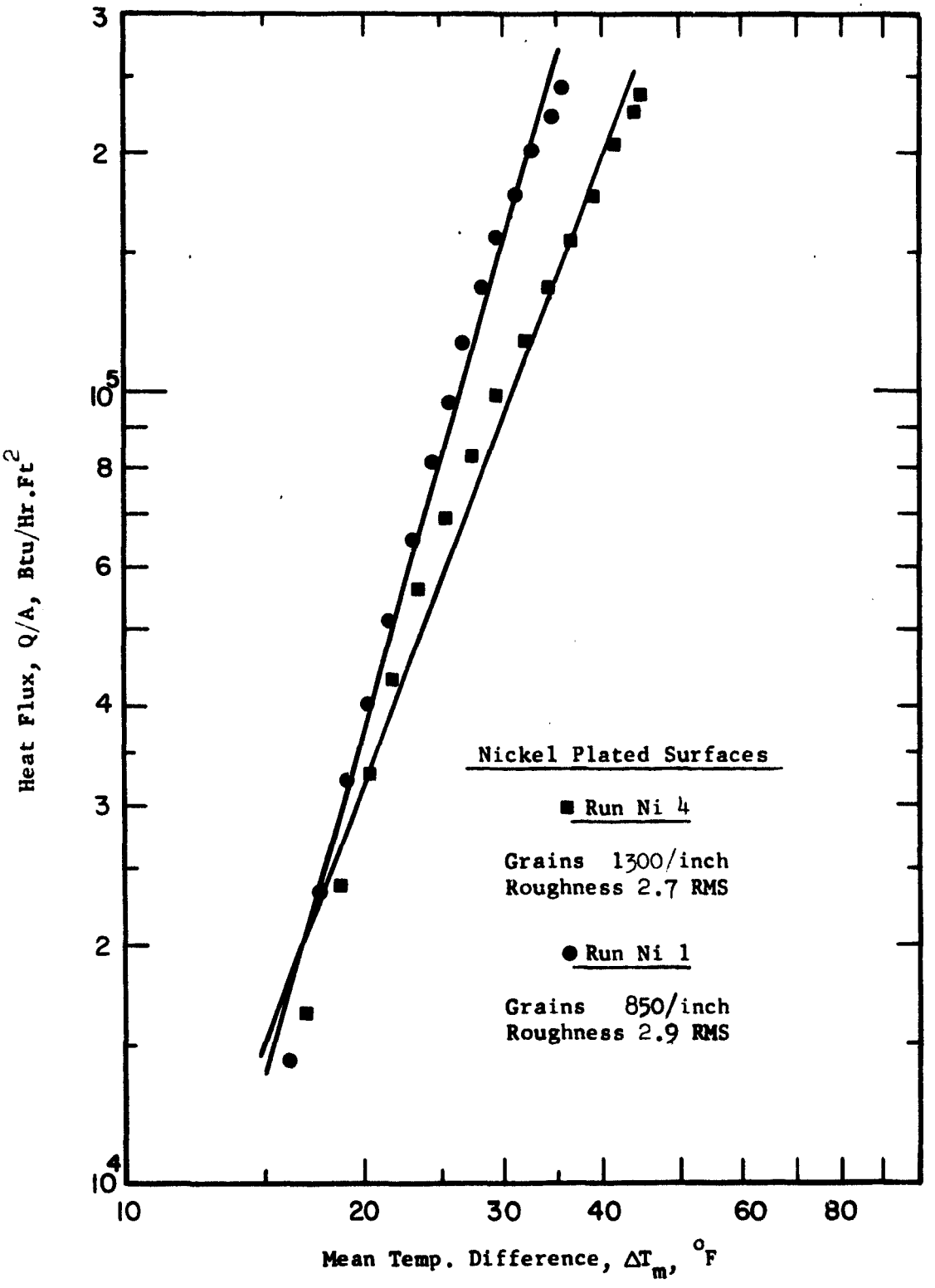

Fig.23 Comparison of Boiling Data for Water on Nickel Plated Surfaces of Different Grain Sizes.

or temperature difference.

Fig. 23 displays the data of runs Ni 1 and Ni 4 which had the greatest grain size deviation among the runs on nickel plated surfaces. Again the trend of the data clearly indicates an increase in heat transfer with increasing grain size. Thus consistent results were obtained with both nickel and copper deposited surfaces.

The above results were somewhat unexpected since one would presume that the smaller the grains, the larger will be the grain boundary area quantitatively per unit area of the surface and hence greater will be the number of potential nucleation sites. According to this view or contention, at a particular ΔT_m heat flux should be higher for the smaller grain-size surface whereas the present experimental results show the opposite.

An explanation for the above behavior was sought from the works of previous investigators (B_3,C_3,C_2)on cavities and grooves. Bankoff's theoretical work (B_3) suggests that critical capillary radius for nucleation at atmospheric pressure lies in the fairly narrow range of 0.2 to 1.2 x 10^{-4} cm. Corty and Foust (C_3) computed the sizes of simplified conical cavities from observed contact angles and measured super heats and found them to be about 10 micro inches or approximately 0.25 x 10^{-4} cm. for pentane, ether and freon 113 boiling on copper and nickel surfaces. Clark et al.(C_2) in their experiments identified active bubble-producing sites as pits with diameters between 0.0003 and 0.003 inch or about 7.5 x 10^{-4} and 7.5 x 10^{-3} cm. In his classic book on grain boundaries McLean (M_3) observes that ordinary grain boundaries such as those found in metals prepared in conventional ways are three atomic

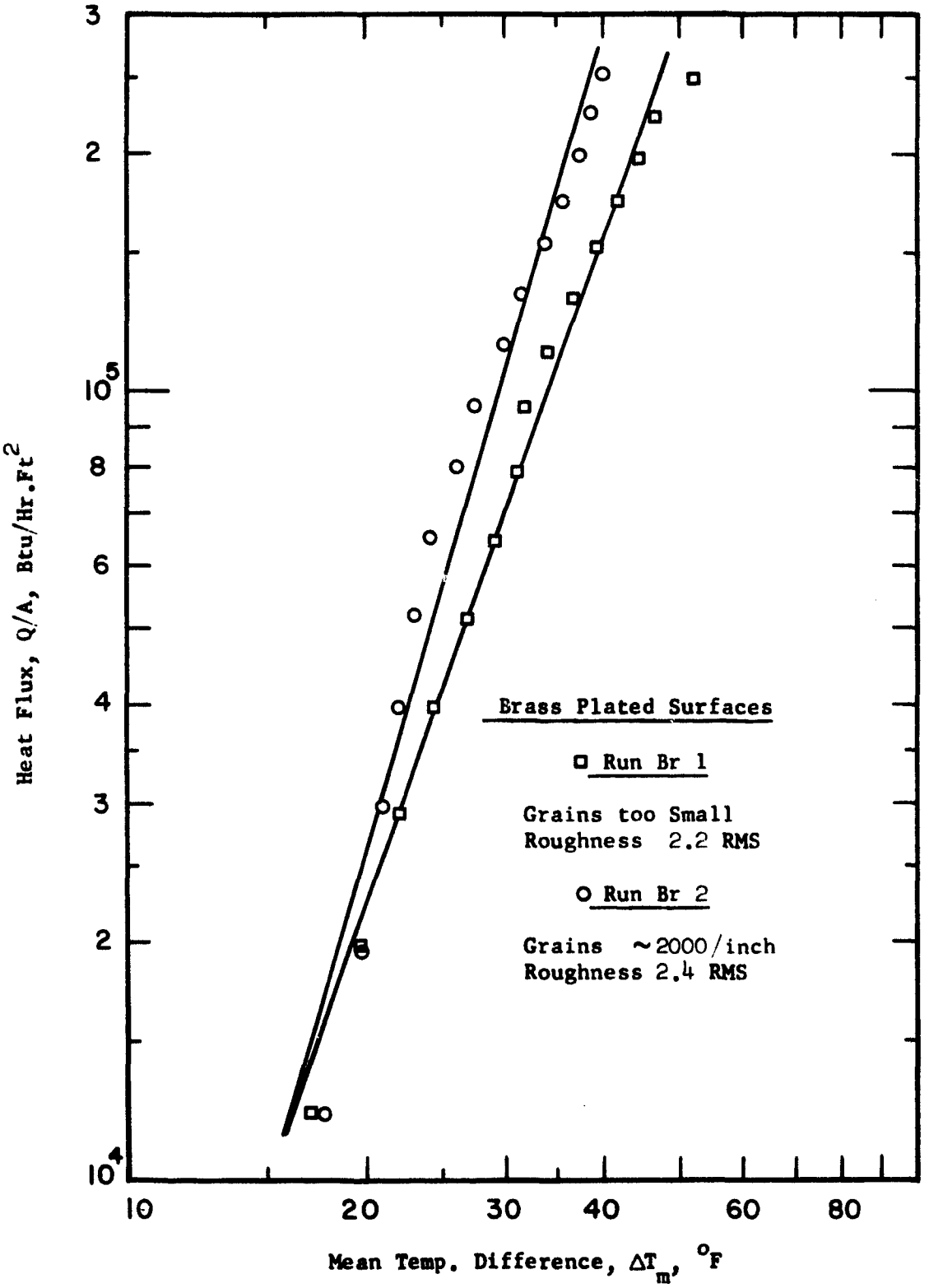

Fig.24 Comparison of Boiling Data for Water on Brass Plated Surfaces of Different Grain Sizes.

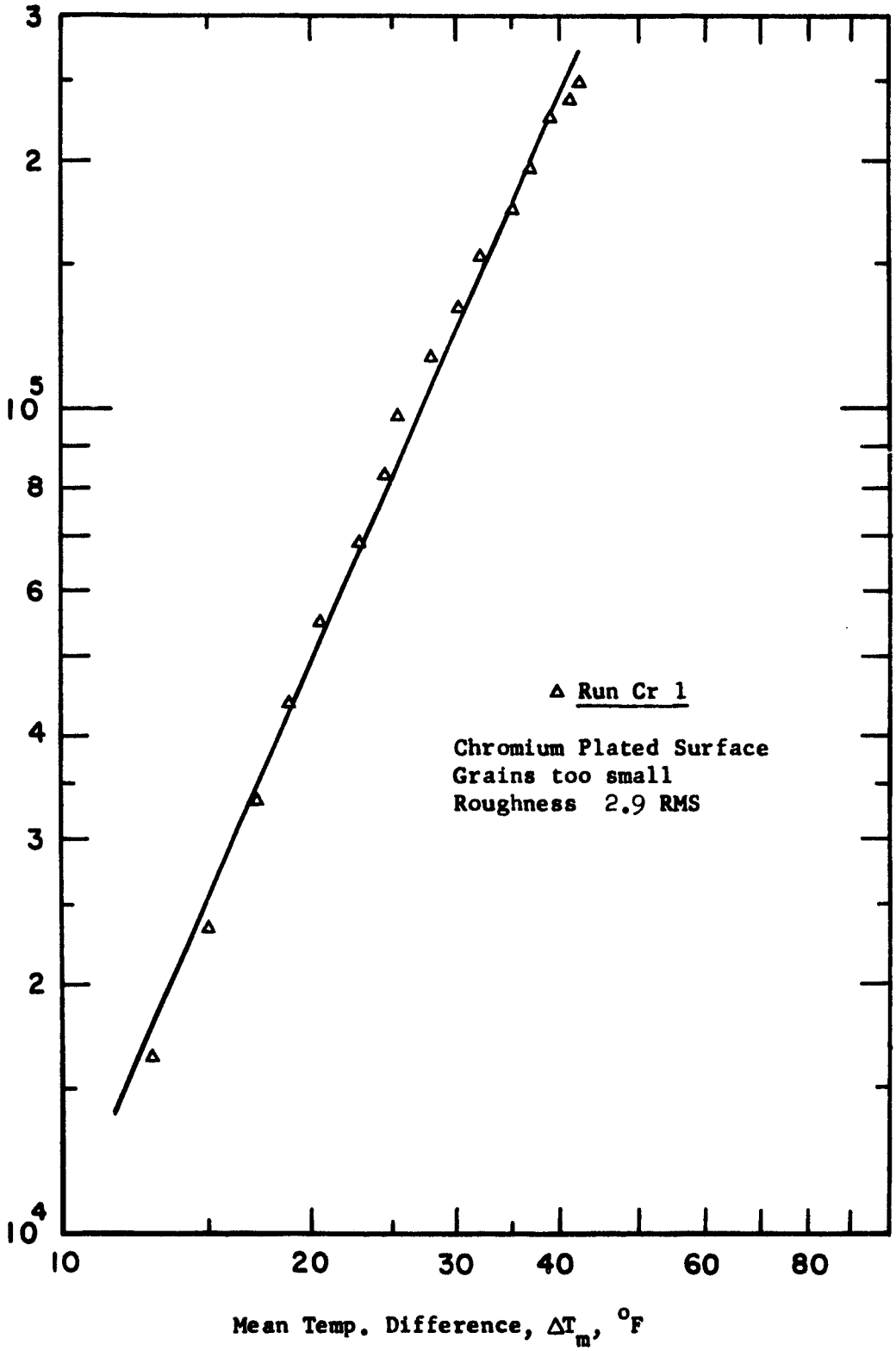

Fig.25 Boiling Data for Water on Chromium Plated Surface.

diameters wide and for a grain size of 10^{-2} cm, the grain boundary width will be of the order of 10^{-7} cm. In the present work, the grain sizes varied from about 1.7×10^{-2} cm. to 1.5×10^{-3} cm. and therefore the grain boundary width probably varied from 10^{-7} cm. to 10^{-8} cm. One might expect the grain boundaries to become narrower as the grain sizes decrease . Such narrowing might possibly render them less favourable to initiate nucleation. Even though there is no evidence available to directly relate the role of grain boundaries in boiling to that played by grooves and cavities, it is conceivable that there might exist a minimum width of the grain boundary which is most favourable for initiation and growth of bubbles. There might also exist an optimum grain size of the heat transfer surface for nucleate boiling to be at a premium rate.

It was attempted to check the above conclusions further by conducting experiments on chrome plated and brass plated surfaces. However these were not very successful mainly because the deposited grains of the above two metals were too small to be counted accurately by the grain size estimation method employed in the present experiments. Estimates of the grain sizes of electrodeposited brass and chromium are available in the literature (B_9). They are of the order of 2×10^{-6} cm. and such small grain sizes could only be measured using more sophisticated metallographic techniques such as x-ray or electron diffraction. Further experiments with deposited surfaces of chromium and brass were therefore discontinued. In any case, the results of the three runs, two on brass and one on chromium electrodeposits are included in Tables 2 to 9 and plotted in Figs. 24 and 25 for comparison with the earlier data on

copper and nickel plated surfaces.

B. Correlation of Boiling Data

Even though many investigators have attempted to derive general correlations for boiling heat transfer (F_2,F_3,L_3,R_8), none of their equations have been found to completely satisfy the voluminous experimental data available in this field. This state of affairs is due to the fact that the above correlations, in spite of including all the conceivable physical properties of the boiling system, are invariably deficient in quantitatively describing the effect of the surface condition of the heater on boiling. The equation of Rohsenow (R_8) incorporates a constant term C_{sf} and exponents r and s as shown below:

$$\frac{C_{\ell}\Delta T}{h_{fg}} = C_{s_f}\left(\frac{Q/A}{\mu_{\ell} h_{fg}} \sqrt{\frac{g_o \sigma}{g(\rho_{\ell}-\rho_v)}}\right)^r \left(\frac{C_{\ell}\mu_{\ell}}{k_{\ell}}\right)^s \qquad (48)$$

where C_{sf} = (constant) β^r where β is the contact angle. Rohsenow inferred that the constant C_{sf} should be a function of the particular fluid-heating surface combination. This seemed to be the case as proven by the author himself on applying his correlation to several sets of experimental data (Table 1, Appendix I).

The exponent 's' accounts for surface cleanliness and takes up a value of 1.0 for water (V_2). 'r' is the reciprocal of the slope obtained by fitting the experimental heat flux - super heat data of a boiling system by the least square method. Rohsenow initially recommended a fixed value of 0.33 for this exponent. However, recent compilation by Vachon et al. (V_2) of their own data and that of other investigators has

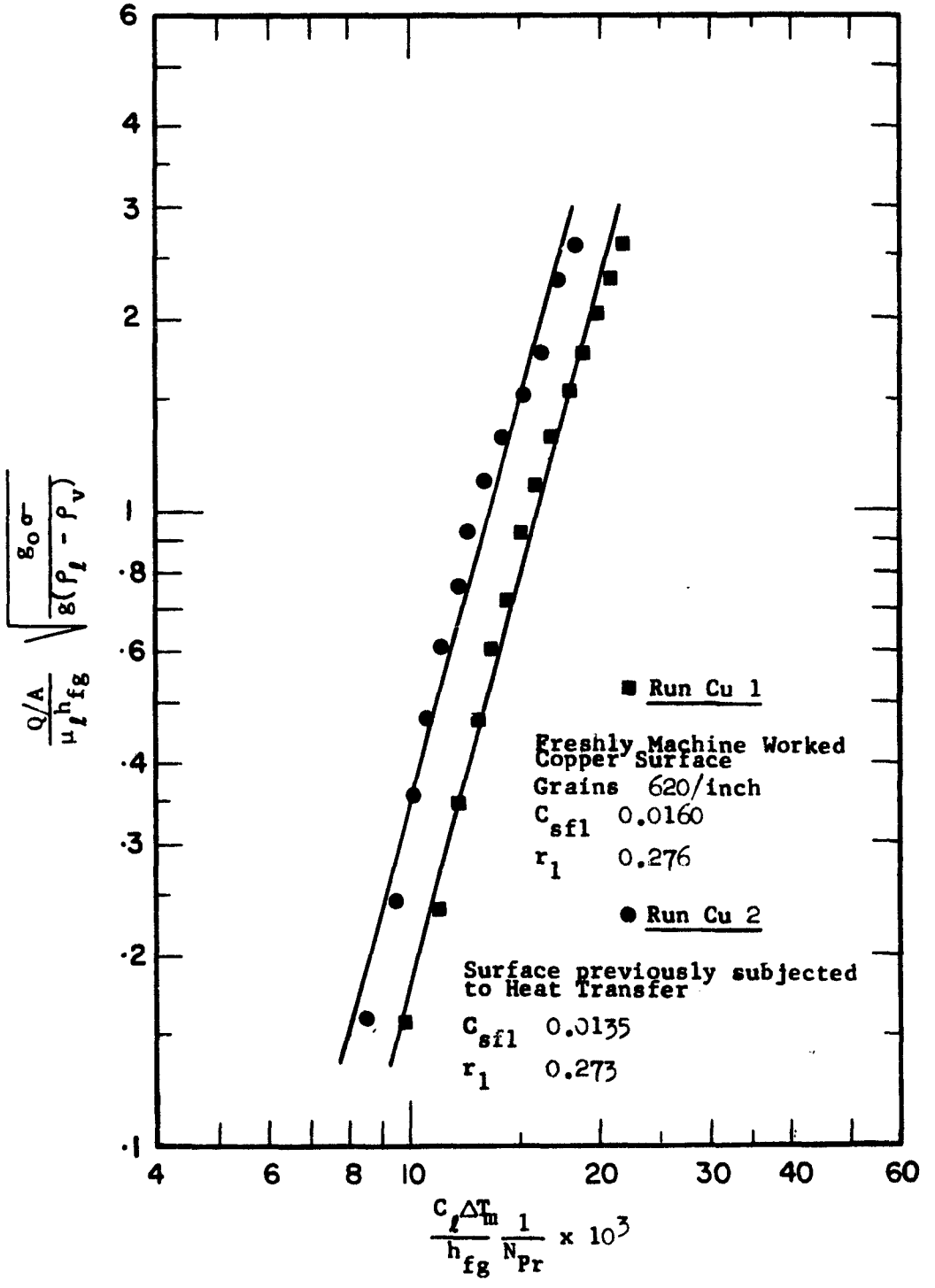

Fig.26 Correlation of Pool-Boiling Data for Water on Copper Surface.

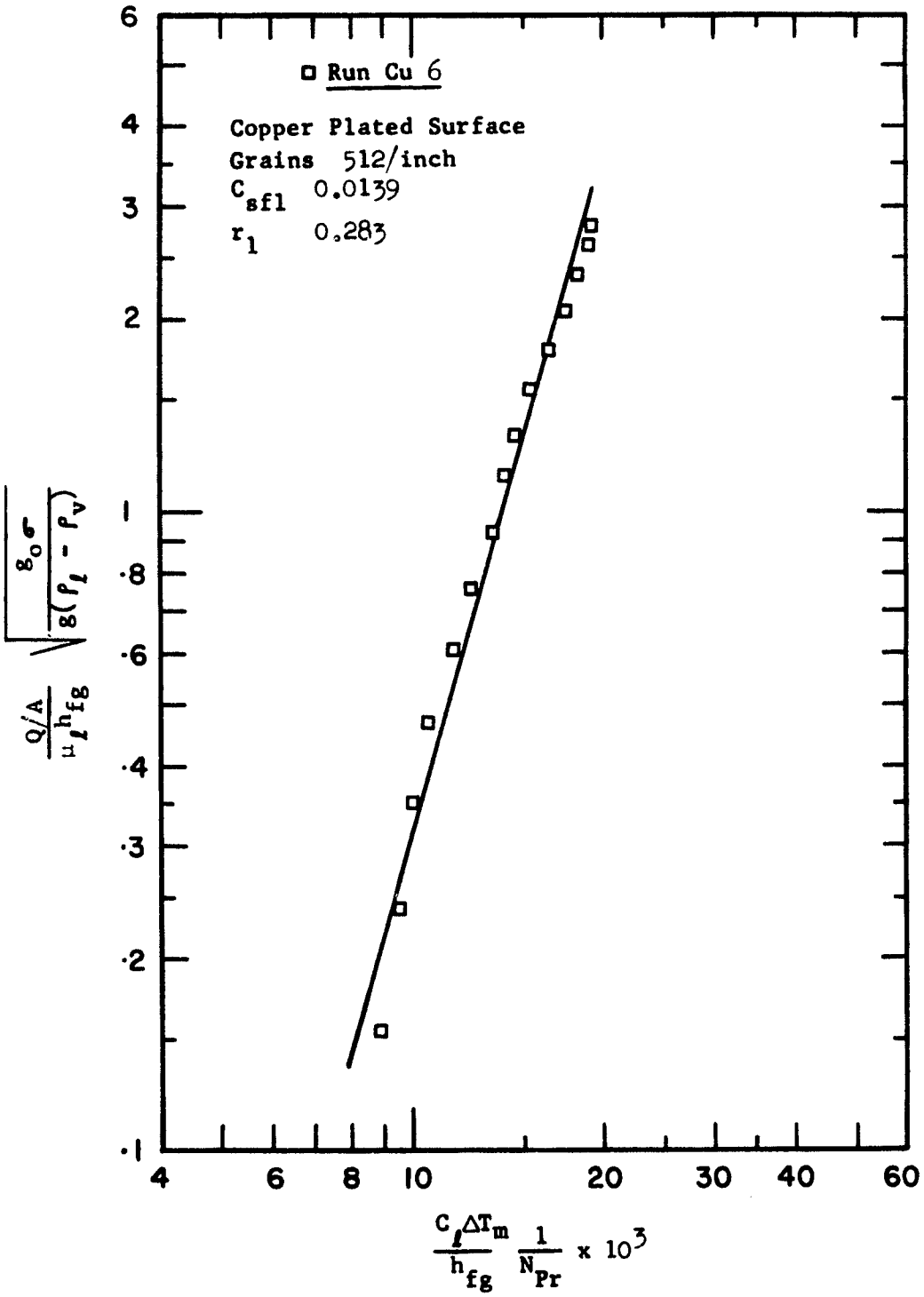

Fig. 27 Correlation of Pool-Boiling Data for Water on Copper Plated Surface.

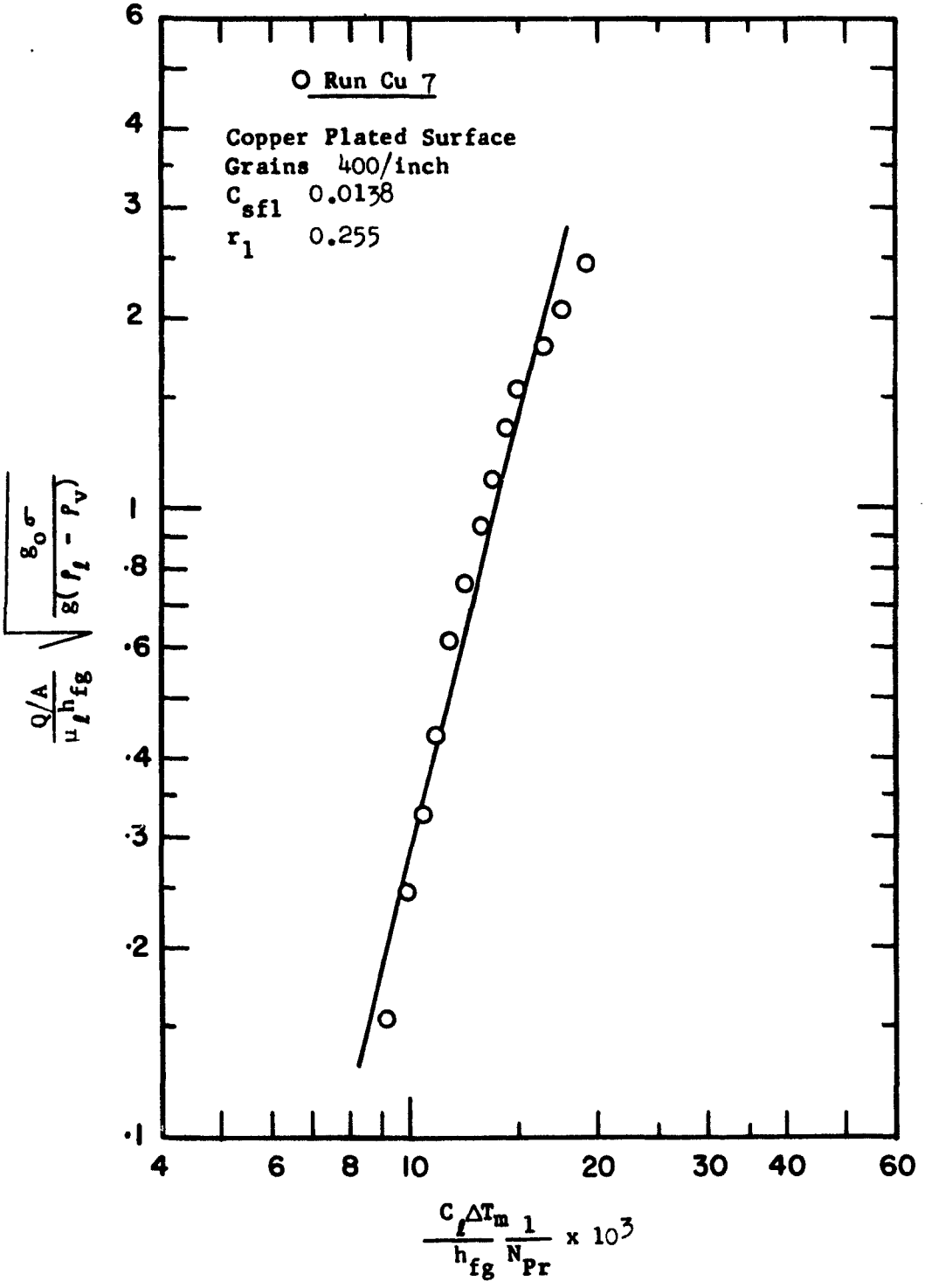

Fig.28 Correlation of Pool-Boiling Data for Water on Copper Plated Surface.

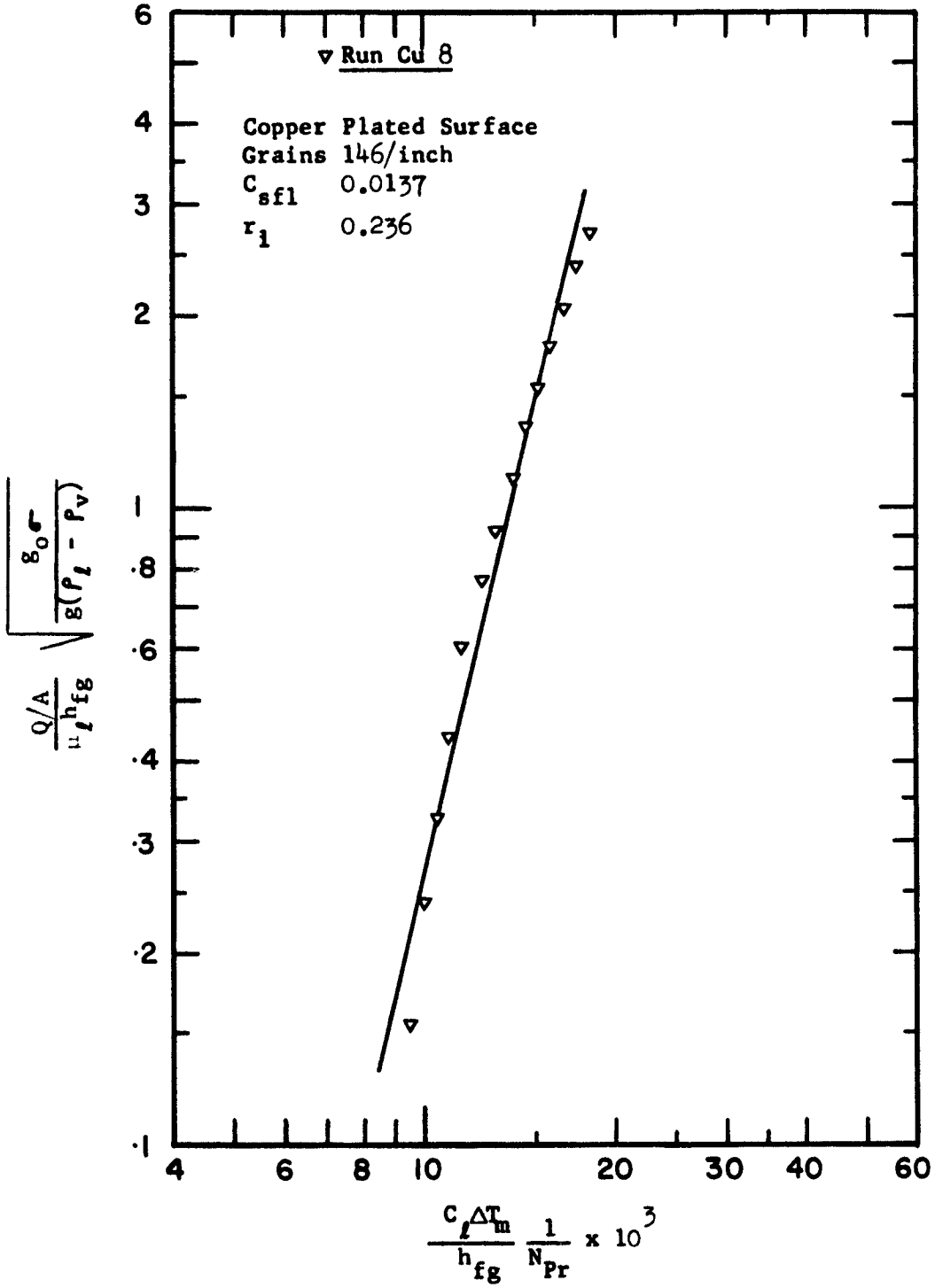

Fig.29 Correlation of Pool-Boiling Data for Water on Copper Plated Surface.

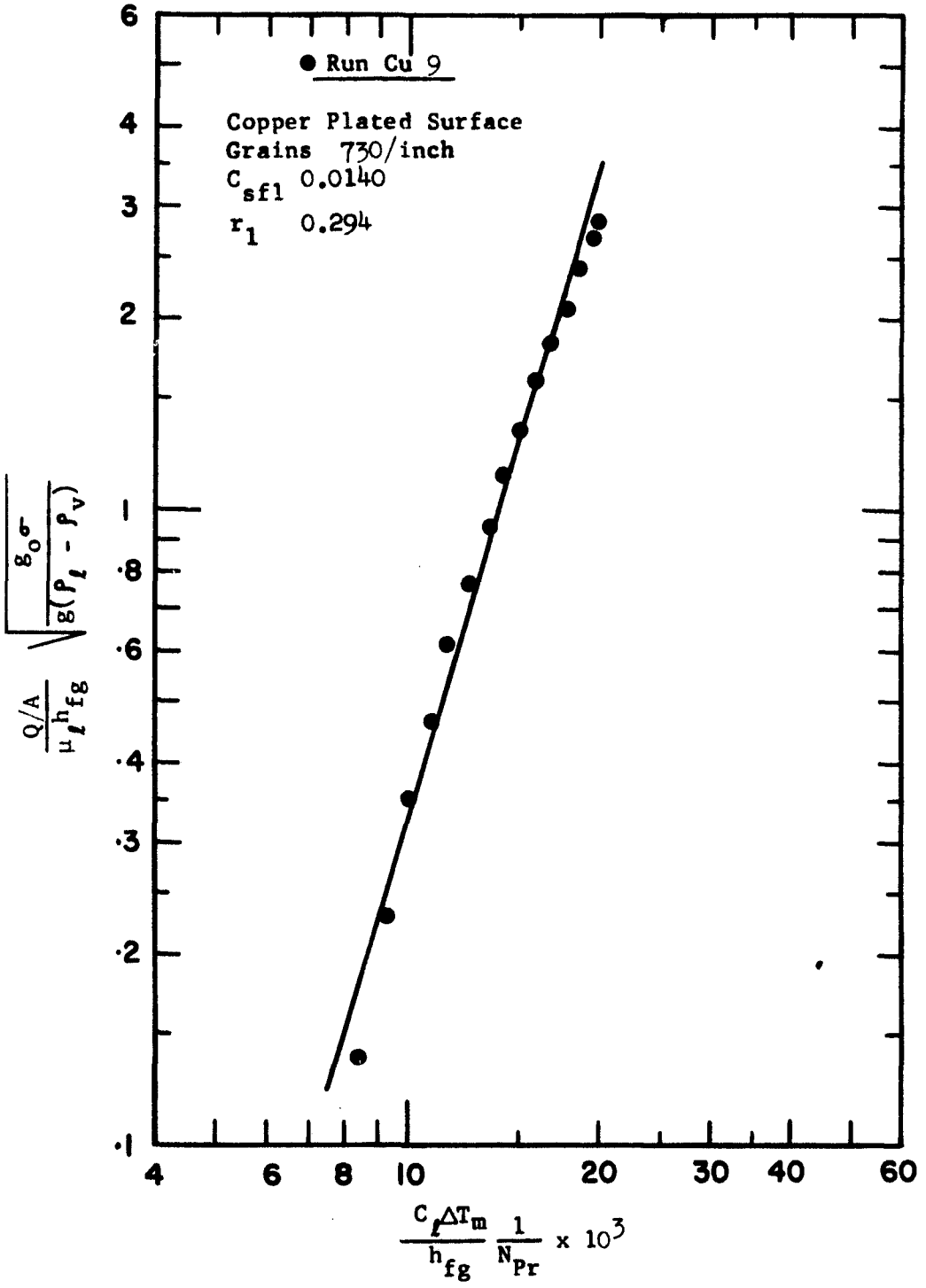

Fig.30 Correlation of Pool-Boiling Data for Water on Copper Plated Surface.

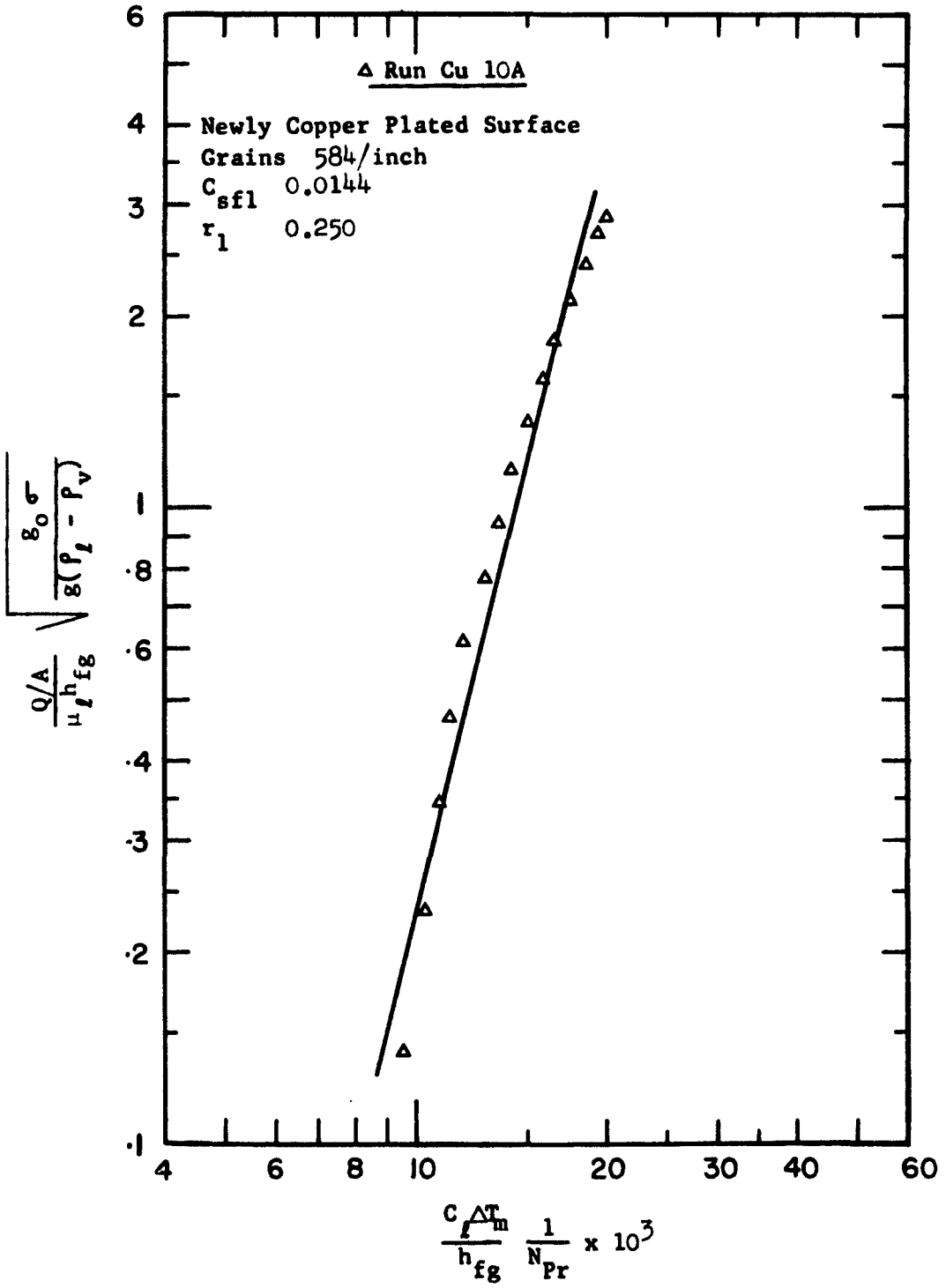

Fig.31 Correlation of Pool-Boiling Data for Water on Copper Plated Surface.

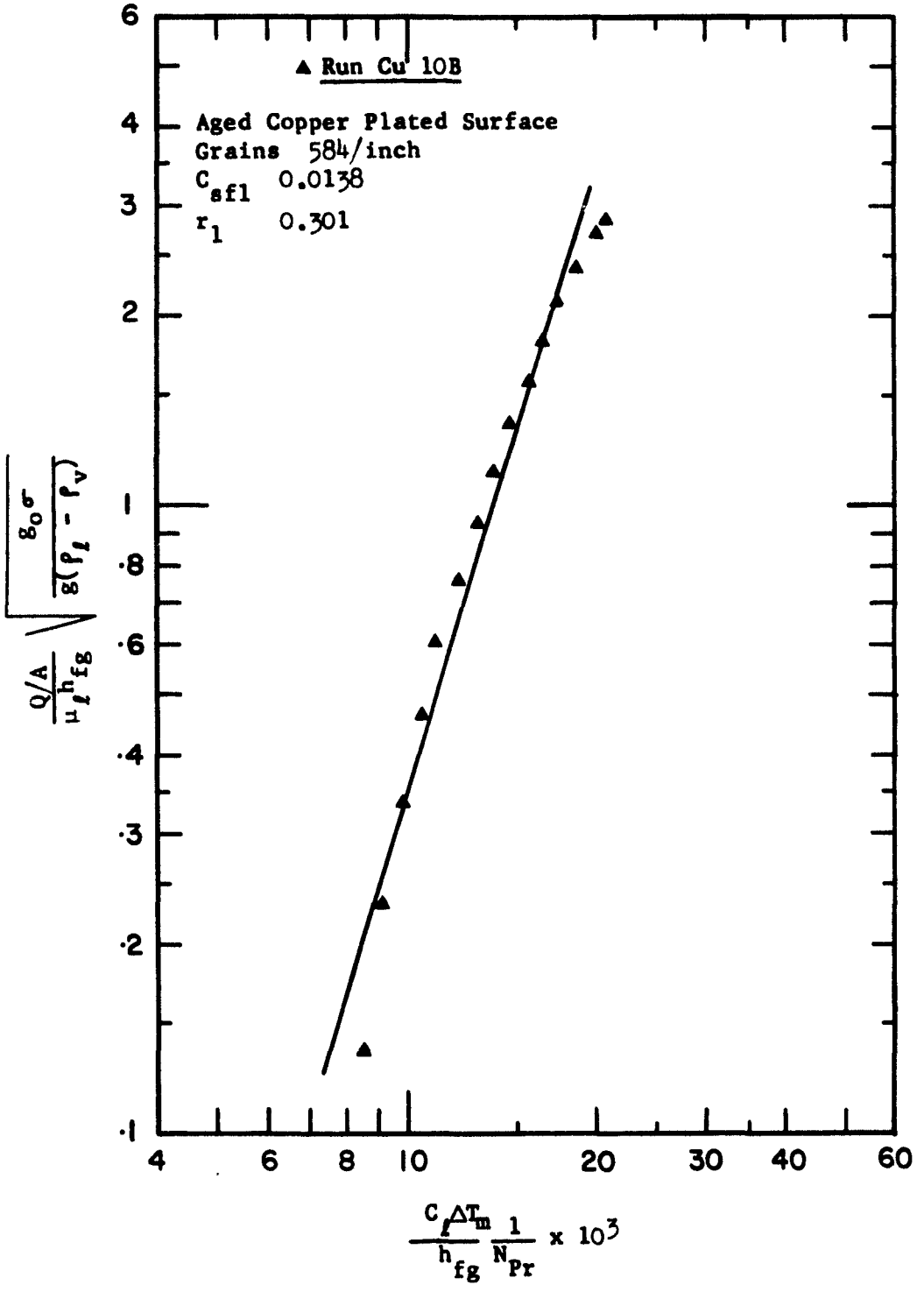

Fig. 32 Correlation of Pool-Boiling Data for Water on Copper Plated Surface.

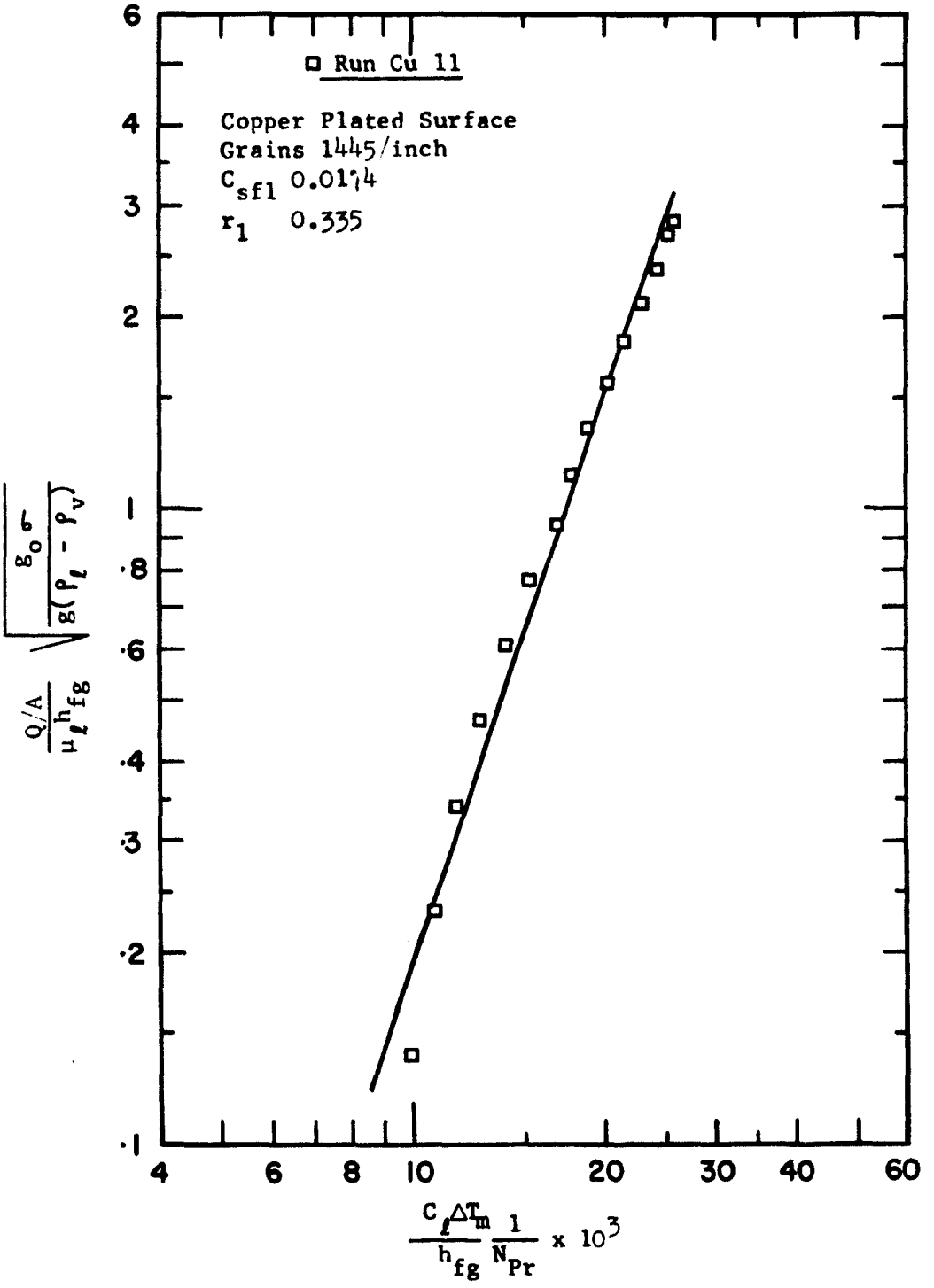

Fig.33 Correlation of Pool-Boiling Data for Water on Copper Plated Surface.

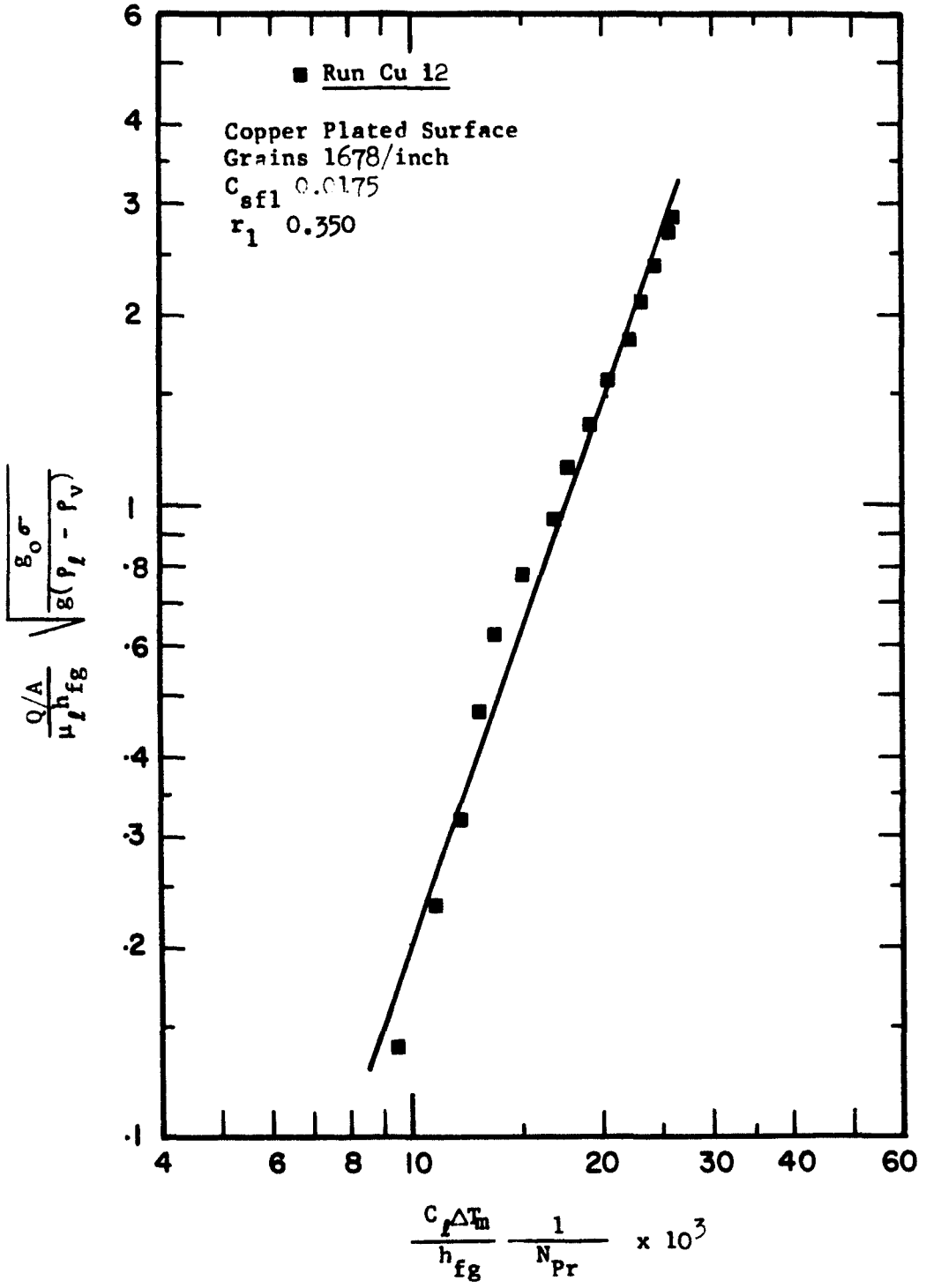

Fig.34 Correlation of Pool-Boiling Data for Water on Copper Plated Surface.

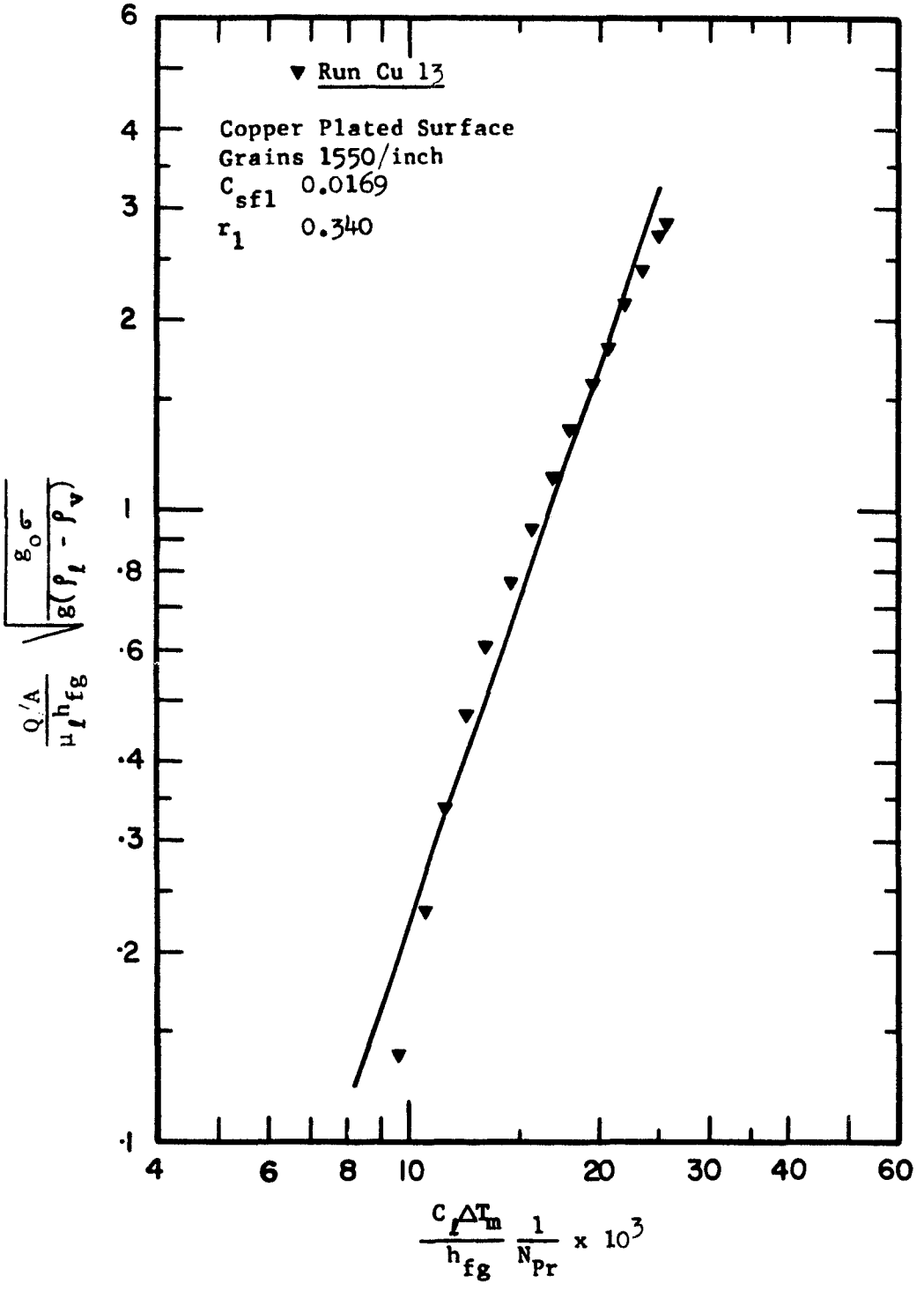

Fig. 35 Correlation of Pool-Boiling Data for Water on Copper Plated Surface.

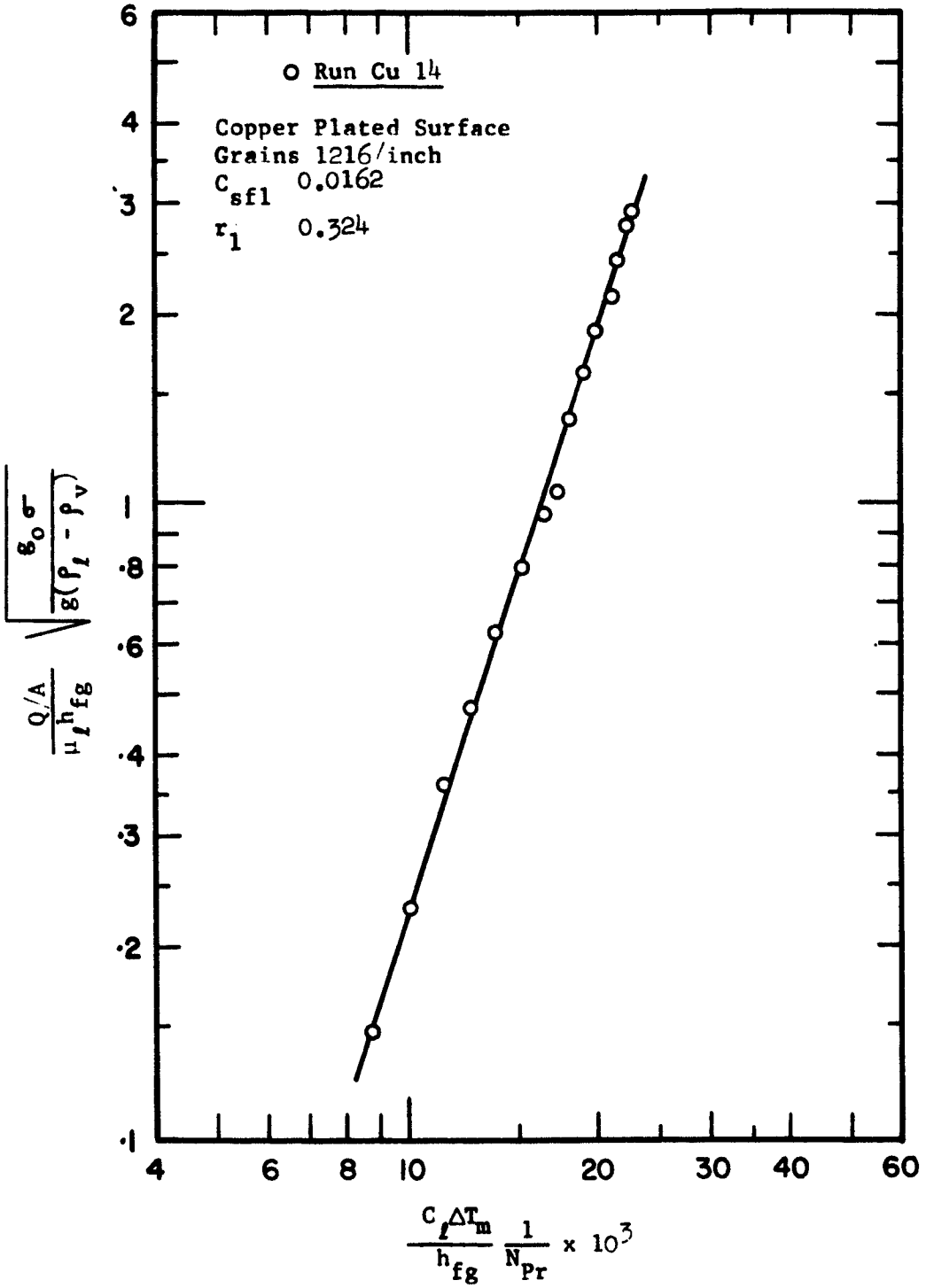

Fig.36 Correlation of Pool-Boiling Data for Water on Copper Plated Surface.

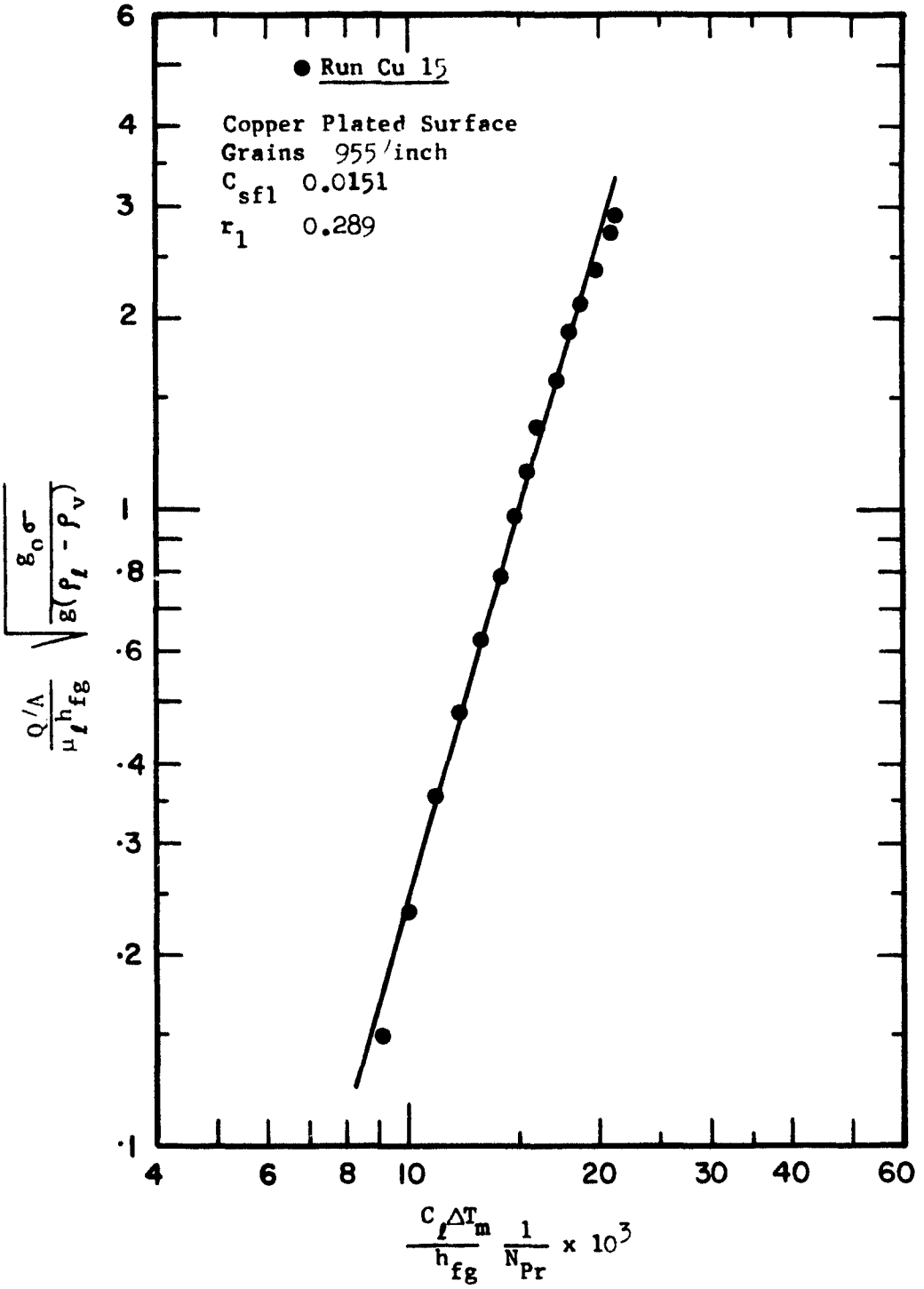

Fig.37 Correlation of Pool-Boiling Data for Water on Copper Plated Surface.

established that values ranging from 0.05 to 0.89 for 'r' are obtained in actual experiments.

Vachon et al.(V_2) investigated the possibility that r and C_{sf} could be functions of both the surface preparation as well as the liquid-surface combination by summarizing the boiling data from literature in such a way that data from a particular liquid-surface combination and a particular preparation technique are grouped under the same headings. Their work provides evidence to support the premise that both r and C_{sf} do vary depending not only on the liquid-surface combination but also on the surface preparation technique.

As discussed in the earlier chapters, the present experimental work attempted to elucidate the effect of metallic grains and grain boundaries of the surface on boiling heat transfer. This was achieved by maintaining the same surface preparation technique, the rms roughness of the surface and the liquid-surface combination in the runs and altering only the sizes of the surface grains by electroplating methods. Then by using the Rohsenow equation to fit the experimental data, it would be possible to deduce whether there is any definite dependency of C_{sf} and r on the surface grains. Such an approach should indicate the differences in boiling heat transfer if any, caused by variation of metallic grain sizes.

Employing the Rohsenow equation, the experimental data for a particular electrodeposited surface with a definite grain size was plotted making use of the least square curve fitting technique. These plots are given as Figures 26 to 37 for copper surfaces. The recommendations of Vachon et al.(V_2) were followed in the computations for these plots as

described below:

1. Values of the intercept C_{sf1}, and exponent r_1, for each surface were obtained, the value of r_1, being the reciprocal of the slope of the least squares fit for each run.

2. Values of the intercept C_{sf2} for each surface were obtained using a value of 0.33 for the exponent r_2 as originally suggested by Rohsenow.

3. Values of C_{sf3} and r_3 for each surface were obtained, the value of r_3 being the reciprocal of the average of the slopes of the least squares curve fits for the data of a particular metal.

Table 9 gives the values of C_{sf1} , r_1 ; C_{sf2} , r_2 and C_{sf3} and r_3 obtained through the computations as described above. These values are also represented by corresponding lines in Figs. 26 to 37. On careful perusal of Table 9 and the figures, it can be seen that C_{sf} and r values for the same surface-liquid combination do vary appreciably depending upon the grain structure even though other variables were kept unchanged. The composite plot (Fig. 38) exhibits this variation clearly for copper plated surfaces. In the present work for copper plated surface with boiling water the C_{sf1} varied from 0.0135 to 0.0175 and the slope r_1 varied from about 0.236 to 0.350 whereas for nickel plated surface-water combination C_{sf1} and r_1 varied from 0.0146 to 0.0167 and 0.273 to 0.379 respectively.

In Table 10 the deviation of r_1 calculated for individual surfaces from a r_2 value of 0.33 and a r_3 value for the whole group of experiments on the same metal surface are given. The deviation of C_{sf1}

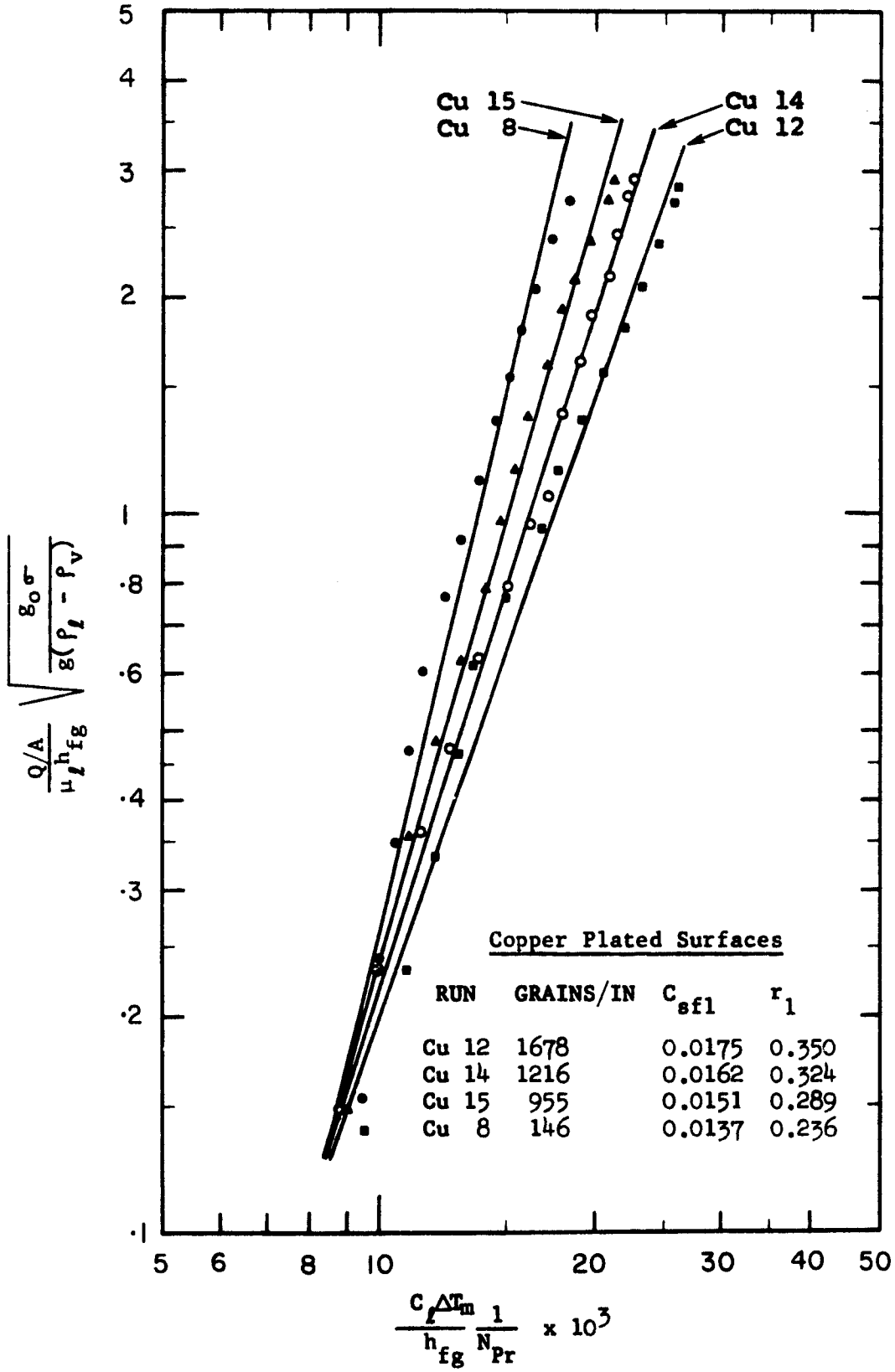

Fig.38 Correlation of Pool-Boiling Data for Water on Copper Plated Surfaces of Different Grain Sizes.

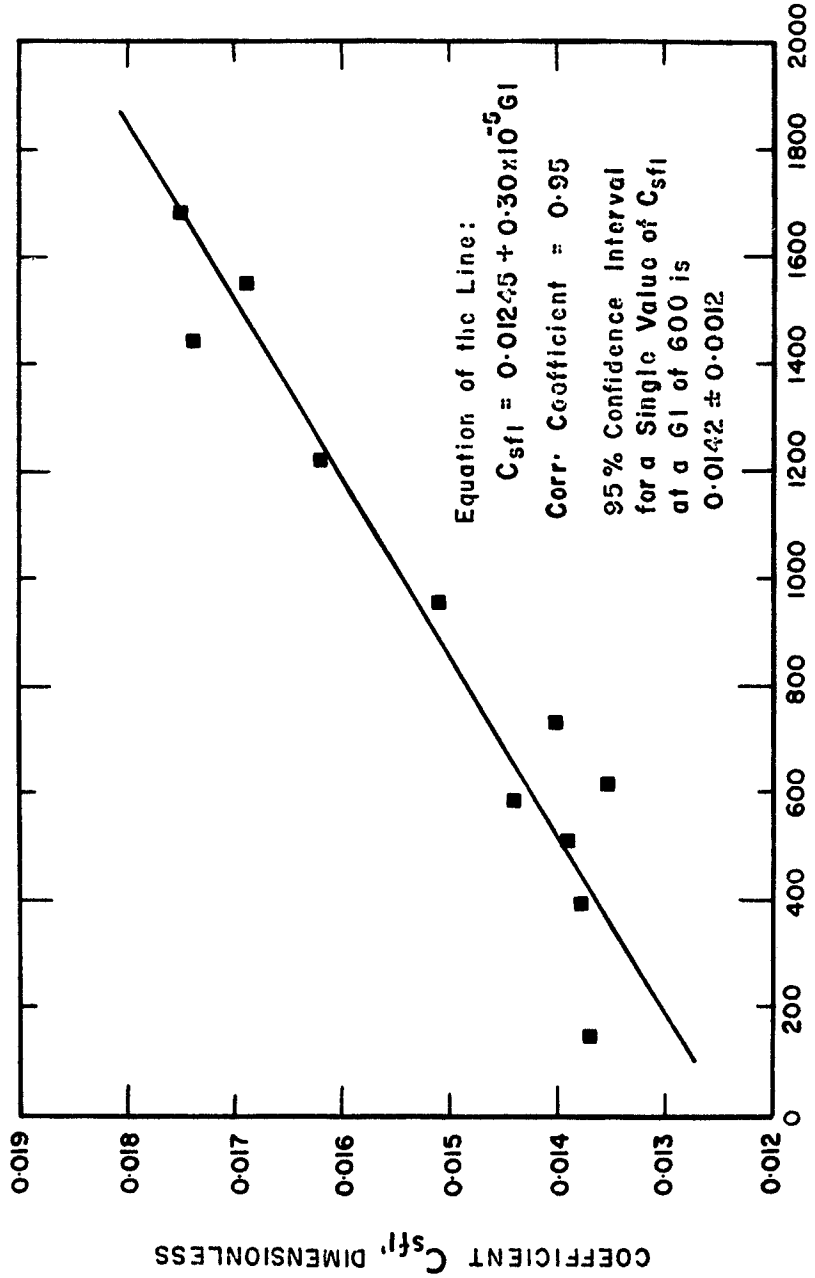

FIG·39 PLOT OF COEFFICIENT C_{sfi} OF ROHSENOW EQUATION VS. GRAINS PER INCH OF COPPER PLATED SURFACES.

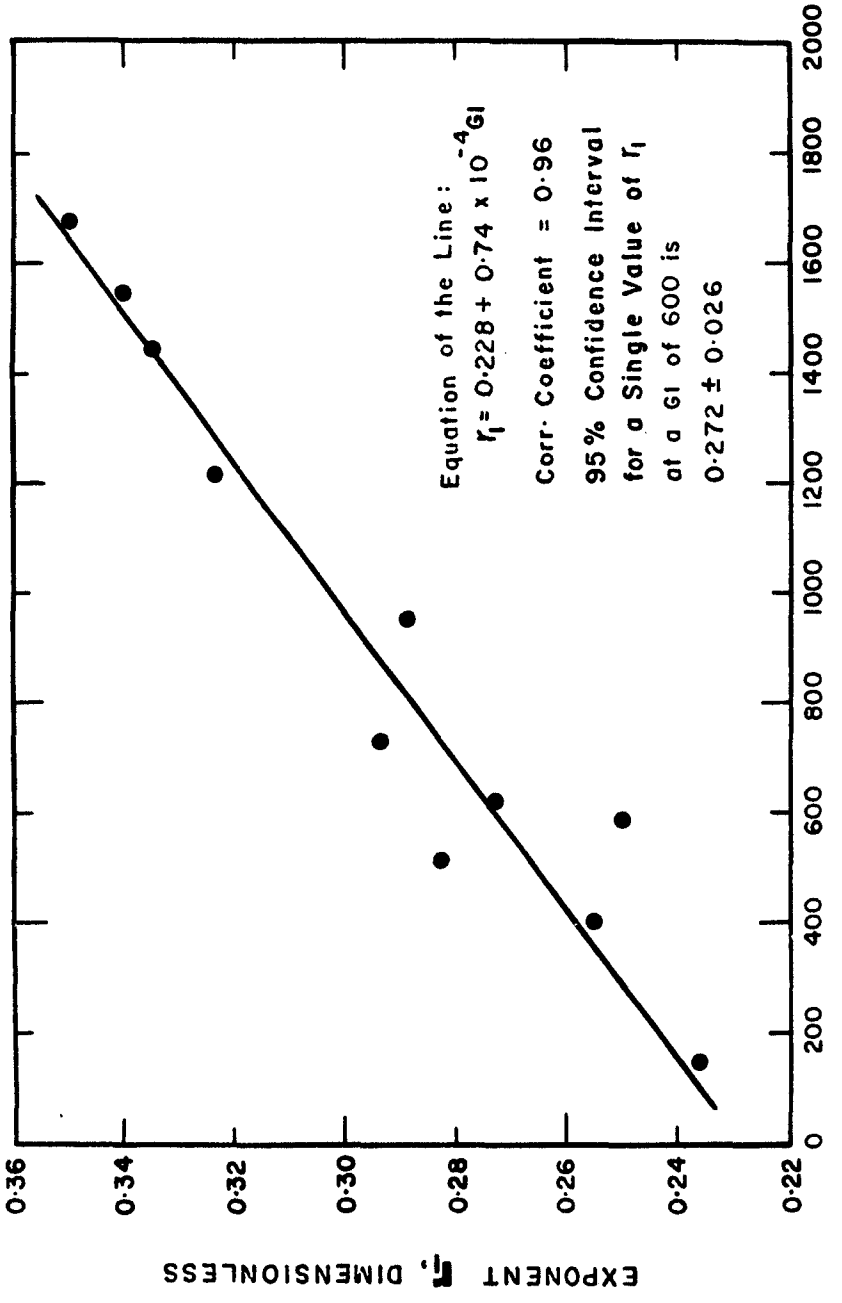

FIG·40 PLOT OF EXPONENT r_f OF ROHSENOW EQUATION Vs.
GRAINS PER INCH OF COPPER PLATED SURFACES.

from corresponding values of C_{sf2} and C_{sf3} are almost negligible as seen from Table 9. Scrutinizing Table 10 one can appreciate that using a fixed value of 0.33 for r_2 gives rise to more deviation proportionately from the individual experimental values of r_1 than the deviations of the corresponding average values of r_3.

For design purposes, proper care should be taken in choosing the values of C_{sf} and r for use with the Rohsenow Correlation. A complete knowledge of the surface characteristics, the surface roughness, the surface preparation techniques used and the surface grain size are prerequisites for choosing the proper values of C_{sf} and r. On the basis of the experimental observations available now, there is sufficient evidence to warrant a reconsideration of the earlier notion (R_8) that a value of Q/A and its corresponding value of ΔT is all that is needed to correlate the boiling data and to evaluate C_{sf} for one particular metal-fluid combination. The present investigation has introduced another parameter namely the surface grain size whose influence on nucleate boiling heat transfer has to be included in any satisfactory correlation.

Having established the influence of grains and grain boundaries on boiling, efforts were made to modify the Rohsenow equation suitably to incorporate these effects. The intercepts C_{sf1} and the exponents r_1 were plotted separately in Fig. 39 and 40 against 'GI', the concentration of the metallic grains of the surface expressed as the number of grains per linear inch. It can be seen from the graphs that C_{sf1} and r_1 show good linear relationships against GI, with the coefficient of correlations of the linear fits of about 0.95 and 0.96 respectively. On including the

observed linearities into the Rohsenow correlation, the following modified equation was obtained for use with the copper surfaces.

$$\frac{C_{\ell}\Delta T}{h_{fg}} = (0.0018\ G + 0.0125)\left(\frac{Q/A}{\mu_{\ell} h_{fg}}\sqrt{\frac{g_o \sigma}{g(\rho_{\ell}-\rho_v)}}\right)^{(0.044G+0.228)} \left(\frac{C_{\ell}\mu_{\ell}}{k_{\ell}}\right)^{1.0} \quad (49)$$

where G is the grain ratio and is defined as the ratio of number of grains per linear inch of a sample to the grains of a surface having 600 grains per linear inch. The number 600 was chosen because the original unplated surface used in the present experiments had about 600 grains per inch and was made from electrolytic copper of 99.98% purity. Other commercially available copper metal surfaces are likely to have grain sizes close to this number and the value of C_{sf} at this grain size is approximately that reported in the literature (Refer Tables 1 and 9). In Table 11 a comparison is made of the experimental values of C_{sf} and r and the calculated values using the above modified correlation. Figure 41 is a plot of the boiling data of all runs on copper plated surfaces correlated with the modified equation. The spread of the experimental data around the correlating line of the plot was estimated to be $\pm$10 per cent.

The problem then leads to an investigation of how the grain size could influence the magnitude of the contact angle 'β' because contact angle is one of the major parameters which seems to contribute significantly to the observed variations in the values of C_{sf} (R_8).

If a growing bubble at a heating surface is considered, as in Figure 1, the contact angle 'β' can be expressed in terms of the surface tension forces acting at the point of contact between liquid, vapor

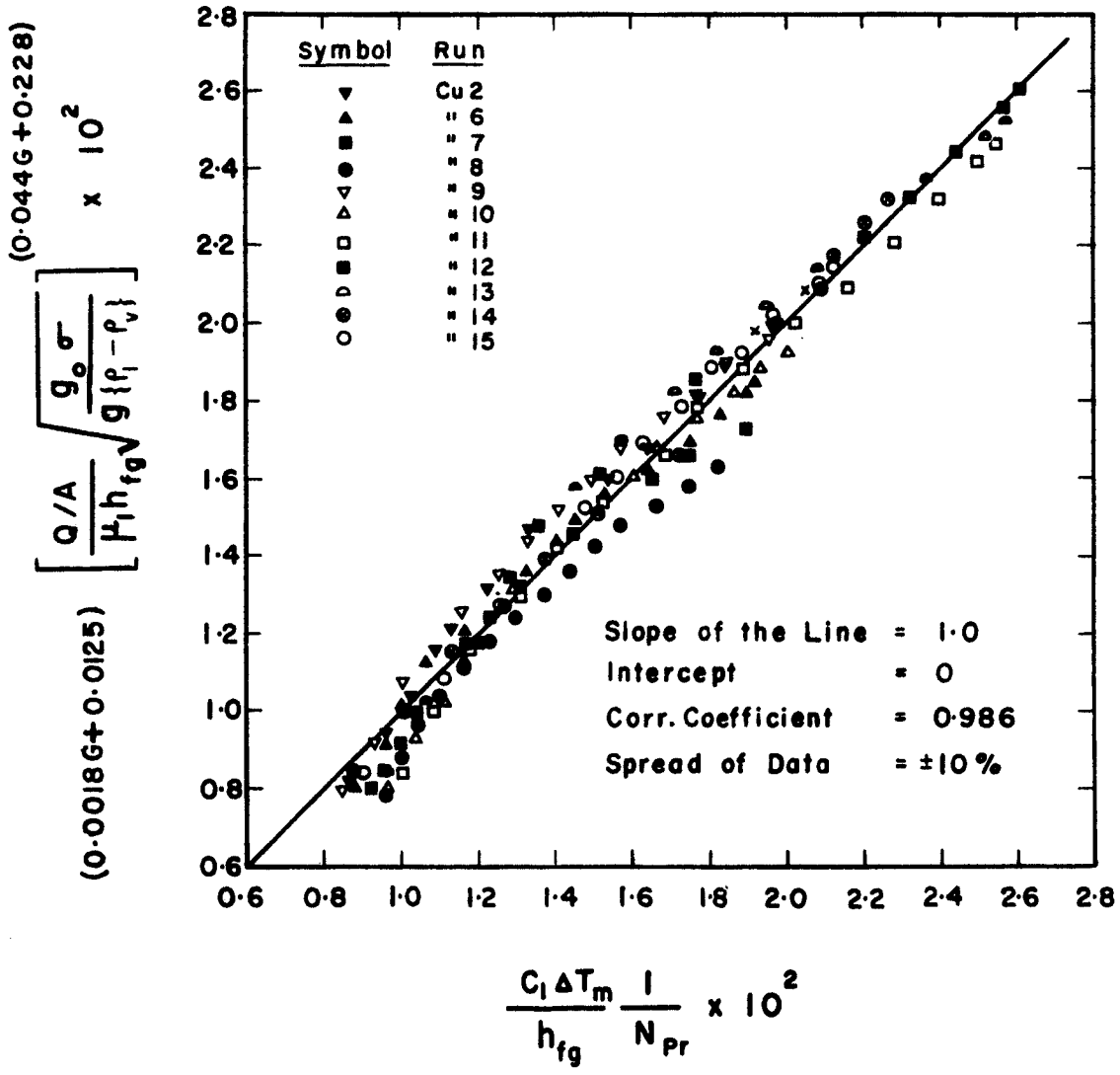

FIG·41 BOILING DATA OF ALL RUNS ON COPPER PLATED SURFACES CORRELATED WITH THE MODIFIED EQUATION

and solid. For the solid grain face the relationship for the contact angle is

$$\cos \beta = \frac{\sigma_{sv} - \sigma_{ls}}{\sigma_{lv}} \qquad (50)$$

For the grain boundary, the above relationship should be modified as follows:

$$\cos \beta = \frac{\sigma_{bv} - \sigma_{ls}}{\sigma_{lv}} \qquad (51)$$

Interfacial tension data σ_{sv} between solid grain face-vapor and σ_{bv}, between grain boundary-vapor are reported in the literature at elevated temperatures for copper metal (M_3,S_7) and are given in Table 14. Their ratio for a high angle boundary is approximately 3:1.

In the present investigation, for a particular liquid-surface combination the fluctuations of the interfacial tensions σ_{sl} and σ_{lv} were probably insignificant and the only variation would have occured in σ_{sv} of Eq. 50 or σ_{bv} of Eq. 51 owing to the variation in ratios of the grains and grain boundaries. If the proper interfacial tension values for the grains and grain boundaries are substituted in Eq. 50 and Eq. 51 respectively, it can be seen that the contact angle β will be higher for the grain boundaries than for the grains. This means the greater the number of gains per unit area of the surface and hence the more grain boundaries quantitatively, the higher will be the effect of contact angle on the bubbles; which in turn will probably show up in the form of a higher C_{sf}. The present experimental observations seem to substantiate such an inference as can be seen from the data in Table 9. However further confirmation of the above deduction depends upon the availability of accurate values of interfacial

tensions σ_{sv} and σ_{bv} on one side and a relationship connecting the contact angle β to C_{sf} and r on the other. Finally as Bankoff* pointed out, the over-all contact angle may not give much information about the microscopic contact angle, which probably varies from point to point on the surface. The future availability of the above two types of contact angle measurements and their inter-relationship may help in further elucidation of nucleate boiling mechanism from surfaces.

---

* Discussion by Bankoff on the paper of Griffith and Wallis (G_3).

CHAPTER VII

CONCLUSIONS AND RECOMMENDATIONS

The following is a summary of the observations obtained and conclusions reached after an analysis of the experimental data of the present investigation:

1. Boiling data obtained on surfaces with various grain sizes were plotted as heat flux Q/A vs mean temperature difference ΔT_m between the surface and saturation temperature. These graphs show a definite effect of grain sizes of the surface on boiling heat transfer. At a given ΔT_m, the heat flux was higher for a surface with a relatively larger grain size. The slope of the boiling curve increased gradually as the grain size of the surface increased.

2. Boiling curves for all grain sizes tend to converge at low values of Q/A.

3. The observations seem to indicate that nucleate boiling is influenced by the grains and associated grain boundaries of the heater surface.

4. Application of the Rohsenow correlation to the boiling data shows that the coefficient C_{sf} and the exponent r of the equation do not remain constant for a particular metal-fluid combination but are influenced by the grain structure of the heat transfer surface.

5. C_{sf} and r tend to decrease as the number of grains decreases (or as the grain size increases).

6. C_{sf} and r plotted separetly against the number of grains per unit length of the surface show linearities.

7. 7. A slightly modified form of the Rohsenow Correlation has been proposed which takes into account the influence of grains and grain boundaries on boiling heat transfer. The modified equation was found to fit the experimental data with a spread of $\pm$ 10 per cent.

The following recommendations are made for future studies:

1. Further boiling investigations should be conducted using surfaces with different sizes of grains preferably in the direction of increasing grain sizes. Such a study will probably indicate whether any optimum grain size exists for the boiling to be highly efficient from a particular metal surface.

2. Boiling studies should be carried out using surfaces produced by other metallurgical techniques.

3. Experimental studies using surfaces with other metal deposits such as zinc, gold, silver, platinum, etc. are the next logical steps.

4. Efforts should be made to produce a uniform radial temperature distribution over the surface of the heat transfer plate.

5. The boiling curves for different grain sizes obtained in the present experiments show a tendency to separate more at higher heat fluxes. Therefore it will be worthwhile to carry out experiments at higher heat fluxes extending up to the critical heat flux. The equipment used in the present study was operated only at 70 per cent of its total capacity.

6. The need for accurate bubble contact angle measurements is evident. The availability of over-all contact angles and microscopic contact angles which probably vary from point to point on the surface and their inter-relationship will facilitate further clarification of the complex phenomenon of nucleate boiling.

APPENDIX I

HEAT TRANSFER DATA

TABLE 1

C_{sf} Values of the Rohsenow Correlation with r=0.33 and s=1.7 (Reference T_1)

Surface-Fluid Combination	C_{sf}
Water - nickel	0.006
Water - platinum	0.013
Water - copper	0.013
Water - brass	0.006
Water - nickel and stainless steel	0.013
Water - stainless steel	0.014
Carbon tetrachloride - copper	0.013
Benzene - chromium	0.010
N-Pentane - chromium	0.015
Ethyl alcohol - copper	0.0027
Isopropyl alcohol - copper	0.0025
35% Potassium carbonate - copper	0.0054
50% Potassium carbonate - copper	0.0027
N-Butyl alcohol - copper	0.0030

TABLE 2

Thermocouple Locations

1. Thermocouples Located in the Copper Plate

T.C. No.	Distance from the Wall in inches	Distance from the Top Surface in inches
t_1	3.015	0.217
t_2	3.015	0.765
t_3	3.015	1.302
t_4	2.003	0.217
t_5	2.003	0.774
t_6	2.003	1.324
t_7	1.000	0.217
t_8	1.000	0.767
t_9	1.000	1.314

2. Thermocouples located on the edge of the Copper Plate

T.C. No.	Distance from the Top Surface in inches
t_{10}	0.313
t_{11}	0.797
t_{12}	1.188

Thermocouple Locations (continued)

3. Thermocouples attached to the bottom surface of the Stainless Steel Fin

T.C. No.	Distance from the wall of the Copper Plate in inches
t_{13}	0.250
t_{14}	1.750

TABLE 3

EXPERIMENTAL TEMPERATURE AND POWER MEASUREMENTS (SPECIMEN DATA)

Run No.	Watt/Hr.	t_1	t_2	t_3	t_4	t_5	t_6	t_7	t_8	t_9
Cu 1	12420	258.15	297.04	329.45	255.59	292.82	318.24	270.74	319.39	368.83
	11016	256.41	292.61	322.39	254.07	288.36	311.36	267.93	309.14	357.76
	9696	254.54	285.85	312.32	252.70	283.19	304.33	263.04	298.29	338.64
	8460	252.11	279.30	302.18	250.33	276.19	294.33	259.19	289.82	324.43
	7350	249.73	274.48	295.25	247.89	270.89	287.22	254.93	282.11	313.25
	6279	247.19	268.18	285.89	245.34	263.78	277.64	251.48	274.37	300.29
	5364	245.19	263.26	278.59	243.62	259.26	271.11	247.37	265.93	287.19
	4521	243.39	259.00	272.43	242.15	255.37	265.85	244.71	259.97	277.39
	3587	241.93	255.04	266.67	240.73	251.37	260.37	241.71	253.45	265.74
	3051	241.11	252.22	262.56	239.85	249.08	257.04	239.78	249.31	258.97
	2424	240.23	249.16	257.85	239.37	246.73	253.48	237.69	244.82	252.08
	1848	238.78	245.85	253.22	238.15	244.34	249.89	235.04	240.23	245.45
	1332	237.27	242.52	248.56	236.67	241.26	245.52	232.54	236.48	240.16
	960	234.12	237.81	241.93	233.71	236.67	239.45	229.19	232.69	235.08

TABLE 4

TEMPERATURE MEASUREMENTS AT THE EDGE OF THE COPPER PLATE

t_{10} °F	t_{11} °F	t_{12} °F;	T_{s4} °F	T_{f} °F	ΔT_4 °F
285.37	314.50	367.86	255.63	211.02	44.61
281.78	309.18	358.62	254.18	210.98	43.20
274.45	297.57	340.52	250.55	210.96	39.59
269.52	290.00	329.69	247.53	210.96	36.57
262.97	280.43	314.50	244.11	210.95	33.16
257.71	273.15	302.11	241.61	210.95	30.66
253.22	266.56	293.11	238.55	210.94	27.61
248.74	259.00	281.37	236.49	210.94	25.55
245.45	254.08	274.22	234.49	210.92	23.57
240.62	248.41	264.59	231.72	210.92	20.80
236.34	242.48	256.41	228.74	210.90	17.84
230.43	235.45	245.41	227.39	210.90	16.49
229.30	232.81	239.00	225.84	210.90	14.94
225.27	228.43	232.93	224.68	210.88	13.80
223.62	226.45	227.77	223.88	210.88	12.50

TABLE 5

COMPUTED MEAN TEMPERATURE DRIVING FORCE, ΔT_m

Run No.	T_{s1}	T_{s2}	T_{s3}	T_l	ΔT_1	ΔT_2	ΔT_3	ΔT_4	ΔT_m
Cu 1	243.25	243.50	248.66	211.34	31.91	32.16	37.32	43.20	37.51
	242.69	243.09	246.62	211.34	31.35	31.75	35.28	39.59	35.47
	242.40	242.67	245.29	211.44	30.96	31.23	33.85	36.57	33.86
	241.61	241.74	243.94	211.32	30.29	30.42	32.62	33.16	32.15
	240.19	240.18	241.23	210.41	29.78	29.77	30.82	30.66	30.48
	239.07	238.86	240.06	210.39	28.68	28.47	29.67	27.61	28.78
	238.16	238.09	238.02	210.41	27.75	27.68	27.61	25.55	27.06
	237.25	237.29	237.05	210.62	26.63	26.67	26.43	23.57	25.70
	236.64	236.60	236.24	210.65	25.99	25.95	25.59	20.80	24.36
	236.44	236.21	235.46	210.74	25.70	25.47	24.72	17.84	23.03
	236.33	236.31	234.45	211.11	25.22	25.20	23.34	16.49	21.95
	235.50	235.63	232.71	211.11	24.39	24.52	21.60	14.94	20.55
	234.61	234.74	230.88	211.09	23.52	23.65	19.79	13.80	19.19
	232.30	232.46	228.05	211.26	21.04	21.20	16.79	12.50	16.81
Cu 2	239.28	237.71	237.45	210.69	28.59	27.02	26.76	43.20	31.49
	238.39	236.86	236.84	210.69	27.70	26.17	26.15	39.59	29.98

Run No.	T_{s1}	T_{s2}	T_{s3}	T_{ℓ}	ΔT_1	ΔT_2	ΔT_3	ΔT_4	ΔT_m
	237.99	236.27	236.88	210.69	27.00	25.28	25.89	33.16	27.83
	236.49	234.81	235.71	210.99	25.50	23.82	24.72	30.66	26.21
	235.09	233.25	233.80	210.99	24.02	22.18	22.73	27.61	24.04
	233.83	232.01	232.76	211.07	22.76	20.94	21.69	25.55	22.66
	232.78	230.69	231.59	211.07	21.71	19.62	20.52	23.57	21.23
	230.84	231.15	232.46	211.09	19.75	20.06	21.37	20.80	20.83
	229.72	230.57	231.25	211.09	18.63	19.48	20.16	17.84	19.28
	228.83	229.79	230.42	211.02	17.81	18.77	19.40	16.49	18.36
	228.14	229.20	229.59	211.02	17.12	18.18	18.57	14.94	17.39
	227.81	228.41	227.92	210.98	16.83	17.43	16.94	13.80	16.17
	226.84	227.14	225.93	210.98	15.86	16.16	14.95	12.50	14.59
Cu 3	237.58	246.78	239.06	210.85	26.73	35.93	28.21	44.61	34.40
	236.48	244.39	237.70	210.88	25.60	33.51	26.82	43.20	32.79
	234.40	241.35	235.92	210.88	23.52	30.47	25.04	39.59	30.20
	233.71	239.46	234.16	210.92	22.79	28.54	23.24	36.57	28.10
	232.50	238.65	233.92	210.95	21.55	27.70	22.97	33.16	26.77

Run No.	T_{s1}	T_{s2}	T_{s3}	T_p	ΔT_1	ΔT_2	ΔT_3	ΔT_4	ΔT_m
	232.15	236.71	232.81	210.95	21.20	25.76	21.86	30.66	25.13
	231.48	235.66	232.19	210.95	20.53	24.71	21.24	27.61	23.74
	230.23	234.34	230.81	210.98	19.25	23.36	19.83	25.55	22.17
	229.38	232.61	230.14	211.01	18.37	21.60	19.13	23.57	20.87
	228.80	231.78	229.08	211.06	17.74	20.72	18.02	20.80	19.38
	228.18	230.27	228.30	211.07	17.11	19.20	17.23	17.84	17.83
	227.62	229.44	227.46	211.09	16.53	18.35	16.37	16.49	16.85
	227.04	228.32	226.59	211.09	15.95	17.23	15.50	14.94	15.75
	226.28	226.68	225.06	211.07	15.21	15.61	13.99	13.80	14.36
	225.10	224.67	223.61	211.07	14.03	13.60	12.54	12.50	12.85
Cu 4	239.27	240.29	244.98	210.22	29.05	30.07	34.76	44.61	36.14
	239.35	240.42	244.30	210.20	29.13	30.22	34.10	43.20	35.49
	237.71	238.89	241.56	210.19	27.52	28.70	31.37	39.59	32.85
	236.30	237.67	239.26	210.17	26.13	27.50	29.09	36.57	30.82
	234.40	235.89	236.81	210.05	24.35	25.84	26.76	33.16	28.20
	234.24	235.60	236.39	210.03	24.21	25.57	26.36	30.66	27.26

Run No.	T_{s1}	T_{s2}	T_{s3}	T_{ℓ}	ΔT_1	ΔT_2	ΔT_3	ΔT_4	ΔT_m
	231.78	233.43	233.70	209.90	21.88	23.53	23.80	27.61	24.69
	230.80	231.62	232.00	209.80	21.00	21.82	22.20	25.55	22.98
	228.79	230.11	230.50	209.80	18.99	20.31	20.70	23.57	21.32
	226.47	227.72	228.67	209.81	16.66	17.91	18.86	20.80	19.07
	225.91	226.73	227.57	209.83	16.08	16.90	17.74	17.84	17.49
	225.70	226.25	226.92	209.85	15.85	16.40	17.07	16.49	16.69
	225.74	226.05	226.00	209.90	15.84	16.15	16.10	14.94	15.77
	225.59	225.56	225.26	209.93	15.66	15.63	15.33	13.80	14.99
	225.23	224.70	224.19	209.95	15.28	14.75	14.24	12.50	13.93
Cu 5	240.27	240.38	238.19	210.41	29.86	29.97	27.78	43.20	32.67
	239.10	238.06	237.05	210.41	28.69	27.65	26.64	39.59	30.58
	237.05	236.74	235.38	210.41	26.64	26.33	24.97	36.57	28.59
	234.77	234.42	234.77	210.35	24.42	24.07	24.42	33.16	26.77
	234.21	233.64	234.06	210.35	23.86	23.29	23.71	30.66	25.56
	232.96	232.64	232.90	210.41	22.55	22.23	22.49	27.61	23.86
	232.01	231.68	231.89	210.42	21.59	21.26	21.47	25.55	22.56

Run No.	T_{s1}	T_{s2}	T_{s3}	T_v	ΔT_1	ΔT_2	ΔT_3	ΔT_4	ΔT_m
	230.68	230.44	230.70	210.42	20.26	20.02	20.28	23.57	21.14
	229.74	229.52	229.94	210.47	19.27	19.05	19.47	20.80	19.74
	229.25	228.90	229.37	210.45	18.80	18.45	18.92	17.84	18.51
	228.08	228.01	228.22	210.44	17.64	17.57	17.78	16.49	17.37
	227.49	227.21	227.42	210.45	17.04	16.76	16.97	14.94	16.36
	225.86	225.78	225.76	210.42	15.44	15.36	15.34	13.80	14.92
	225.25	225.14	224.95	210.44	14.81	14.70	14.51	12.50	14.01
Cu 6	238.75	240.97	239.13	211.41	27.34	29.56	27.72	44.61	32.80
	238.04	240.15	239.12	211.41	26.63	28.74	27.71	43.20	32.18
	236.98	239.29	239.07	211.40	25.58	27.89	27.67	39.59	30.91
	236.21	238.90	238.22	211.40	24.81	27.50	26.82	36.57	29.57
	235.51	237.59	237.06	211.43	24.08	26.16	25.63	33.16	27.75
	233.95	235.88	235.66	211.41	22.54	24.47	24.25	30.66	25.98
	233.26	235.33	235.15	211.41	21.85	23.92	23.74	27.61	24.75
	232.65	234.57	234.61	211.42	21.23	23.15	23.19	25.55	23.73
	231.85	233.84	233.90	211.45	20.40	22.39	22.45	23.57	22.63

Run No.	T_{s1}	T_{s2}	T_{s3}	T_{ℓ}	ΔT_1	ΔT_2	ΔT_3	ΔT_4	ΔT_m
	230.80	232.50	232.51	211.45	19.35	21.05	21.06	20.80	20.89
	230.87	232.22	232.29	211.52	19.35	20.70	20.77	17.84	19.86
	228.83	230.28	230.18	211.47	17.36	18.81	18.71	16.49	18.04
	228.26	228.94	229.66	211.47	16.79	17.47	18.19	14.94	17.05
	227.63	228.13	228.85	211.45	16.18	16.68	17.40	13.80	16.17
	227.18	227.26	227.64	211.43	15.75	15.83	16.21	12.50	15.07
Cu 7	238.27	241.16	241.30	211.47	26.80	29.69	29.83	39.59	32.34
	236.92	238.68	238.46	211.47	25.45	27.21	26.99	36.57	29.61
	235.98	237.34	237.33	211.50	24.48	25.84	25.83	33.16	27.79
	234.06	235.13	235.04	211.50	22.56	23.63	23.54	30.66	25.48
	233.23	233.68	234.98	211.47	21.76	22.21	23.51	27.61	24.26
	232.33	232.54	234.78	211.52	20.81	21.02	23.26	25.55	23.26
	231.69	231.49	234.04	211.52	20.17	19.97	22.52	23.57	22.11
	230.91	230.71	233.18	211.53	19.38	19.18	21.65	20.80	20.74
	230.50	230.08	232.90	211.52	18.98	18.56	21.38	17.84	19.64
	229.87	229.51	232.14	211.52	18.35	17.99	20.62	16.49	18.76

Run No.	T_{s1}	T_{s2}	T_{s3}	T_{ℓ}	ΔT_1	ΔT_2	ΔT_3	ΔT_4	ΔT_m
	229.21	228.93	231.28	211.50	17.71	17.43	19.78	14.94	17.80
	228.62	228.42	230.18	211.50	17.12	16.92	18.68	13.80	16.85
	227.97	227.77	228.65	211.50	16.47	16.27	17.15	12.50	15.62
Cu 8	246.60	242.93	234.05	211.31	35.29	31.62	22.74	43.20	31.09
	245.27	242.08	233.85	211.30	33.97	30.78	22.55	39.59	29.75
	243.44	240.64	233.38	211.31	32.13	29.33	22.07	36.57	28.27
	241.18	239.21	233.22	211.21	29.87	27.90	21.91	33.16	26.81
	239.18	237.85	233.37	211.32	27.86	26.53	22.05	30.66	25.76
	237.47	236.61	233.42	211.34	26.13	25.27	22.08	27.61	24.55
	235.98	235.26	233.01	211.34	24.64	23.92	21.67	25.55	23.41
	234.55	233.93	232.01	211.35	23.20	22.58	20.66	23.57	22.04
	233.69	233.13	231.73	211.34	22.35	21.79	20.39	20.80	20.92
	232.84	232.45	231.08	211.34	21.50	21.11	19.74	17.84	19.61
	231.88	231.62	230.50	211.34	20.54	20.28	19.16	16.49	18.74
	231.20	231.07	229.98	211.34	19.86	19.73	18.64	14.94	17.92
	230.57	230.34	229.24	211.34	19.25	19.00	17.90	13.80	17.08

Run No.	T_{s1}	T_{s2}	T_{s3}	T_{ℓ}	ΔT_1	ΔT_2	ΔT_3	ΔT_4	ΔT_m
	229.72	229.52	228.42	211.34	18.38	18.20	17.08	12.50	16.13
Cu 9	244.42	241.20	239.60	210.54	33.88	30.66	29.06	44.61	34.00
	243.82	240.60	239.14	210.53	33.29	30.07	28.61	43.20	33.25
	241.76	238.84	238.49	210.54	31.22	28.30	27.95	39.59	31.44
	241.00	238.48	238.17	210.59	30.41	27.89	27.58	36.47	30.30
	239.56	237.47	237.21	210.59	28.97	26.88	26.62	33.16	28.63
	238.04	236.34	235.82	210.61	27.43	25.73	25.21	30.66	26.96
	236.88	235.60	234.96	210.62	26.26	24.98	24.34	27.61	25.50
	235.31	234.63	233.89	210.62	24.69	24.01	23.27	25.55	24.15
	233.33	233.52	232.91	210.62	22.71	22.90	22.29	23.57	22.80
	231.94	232.88	231.81	210.64	21.30	22.24	21.17	20.80	21.31
	231.07	231.55	230.55	210.65	20.42	20.90	19.90	17.84	19.58
	230.64	230.69	229.33	210.65	19.99	20.04	18.68	16.49	18.45
	230.05	229.94	227.69	210.66	19.39	19.28	17.03	14.94	17.08
	228.96	228.86	226.49	210.67	18.29	18.19	15.82	13.80	15.92
	227.24	227.38	224.99	210.68	16.56	16.70	14.31	12.50	14.46

Run No.	T_{s1}	T_{s2}	T_{s3}	T_{ℓ}	ΔT_1	ΔT_2	ΔT_3	ΔT_4	ΔT_m
Cu 10A	237.70	247.63	238.73	211.28	26.42	36.35	27.45	44.61	34.14
	237.27	246.24	237.61	211.29	25.98	34.95	26.32	43.20	32.91
	237.72	244.72	237.84	211.30	26.42	33.42	26.54	39.59	31.69
	237.06	243.06	236.79	211.30	25.76	31.76	25.49	36.57	29.98
	235.95	241.43	236.16	211.31	24.64	30.12	24.85	33.16	28.32
	235.83	240.43	235.22	211.31	24.52	29.12	23.91	30.66	26.98
	234.75	239.26	234.22	211.31	23.44	27.95	22.91	27.61	25.36
	234.15	238.17	233.18	211.32	22.83	26.85	21.86	25.55	24.05
	233.47	236.93	232.89	211.32	22.15	25.61	21.57	23.57	23.06
	232.59	235.43	232.69	211.32	21.27	24.11	21.37	20.80	21.81
	231.70	233.85	232.29	211.34	20.30	22.51	20.95	17.84	20.40
	231.31	232.52	231.82	211.34	19.97	21.18	20.48	16.49	19.50
	231.08	231.59	231.28	211.34	19.74	20.25	19.94	14.94	18.61
	230.33	230.39	230.35	211.34	18.99	19.05	19.01	13.80	17.57
	229.62	229.13	229.07	211.34	18.28	17.79	17.73	12.50	16.32

Run No.	T_{s1}	T_{s2}	T_{s3}	T_{ℓ}	ΔT_1	ΔT_2	ΔT_3	ΔT_4	ΔT_m
Cu 10B	236.29	247.54	241.65	211.33	24.96	36.21	30.32	44.61	35.30
	235.74	246.58	240.40	211.33	24.41	35.25	20.07	43.20	34.11
	234.77	243.89	238.44	211.33	23.44	32.56	27.11	39.59	31.58
	233.95	241.75	236.87	211.34	22.61	30.41	25.53	36.57	29.52
	233.77	240.59	235.89	211.33	22.44	29.26	24.56	33.16	27.88
	233.44	239.81	235.08	211.33	22.11	28.48	23.75	30.66	26.63
	232.68	238.42	233.99	211.35	21.33	27.07	22.64	27.61	24.93
	231.85	237.05	232.91	211.38	20.47	25.67	21.53	25.55	23.51
	230.96	235.24	231.86	211.38	19.58	23.86	20.48	23.56	22.04
	230.04	233.52	230.71	211.38	18.66	22.14	19.33	20.80	20.33
	229.59	232.05	230.42	211.38	18.21	20.67	19.04	17.84	19.02
	229.21	230.97	229.59	211.39	17.82	19.58	18.20	16.49	18.01
	228.74	229.68	228.44	211.40	17.34	18.28	17.04	14.94	16.75
	227.94	228.57	227.24	211.40	16.54	17.17	15.84	13.80	15.60
	227.10	227.10	226.12	211.40	15.70	15.70	14.72	12.50	14.38

Run No.	T_{s1}	T_{s2}	T_{s3}	T_{ℓ}	ΔT_1	ΔT_2	ΔT_3	ΔT_4	ΔT_m
Cu 11	240.53	248.33	258.96	211.20	29.33	37.13	47.76	44.61	43.29
	239.00	247.16	258.50	211.20	27.80	35.96	47.30	43.20	42.76
	238.61	246.51	257.30	211.20	27.41	35.31	46.10	39.59	40.86
	238.26	245.70	255.30	211.21	27.05	34.49	44.09	36.57	38.92
	237.47	244.17	253.07	211.21	26.26	32.96	41.86	33.16	36.60
	236.70	243.30	250.43	211.20	25.50	32.10	39.23	30.66	34.50
	235.77	241.41	247.76	211.18	24.59	30.23	36.58	27.61	32.01
	235.10	240.33	245.29	211.18	23.92	29.15	34.11	25.55	30.06
	234.33	239.13	244.10	211.18	23.15	27.95	32.92	23.57	28.68
	233.60	237.27	240.71	211.18	22.42	26.09	29.53	20.80	25.94
	232.48	235.41	239.13	211.18	21.30	24.23	27.95	17.84	23.95
	231.90	233.92	236.35	211.18	20.72	22.74	25.17	16.49	21.97
	231.06	232.44	233.55	211.18	19.88	21.26	22.37	14.94	19.92
	230.28	231.05	231.67	211.18	19.10	19.87	20.49	13.80	18.42
	229.49	229.44	229.86	211.18	18.31	18.26	18.68	12.50	16.85

Run No.	T_{s1}	T_{s2}	T_{s3}	T_{ℓ}	ΔT_1	ΔT_2	ΔT_3	ΔT_4	ΔT_m
Cu 12	240.24	249.64	260.35	210.95	29.29	38.69	49.40	44.61	44.57
	239.78	240.50	259.86	210.95	28.83	38.55	48.91	43.20	43.91
	239.81	248.47	257.80	210.93	28.88	37.54	46.87	39.59	41.78
	239.83	247.49	255.38	210.90	28.93	36.59	44.48	36.57	39.67
	239.50	246.24	253.63	210.90	28.60	35.34	42.73	33.16	37.64
	238.64	244.12	250.46	210.88	27.76	33.24	39.58	30.66	35.04
	237.39	242.23	248.29	210.88	26.51	31.35	37.41	27.61	32.74
	236.01	240.52	245.13	210.88	25.13	29.64	34.25	25.55	30.30
	234.95	239.08	243.57	210.85	24.10	28.23	32.72	23.57	28.70
	233.82	237.89	238.57	210.85	22.97	27.04	27.72	20.80	25.38
	233.44	236.64	235.98	210.85	22.59	25.79	25.13	17.84	23.11
	233.26	235.12	234.77	210.82	22.44	24.30	23.95	16.49	21.87
	233.02	234.44	232.73	210.82	22.20	23.62	21.91	14.94	20.37
	231.73	232.29	230.60	210.72	21.01	21.57	19.88	13.80	18.63
	230.83	230.82	226.89	210.72	20.11	20.10	16.17	12.50	16.24

Run No.	T_{s1}	T_{s2}	T_{s3}	T_{ℓ}	ΔT_1	ΔT_2	ΔT_3	ΔT_4	ΔT_m
Cu 13	234.98	248.36	260.64	211.38	23.60	36.98	49.26	44.61	43.81
	235.00	247.48	259.79	211.38	23.62	36.10	48.41	43.20	42.85
	234.82	246.15	256.66	211.36	23.46	34.79	45.30	39.59	40.17
	234.26	244.46	253.58	211.34	22.92	33.12	42.24	36.57	37.57
	233.42	242.62	251.46	211.34	22.08	31.28	40.12	33.16	3 .22
	232.84	241.06	248.97	211.32	21.52	29.74	37.65	30.66	33.05
	232.39	239.20	246.87	211.32	21.07	27.88	35.55	27.61	30.84
	232.00	237.57	244.78	211.32	20.68	26.25	33.46	25.55	28.95
	231.43	235.76	242.19	211.35	20.08	24.41	30.84	23.57	26.79
	230.89	234.66	239.74	211.36	19.53	23.30	28.38	20.80	24.65
	230.52	233.92	237.63	211.36	19.16	22.56	26.27	17.84	22.71
	230.11	232.63	235.55	211.36	18.75	21.27	24.19	16.49	21.10
	229.77	231.51	233.91	211.36	18.41	20.15	22.55	14.94	19.67
	229.16	230.10	231.95	211.36	17.80	18.74	20.59	13.80	18.14
	228.39	228.65	229.44	211.38	17.01	17.27	18.06	12.50	16.28

Run No.	T_{s1}	T_{s2}	T_{s3}	T_{ℓ}	ΔT_1	ΔT_2	ΔT_3	ΔT_4	ΔT_m
Cu 14	237.51	251.42	246.61	211.05	26.46	40.37	35.56	44.61	38.64
	237.27	250.65	245.94	211.05	26.22	39.60	34.89	43.20	37.76
	237.21	247.84	246.40	211.05	26.16	36.79	35.35	39.59	36.34
	236.67	246.05	247.66	211.06	25.61	34.99	36.60	36.57	35.62
	235.87	244.29	246.39	211.07	24.80	33.22	35.32	33.16	33.67
	235.48	242.44	245.95	211.07	24.41	31.37	34.88	30.66	32.35
	234.66	240.90	245.21	211.07	23.59	29.83	34.14	27.61	30.78
	233.97	239.92	243.99	211.07	22.90	28.85	32.92	25.55	29.41
	233.30	238.07	242.52	211.07	22.23	27.00	31.45	23.57	27.76
	232.23	236.57	240.87	211.08	21.15	25.49	29.79	20.80	25.86
	231.19	234.56	238.17	211.08	20.11	23.48	27.09	17.84	23.33
	230.61	232.89	235.68	211.08	19.53	21.81	24.60	16.49	21.45
	230.10	231.21	232.84	211.08	19.02	20.13	21.76	14.94	19.35
	229.49	229.78	229.44	211.07	18.42	18.71	18.37	13.80	17.18
	228.21	227.77	226.45	211.07	17.14	16.70	15.38	12.50	14.97

Run No.	T_{s1}	T_{s2}	T_{s3}	T_{ℓ}	ΔT_1	ΔT_2	ΔT_3	ΔT_4	ΔT_m
Cu 15	228.98	239.77	247.83	210.75	18.23	29.02	37.08	44.61	36.33
	228.45	239.11	247.56	210.75	17.70	28.36	36.81	43.20	35.65
	229.19	238.10	245.68	210.73	18.46	27.37	34.95	39.59	33.64
	229.25	237.43	244.38	210.72	18.53	26.71	33.66	36.57	32.08
	229.77	236.96	243.51	210.70	19.07	26.26	32.81	33.16	30.69
	229.56	235.66	242.62	210.68	18.88	24.98	31.94	30.66	29.31
	229.95	235.05	240.95	210.66	19.29	24.39	30.29	27.61	27.62
	230.13	234.23	239.76	210.65	19.48	23.58	29.11	25.55	26.36
	229.72	233.68	238.62	210.62	19.10	23.06	28.00	23.57	25.18
	229.73	233.04	237.75	210.62	19.11	22.42	27.13	20.80	23.88
	229.46	231.93	236.23	210.61	18.85	21.32	25.62	17.84	22.13
	228.70	230.51	234.30	210.59	18.11	19.92	23.71	16.49	20.55
	228.36	229.49	231.98	210.59	17.77	18.90	21.39	14.94	18.84
	227.89	228.16	229.74	210.59	17.30	17.57	19.15	13.80	17.21
	226.92	226.73	227.43	210.59	16.33	16.14	16.84	12.50	15.45

Run No.	T_{s1}	T_{s2}	T_{s3}	T_l	ΔT_1	ΔT_2	ΔT_3	ΔT_4	ΔT_m
Ni 1	232.29	244.22	247.48	210.85	21.44	33.37	36.63	44.61	37.28
	232.45	244.05	248.13	210.85	21.60	33.20	37.28	43.20	37.15
	233.07	243.48	246.89	210.85	22.22	32.63	36.04	39.59	35.50
	233.18	242.41	245.25	210.85	22.33	31.56	34.40	36.57	33.70
	233.32	241.62	244.07	210.88	22.44	30.74	33.19	33.16	32.04
	233.33	240.85	243.74	210.88	22.45	29.97	32.86	30.66	31.03
	233.54	239.57	242.59	210.88	22.66	28.69	31.71	27.61	29.40
	233.86	238.83	241.65	210.92	22.94	27.91	30.73	25.55	28.23
	233.52	237.70	239.93	210.95	22.60	26.75	28.98	23.57	26.63
	233.57	236.50	239.56	210.95	22.62	25.55	28.61	20.80	25.43
	233.26	235.01	238.14	210.95	22.31	24.06	27.19	17.84	23.63
	233.13	233.69	237.13	210.95	22.18	22.74	26.18	16.49	22.50
	232.93	232.09	234.91	210.95	21.98	21.14	23.96	14.94	20.72
	232.36	230.82	233.32	210.95	21.41	19.87	22.37	13.80	19.38
	231.10	228.89	231.10	210.95	20.15	17.94	20.15	12.50	17.53

Run No.	T_{s1}	T_{s2}	T_{s3}	T_l	ΔT_1	ΔT_2	ΔT_3	ΔT_4	ΔT_m
Ni 2	230.69	239.59	246.34	211.05	19.64	28.54	35.29	45.42	35.73
	231.73	239.28	245.22	211.05	20.68	28.23	34.17	43.20	34.61
	231.49	238.35	244.14	211.05	20.44	27.30	33.09	39.59	32.91
	231.14	237.57	242.78	211.08	20.06	26.49	31.70	36.57	31.25
	230.92	236.52	241.52	211.08	19.84	25.44	30.44	33.16	29.50
	230.50	236.34	240.62	211.11	19.39	25.23	29.51	30.66	28.32
	230.54	235.41	239.42	211.12	19.42	24.29	28.30	27.61	26.72
	230.33	234.58	238.62	211.14	19.19	23.44	27.48	25.55	25.59
	230.52	233.73	238.12	211.16	19.36	22.57	26.96	23.57	24.62
	230.22	232.77	236.97	211.18	19.14	21.59	25.79	20.80	23.10
	229.93	231.76	236.02	211.24	18.69	20.52	24.78	17.84	21.57
	229.64	230.48	234.62	211.31	18.33	19.17	23.31	16.49	20.22
	229.39	229.42	233.23	211.34	18.05	18.08	21.89	14.94	18.90
	229.21	228.48	231.62	211.38	17.83	17.10	20.24	13.80	17.62
	228.52	227.31	230.02	211.41	17.11	15.90	18.61	12.50	16.23

Run No.	T_{s1}	T_{s2}	T_{s3}	T_{ℓ}	ΔT_1	ΔT_2	ΔT_3	ΔT_4	ΔT_m
Ni 3	244.93	254.86	255.03	210.45	34.48	44.41	44.58	45.42	44.21
	244.04	253.19	253.02	210.49	33.55	42.70	42.53	43.20	42.26
	242.55	251.10	250.25	210.52	32.03	40.58	39.73	39.59	39.45
	241.07	248.89	248.02	210.55	30.52	38.34	37.47	36.57	37.03
	239.57	246.61	245.69	210.55	29.02	36.06	35.14	33.16	34.45
	238.64	244.94	243.92	210.57	28.07	34.37	33.35	30.66	32.54
	237.40	243.09	241.59	210.57	26.83	32.52	31.02	27.61	30.17
	236.57	241.66	240.44	210.65	25.92	31.01	29.79	25.55	28.67
	235.68	240.05	238.44	210.68	25.00	29.37	27.76	23.57	26.80
	234.38	238.03	236.58	210.68	23.70	27.35	25.90	20.80	24.68
	233.14	235.29	234.57	210.68	22.46	24.61	23.89	17.84	22.29
	232.76	233.96	233.07	210.68	22.08	23.28	22.39	16.49	20.93
	232.63	232.79	232.37	210.68	21.95	22.11	21.69	14.94	19.92
	231.97	231.06	230.95	210.68	21.29	20.38	20.27	13.80	18.55
	230.52	228.84	228.74	210.68	19.84	18.16	18.06	12.50	16.64

Run No.	T_{s1}	T_{s2}	T_{s3}	T_p	ΔT_1	ΔT_2	ΔT_3	ΔT_4	ΔT_m
Ni 4	251.20	255.35	259.07	211.48	39.20	43.35	47.07	44.61	45.12
	250.27	253.61	257.67	211.45	38.82	42.16	46.22	43.20	44.07
	249.00	251.91	255.39	211.43	37.57	40.48	43.96	39.59	41.62
	247.41	249.53	253.06	211.41	36.00	38.12	41.65	36.57	39.14
	245.86	247.56	250.54	211.38	34.48	36.18	39.16	33.16	36.57
	244.05	245.54	248.11	211.34	32.71	34.20	36.77	30.66	34.28
	242.76	243.43	246.08	211.31	31.45	32.12	34.77	27.61	32.00
	240.44	240.81	243.27	211.29	29.15	29.52	31.98	25.55	29.49
	239.14	238.64	241.26	211.26	27.88	27.38	30.00	23.57	27.51
	237.29	236.90	239.55	211.22	26.07	25.68	28.33	20.80	25.52
	235.53	234.71	237.72	211.16	24.37	23.55	26.56	17.84	23.35
	233.69	232.76	235.97	211.11	22.58	21.65	24.86	16.49	21.69
	232.81	231.44	234.48	211.06	21.75	20.38	23.42	14.94	20.30
	231.65	229.91	232.30	211.01	20.64	18.90	21.29	13.80	18.64
	230.33	227.92	230.36	210.95	19.38	16.97	19.41	12.50	16.95

Run No.	T_{s1}	T_{s2}	T_{s3}	T_{ℓ}	ΔT_1	ΔT_2	ΔT_3	ΔT_4	ΔT_m
Cr 1	243.97	252.68	253.19	211.08	32.89	41.60	42.11	45.42	42.40
	242.38	251.52	251.77	211.02	31.36	40.50	40.75	44.61	41.25
	241.73	250.53	247.99	210.98	30.75	39.55	37.01	43.20	38.95
	240.17	248.36	246.86	210.96	29.21	37.40	35.90	39.59	36.89
	239.49	246.83	245.40	210.96	28.53	35.87	34.44	36.57	35.02
	238.25	244.41	252.18	210.95	27.30	33.46	31.23	33.16	32.04
	236.87	242.50	240.43	210.95	25.92	31.55	29.48	30.66	30.07
	235.49	240.87	238.90	210.94	24.55	29.93	27.96	27.61	28.11
	234.48	238.70	235.54	210.94	23.54	27.76	24.60	25.55	25.51
	233.66	237.45	235.20	210.92	22.74	26.53	24.28	23.57	24.49
	233.02	235.96	233.99	210.92	22.10	25.04	23.07	20.80	22.82
	232.20	234.26	231.77	210.90	21.40	23.36	20.87	17.84	20.61
	231.12	232.18	229.80	210.90	20.22	21.28	18.90	16.49	18.83
	230.30	230.55	227.94	210.90	19.40	19.65	17.04	14.94	17.17
	229.00	228.31	225.19	210.88	18.12	17.43	14.31	13.80	15.07
	227.59	226.14	222.17	210.88	16.71	15.26	11.29	12.50	12.81

Run No.	T_{s1}	T_{s2}	T_{s3}	T_{ℓ}	ΔT_1	ΔT_2	ΔT_3	ΔT_4	ΔT_m
Br 1	249.87	263.28	266.51	211.07	38.80	52.21	55.44	51.41	52.01
	249.02	257.31	255.93	211.07	37.95	46.24	44.86	51.06	46.51
	247.13	255.30	253.48	211.07	36.06	44.23	42.41	49.22	44.35
	245.53	252.84	251.42	211.07	34.46	41.77	40.35	44.72	41.55
	244.15	250.95	249.77	211.07	33.08	39.88	38.70	41.00	39.29
	242.61	248.48	248.88	211.08	31.53	37.40	37.80	36.29	36.94
	241.10	246.13	245.09	211.08	30.02	35.05	34.01	33.45	33.86
	239.69	243.94	243.63	211.11	28.58	32.83	32.52	29.91	31.64
	238.65	241.40	245.09	211.14	27.51	30.26	33.95	27.36	30.94
	237.56	239.32	244.65	211.18	26.38	28.14	33.47	23.68	29.17
	236.86	237.49	241.74	211.21	25.65	26.28	30.53	21.75	26.88
	235.74	235.27	237.53	211.24	24.50	24.03	26.29	21.36	24.32
	234.54	233.59	234.27	211.28	23.26	22.31	22.99	19.68	21.93
	233.09	231.91	231.42	211.31	21.78	20.60	20.11	17.73	19.65
	231.18	229.42	228.14	211.31	19.87	18.11	16.83	15.66	16.96

Run No.	T_{s1}	T_{s2}	T_{s3}	T_{ℓ}	ΔT_1	ΔT_2	ΔT_3	ΔT_4	ΔT_m
Br 2	243.21	243.03	248.71	210.98	32.23	32.05	37.73	51.41	39.96
	241.19	240.54	247.38	210.99	30.20	29.55	36.39	51.06	38.60
	240.09	239.65	246.23	211.01	29.08	28.64	35.22	49.22	37.31
	239.04	239.16	245.36	211.01	28.03	28.15	34.35	44.72	35.50
	238.03	238.18	244.50	211.02	27.01	27.16	33.48	41.00	33.81
	236.92	237.63	242.68	211.05	25.87	26.58	31.63	36.29	31.48
	235.88	236.46	241.66	211.07	24.81	25.39	30.59	33.45	29.91
	234.54	235.24	239.35	211.09	23.45	24.15	28.26	29.91	27.54
	233.83	234.08	238.21	211.11	22.72	22.97	27.10	27.36	26.01
	233.09	232.88	236.96	211.11	21.98	21.77	25.85	23.68	24.13
	232.38	232.12	236.20	211.13	21.25	20.99	25.07	21.75	23.03
	231.32	231.05	234.79	211.15	20.17	19.90	23.64	21.36	21.98
	230.78	230.03	234.27	211.15	19.63	18.88	23.12	19.68	21.03
	229.54	228.91	232.75	211.18	18.36	17.73	21.57	17.73	19.47
	228.55	227.45	230.89	211.20	17.35	16.25	19.69	15.66	17.68

TABLE 6

TEMPERATURE MEASUREMENTS AND COMPUTED HEAT LOSS FROM THE STAINLESS STEEL FIN

Run No.	Q Btu	t_{13}	t_{14}	θ_0	θ_1	θ_m	Heat Loss Btu
A	42200	229.10	215.16	231.50	212.86	222.18	1631
	39063	227.28	214.90	229.44	212.80	221.12	1591
	33985	224.40	214.42	226.10	212.72	219.41	1530
	29610	223.50	214.41	225.12	212.68	218.90	1481
	25953	223.22	214.20	224.83	212.63	218.48	1452
	22656	220.95	213.70	224.24	212.52	217.38	1398
	19427	220.20	212.60	221.51	211.35	216.43	1357
	16253	219.48	211.90	220.75	210.59	215.67	1318
	14003	218.80	210.92	220.14	209.60	214.87	1273
	11400	218.36	210.15	219.81	208.75	214.28	1235
	9339	217.94	209.83	219.32	208.50	213.91	1207
	7395	217.46	208.62	218.98	207.14	213.06	1132
	5850	216.95	208.35	218.50	206.90	212.70	1090
	4248	216.60	208.50	218.02	207.12	212.57	1070
	3225	216.22	208.55	217.57	207.33	212.45	1052
B	36180	226.12	217.91	227.50	216.54	222.02	1561
	33223	224.62	216.88	225.97	215.55	220.76	1520
	31157	223.33	214.70	224.82	213.28	219.05	1463
	27248	222.10	212.72	223.73	211.03	217.38	1401
	24895	221.30	212.14	222.81	210.75	216.78	1362
	22372	220.32	211.50	221.50	210.02	215.94	1330
	18721	219.43	211.16	220.84	209.76	215.28	1291
	15737	218.93	211.00	220.32	209.64	214.96	1270
	13347	218.70	210.72	220.12	209.40	214.76	1256
	10690	218.20	210.42	219.56	209.12	214.01	1225
	9036	217.80	210.30	219.10	208.98	214.01	1200
	7200	217.42	210.12	218.71	208.91	213.81	1181

Run No.	Q Btu	t_{13}	t_{14}	θ_0	θ_1	θ_m	Heat Loss Btu
	6284	217.00	210.03	218.24	208.84	213.54	1154
	5717	216.90	209.61	218.21	208.41	213.31	1132
	4337	216.71	209.58	217.98	208.38	213.18	1117

TABLE 7

HEAT FLUX vs TEMPERATURE DIFFERENCE

Run No.	Total Heat Input, Q Btu/Hr.	Fin Loss Btu/Hr.	% Heat Loss	Heat Flux Q/A, Btu/Hr.Ft^2	ΔT_m, ^oF
Cu 1	42390	1643	3.9	209740	37.51
	37598	1576	4.2	185600	35.47
	33092	1513	4.6	162890	33.86
	28874	1453	5.0	141620	32.15
	25086	1400	5.6	122530	30.48
	21430	1349	6.3	104100	28.78
	18307	1305	7.1	88360	27.06
	15430	1264	8.2	73860	25.70
	12242	1220	10.0	57790	24.36
	10413	1193	11.5	48570	23.03
	8273	1164	14.0	37790	21.95
	6307	1136	18.0	27880	20.55
	4546	1111	25.5	19000	19.19
	3277	1094	33.4	12610	16.81
Cu 2	42390	1643	3.9	209740	31.49
	37598	1576	4.2	185590	29.98
	28874	1453	5.0	141620	27.83
	21563	1351	6.3	121800	26.21
	18430	1307	7.1	104770	24.04
	15430	1264	8.2	88980	22.66
	12901	1229	9.5	73860	21.23
	10524	1195	11.4	61120	20.83
	8273	1164	14.0	49130	19.28
	6451	1138	17.6	37790	18.36
	5457	1124	20.6	28610	17.39
	4669	1113	23.8	19620	16.17
	3276	1094	33.4	12600	14.59

Run No.	Total Heat Input, Q Btu/Hr.	Fin Loss Btu/Hr.	% Heat Loss	Heat Flux Q/A, Btu/Hr.Ft^2	ΔT_m, ^oF
Cu 3	44946	1679	3.7	222630	34.40
	42390	1643	3.9	209740	32.79
	37424	1574	4.2	184720	30.20
	33256	1515	4.6	163710	28.10
	28874	1453	5.0	141620	26.77
	25086	1400	5.6	122530	25.13
	21563	1351	6.3	104770	23.74
	18430	1307	7.1	88980	22.17
	15655	1268	8.1	75000	20.87
	12952	1230	9.5	61370	19.38
	10505	1195	11.4	49040	17.83
	8191	1163	14.2	37380	16.85
	6379	1137	17.8	28240	15.75
	4577	1112	24.3	19160	14.36
	3276	1094	33.4	12600	12.85
Cu 4	44273	1670	3.8	219240	36.14
	42389	1643	3.9	209750	35.49
	37423	1574	4.2	184710	32.85
	33092	1513	4.6	162890	30.82
	28874	1453	5.0	141620	28.20
	25086	1400	5.6	122530	27.26
	21563	1351	6.3	104770	24.69
	18430	1307	7.1	88980	22.98
	15543	1266	8.1	74430	21.32
	12901	1229	9.5	61110	19.07
	10505	1195	11.3	49040	17.49
	8273	1164	14.2	37790	16.69
	6343	1137	17.9	28060	15.77
	4669	1113	23.8	19620	14.99
	3225	1093	33.9	12350	13.93

Run No.	Total Heat Input, Q Btu/Hr.	Fin Loss Btu/Hr.	% Heat Loss	Heat Flux Q/A, Btu/Hr.Ft^2	ΔT_m, °F
Cu 5	42390	1643	3.9	209740	32.67
	37598	1576	4.2	185590	30.58
	33092	1513	4.6	162890	28.59
	28874	1453	5.0	141620	26.77
	25229	1402	5.6	123200	25.56
	21696	1353	6.2	105450	23.86
	18430	1307	7.1	88980	22.56
	15543	1266	8.1	74430	21.14
	12799	1227	9.6	60600	19.74
	10505	1195	11.4	49040	18.51
	8191	1163	14.2	37380	17.37
	6307	1136	18.0	27880	16.36
	4669	1113	23.8	19620	14.92
	3276	1094	33.4	12610	14.01
Cu 6	44703	1676	3.7	221400	32.80
	42390	1643	3.9	209740	32.18
	37772	1579	4.2	186470	30.91
	33256	1515	4.6	163710	29.57
	29181	1458	5.0	143170	27.75
	25229	1402	5.6	123250	25.98
	21563	1351	6.3	104770	24.75
	18737	1311	7.0	90530	23.73
	15486	1265	8.2	74140	22.63
	12696	1226	9.7	60080	20.89
	10413	1194	11.5	48590	19.86
	8191	1163	14.2	37380	18.04
	6343	1137	17.9	28060	17.05
	4577	1112	24.3	19160	16.17
	3200	1092	34.1	12220	15.07

Run No.	Total Heat Input, Q Btu/Hr.	Fin Loss Btu/Hr.	% Heat Loss	Heat Flux Q/A, Btu/Hr.Ft^2	ΔT_m, ^oF
Cu 7	39325	1600	4.1	194300	32.34
	33584	1520	4.5	165360	29.61
	29335	1460	5.0	143950	27.79
	25229	1402	5.6	123250	25.48
	21830	1354	6.2	106120	24.26
	18430	1307	7.1	88980	23.26
	15543	1266	8.1	74430	22.11
	12799	1227	9.6	60600	20.74
	10505	1195	11.4	49040	19.64
	8232	1163	14.1	37580	18.76
	6307	1136	18.0	27880	17.80
	4669	1113	23.8	19620	16.85
	3200	1092	34.1	12220	15.62
Cu 8	43792	1663	3.8	216810	31.09
	38922	1595	4.1	192270	29.75
	33256	1515	4.6	163710	28.27
	29181	1458	5.0	143170	26.81
	25229	1402	5.6	123250	25.76
	21830	1354	6.2	106120	24.55
	18430	1307	7.1	88980	23.41
	15318	1263	8.2	73290	22.04
	12901	1229	9.5	61120	20.92
	10367	1193	11.5	48340	19.61
	8191	1163	14.2	37380	18.74
	6307	1136	18.0	27880	17.92
	4577	1112	24.3	19160	17.08
	3200	1092	34.1	12220	16.13

Run No.	Total Heat Input, Q Btu/Hr.	Fin Loss Btu/Hr.	% Heat Loss	Heat Flux Q/A, Btu/Hr.Ft^2	ΔT_m, ^oF
Cu 9	44893	1679	3.7	229460	34.00
	42390	1643	3.9	216350	33.25
	37946	1581	4.2	193090	31.44
	32765	1508	4.6	165970	30.30
	29181	1458	5.0	147210	28.63
	25229	1402	5.6	126520	26.96
	21563	1351	6.3	107330	25.50
	18430	1307	7.1	90920	24.15
	15543	1266	8.1	75810	22.80
	12799	1227	9.6	61440	21.31
	10505	1195	11.4	49430	19.58
	81'	1163	14.2	37320	18.45
	6451	1138	17.6	28210	17.08
	4608	1112	24.1	18560	15.92
	3174	1092	34.4	11050	14.46
Cu 10A	44703	1676	3.7	228470	34.14
	42390	1643	3.9	216350	32.91
	37598	1576	4.2	191270	31.69
	33256	1515	4.6	168540	29.98
	28874	1453	5.0	145600	28.32
	25086	1400	5.6	125770	26.98
	21696	1352	6.2	108020	25.36
	18430	1307	7.1	90920	24.05
	15430	1264	8.2	75220	23.06
	12799	1227	9.6	61440	21.81
	10413	1194	11.4	48950	20.40
	8191	1163	14.2	37320	19.50
	6307	1136	18.0	27460	18.61
	4602	1112	24.2	18560	17.57
	3174	1092	34.4	11050	16.32

Run No.	Total Heat Input, Q Btu/Hr.	Fin Loss Btu/Hr.	% Heat Loss	Heat Flux Q/A, Btu/Hr.Ft^2	ΔT_m, ^oF
Cu 10B	44703	1676	3.7	228470	35.30
	42389	1643	3.9	216350	34.11
	37598	1576	4.2	191270	31.58
	32929	1510	4.6	166820	29.52
	28874	1453	5.0	145600	27.88
	25086	1400	5.6	125760	26.63
	21563	1351	6.2	107330	24.93
	18430	1307	7.1	90930	23.51
	15430	1264	8.2	75220	22.04
	12696	1226	9.7	60900	20.33
	10321	1193	11.6	48470	19.02
	8191	1163	14.2	37320	18.01
	6164	1134	18.4	26710	16.75
	4608	1112	24.1	18560	15.60
	3123	1091	34.9	10790	14.38
Cu 11	44514	1673	3.8	227480	43.29
	42205	1641	3.9	219390	42.76
	37424	1574	4.2	190360	40.86
	33092	1513	4.6	167680	38.92
	28874	1453	5.0	145600	36.60
	25086	1400	5.6	125770	34.50
	21430	1349	6.3	106630	32.01
	18430	1307	7.1	90920	30.06
	15430	1264	8.2	75220	28.68
	12799	1227	9.6	61440	25.95
	10321	1193	11.6	48470	23.95
	8191	1163	14.2	37320	21.97
	6236	1135	18.2	27080	19.92
	4608	1112	24.1	18560	18.42
	3174	1092	34.4	11050	16.85

Run No.	Total Heat Input, Q Btu/Hr.	Fin Loss Btu/Hr.	% Heat Loss	Heat Flux Q/A, Btu/Hr.Ft^2	ΔT_m, $^\circ$F
Cu 12	44514	1673	3.8	227480	44.57
	42574	1646	3.9	217320	43.91
	37424	1574	4.2	190360	41.78
	32765	1508	4.6	165970	39.67
	28874	1453	5.0	145600	37.64
	25086	1400	5.6	125770	35.04
	21563	1351	6.3	107330	32.74
	18431	1307	7.1	90920	30.30
	15543	1266	8.1	75810	28.70
	12799	1227	9.6	61440	25.38
	10505	1195	11.4	49430	23.11
	8191	1163	14.2	37320	21.87
	6164	1134	18.4	26710	20.37
	4608	1112	24.1	18560	18.63
	3174	1092	34.4	11050	16.24
Cu 13	44514	1673	3.8	227480	43.81
	42574	1646	3.9	217320	42.85
	37946	1581	4.2	193090	40.17
	33092	1513	4.6	167680	37.57
	28720	1451	5.1	144790	35.22
	25229	1402	5.6	126520	33.05
	21563	1351	6.3	107330	30.84
	18430	1307	7.1	90920	28.95
	15430	1264	8.2	75220	26.79
	12799	1227	9.6	61440	24.65
	10321	1193	11.6	48470	22.71
	8355	1165	13.9	38180	21.10
	6236	1135	18.2	27080	19.67
	4608	1112	24.1	18560	18.14
	3174	1092	34.4	11050	16.28

Run No.	Total Heat Input, Q Btu/Hr.	Fin Loss Btu/Hr.	% Heat Loss	Heat Flux Q/A, Btu/Hr.Ft^2	ΔT_m, ^oF
Cu 14	45651	1689	3.7	233430	38.64
	43310	1656	3.8	221180	37.76
	38294	1586	4.1	194910	36.34
	33584	1520	4.5	170260	35.62
	29795	1466	4.9	150420	33.67
	25802	1410	5.5	129520	32.35
	21963	1356	6.2	109420	30.78
	18798	1311	7.0	84320	29.41
	15881	1270	8.0	77580	27.76
	13208	1233	9.3	63590	25.86
	10690	1198	11.2	50400	23.33
	8437	1166	13.8	38610	21.45
	6594	1140	17.3	28580	19.35
	4608	1112	24.1	18560	17.18
	3328	1094	32.9	11860	14.97
Cu 15	45461	1687	3.7	232430	36.33
	42758	1649	3.9	218280	35.65
	37598	1576	4.2	191270	33.64
	33420	1517	4.5	169400	32.08
	30391	1475	4.9	153540	30.69
	25516	1406	5.5	128020	29.31
	21963	1356	6.2	109420	27.62
	18676	1310	7.0	92210	26.36
	15993	1272	8.0	78170	25.18
	13106	1232	9.4	63050	23.88
	10597	1195	11.3	49920	22.13
	8437	1166	13.8	38610	20.55
	6522	1139	17.5	28580	18.84
	4608	1112	24.1	18560	17.21
	3328	1094	32.9	11860	15.45

Run No.	Total Heat Input, Q Btu/Hr.	Fin Loss Btu/Hr.	% Heat Loss	Heat Flux Q/A, Btu/Hr.Ft^2	ΔT_m, ^oF
Ni 1	45326	1685	3.7	232030	37.28
	43420	1658	3.8	222160	37.15
	37946	1581	4.2	200580	35.50
	32765	1508	4.6	177340	33.70
	29335	1460	5.0	154480	32.04
	25802	1410	5.5	136060	31.03
	21963	1356	6.2	115450	29.40
	18430	1307	7.1	94270	28.23
	15881	1271	8.0	79080	26.63
	13106	1232	9.4	62900	25.43
	10597	1195	11.2	49200	23.63
	8355	1165	13.9	39380	22.50
	6307	1136	18.0	30870	20.72
	4608	1112	24.1	23380	19.38
	3225	1093	33.9	14030	17.53
Ni 2	46970	1708	3.6	242440	35.73
	42390	1644	3.9	221510	34.61
	38120	1583	4.2	201150	32.91
	33584	1520	4.5	177820	31.25
	29335	1460	5.0	155760	29.50
	25516	1406	5.5	134420	28.32
	22096	1358	6.1	115170	26.72
	18799	1312	7.0	96720	25.59
	15881	1271	8.0	81190	24.62
	13208	1233	9.3	65000	23.10
	10690	1198	11.2	51130	21.57
	8437	1166	13.8	40460	20.22
	6379	1137	17.8	32280	18.90
	4669	1113	23.8	23310	17.62
	3328	1094	32.9	14260	16.23

Run No.	Total Heat Input, Q Btu/Hr.	Fin Loss Btu/Hr.	% Heat Loss	Heat Flux Q/A, Btu/Hr.Ft^2	ΔT_m, ^oF
Ni 3	47857	1720	3.6	244980	44.21
	43792	1663	3.8	223700	42.26
	37772	1579	4.2	192180	39.45
	33748	1522	4.5	171110	37.03
	29488	1462	5.0	148810	34.45
	26461	1420	5.4	132960	32.54
	22096	1358	6.1	110110	30.17
	19167	1317	6.9	94780	28.67
	16106	1274	7.9	78760	26.80
	13311	1235	9.3	64120	24.68
	10597	1196	11.3	49920	22.29
	8437	1166	13.8	38610	20.93
	6451	1138	17.6	28210	19.92
	4587	1112	24.2	18450	18.55
	3225	1093	33.9	11320	16.64
Ni 4	45474	1686	3.7	237020	45.12
	43433	1658	3.8	226330	44.07
	39107	1597	4.1	203690	41.62
	33758	1522	4.5	175680	39.14
	29651	1464	4.9	154180	36.57
	25810	1410	5.5	134070	34.28
	22235	1360	6.1	115360	32.00
	19050	1315	6.9	98680	29.49
	15998	1272	8.0	82700	27.51
	13417	1236	9.2	69190	25.52
	10877	1200	11.0	55900	23.35
	8439	1166	13.8	43130	21.69
	6524	1139	17.5	33110	20.30
	4732	1114	23.5	23720	18.64
	3329	1094	32.9	16380	16.95

Run No.	Total Heat Input, Q Btu/Hr.	Fin Loss Btu/Hr.	% Heat Loss	Heat Flux, Q/A Btu/Hr.Ft^2	ΔT_m, °F
Cr 1	47482	1715	3.6	247460	42.40
	45285	1684	3.7	235960	41.25
	43139	1654	3.8	224730	38.95
	37608	1576	4.2	195790	36.89
	33593	1520	4.5	174770	35.02
	29343	1460	5.0	152530	32.04
	25523	1406	5.5	132530	30.07
	22369	1362	6.1	116020	28.11
	18804	1312	7.0	97370	25.51
	15998	1272	8.0	82680	24.49
	13315	1235	9.3	68640	22.82
	10693	1198	11.2	54910	20.61
	8603	1168	13.6	43980	18.83
	6596	1140	17.3	33470	17.17
	4670	1113	23.8	23400	15.07
	3328	1094	32.9	16370	12.81
Br 1	48779	1733	3.6	249810	52.01
	43754	1663	3.8	223500	46.51
	38885	1594	4.1	198010	44.35
	34413	1531	4.4	174600	41.55
	30214	1472	4.9	152610	39.29
	26192	1416	5.4	131560	36.94
	22590	1365	6.0	112700	33.86
	19255	1318	6.8	95240	31.64
	16186	1275	7.9	79170	30.94
	13349	1235	9.3	64320	29.17
	10877	1200	11.0	51380	26.88
	8631	1169	13.5	39620	24.32
	6644	1141	17.2	29220	21.93
	4855	1116	23.0	19850	19.65
	3380	1095	32.4	12130	16.96

Run No.	Total Heat Input, Q Btu/Hr.	Fin Loss Btu/Hr.	% Heat Loss	Heat Flux, Q/A Btu/Hr.Ft^2	ΔT_m, ^oF
Br 2	49298	1741	3.5	252530	39.96
	44123	1668	3.8	225430	38.60
	39002	1596	4.1	198620	37.31
	34468	1532	4.4	174890	35.50
	30368	1474	4.9	153420	33.81
	26383	1418	5.4	132560	31.48
	22679	1366	6.0	113170	29.91
	19337	1319	6.8	95670	27.54
	16298	1277	7.8	79760	26.01
	13519	1238	9.2	65220	24.13
	10938	1201	11.0	51700	23.03
	8603	1168	13.6	39480	21.98
	6715	1142	17.0	29590	21.03
	4855	1116	23.0	19850	19.47
	3380	1095	32.4	12130	17.68

TABLE 8

SLOPE AND COEFFICIENT OF CORRELATION OF Q/A vs ΔT_m PLOTS

Run No.	Grains/inch	Slope of the Q/A vs ΔT Plot	Correlation Coefficient
Cu 12	1678	2.802	0.990
13	1550	2.864	0.987
11	1445	2.938	0.992
14	1216	3.073	0.998
15	955	3.438	0.997
9	730	3.337	0.991
2	620	3.562	0.987
10A	584	3.845	0.980
6	512	3.453	0.988
7	400	3.733	0.975
8	146	4.091	0.983
Ni 4	1300	2.592	0.991
3	1033	2.953	0.981
1	850	3.642	0.997
2	675	3.482	0.993
Cr 1	too small	2.297	0.997
Br 1	too small	2.781	0.993
2	~2000	3.441	0.982

TABLE 9

EVALUATION OF CONSTANTS OF THE
ROHSENOW CORRELATION FOR HEAT TRANSFER SURFACES OF VARYING GRAIN SIZE

Run No.	Grains per inch	C_{sf1}	Slope	$r_1=1/\text{Slope}$	C_{sf2}	r_2	C_{sf3}	r_3
Cu 12	1678	0.0175	2.858	0.350	0.0175	0.33	0.0175	0.30
13	1550	0.0169	2.943	0.340	0.0169	0.33	0.0168	0.30
11	1445	0.0174	2.987	0.335	0.0174	0.33	0.0174	0.30
14	1216	0.0162	3.085	0.324	0.0162	0.33	0.0162	0.30
15	955	0.0151	3.461	0.289	0.0151	0.33	0.0151	0.30
9	730	0.0140	3.401	0.294	0.0140	0.33	0.0140	0.30
10A	584	0.0144	4.008	0.250	0.0145	0.33	0.0144	0.30
6	512	0.0139	3.535	0.283	0.0139	0.33	0.0139	0.30
7	400	0.0138	3.926	0.255	0.0140	0.33	0.0139	0.30
8	146	0.0137	4.234	0.236	0.0139	0.33	0.0138	0.30
*2	620	0.0135	3.658	0.273	0.0136	0.33	0.0136	0.30
*1	620	0.0160	3.625	0.276	0.0162	0.33	0.0161	0.30
Ni 4	1300	0.0167	2.641	0.379	0.0167	0.33	0.0167	0.31
3	1033	0.0166	3.067	0.326	0.0166	0.33	0.0166	0.31
1	850	0.0160	3.664	0.273	0.0159	0.33	0.0159	0.31
2	675	0.0146	3.530	0.283	0.0146	0.33	0.0146	0.31
Cr 1	too small	0.0145	2.312	0.433	0.0147	0.33	-	-
Br 1	too small	0.0162	3.565	0.281	0.0162	0.33	-	-
2	2000	0.0186	2.443	0.409	0.0185	0.33	-	-

* Data of Runs Cu 1 and Cu 2 were obtained on the original unplated copper surface. Cu 1 was the first run carried out on the freshly machined surface.

TABLE 10

PERCENT DEVIATION OF EXPONENTS r_2 AND r_3 FROM r_1 IN ROHSENOW CORRELATION

Run No.	Percent Deviation of r_2 and r_3 Values from r_1 Values	Percent of r_2 Values within Deviation Percentage	Percent of r_3 Values within Deviation Percentage
Cu 1 to Cu 15	10%	50.0%	50.0%
	20%	75.0%	87.5%
	25%	81.3%	93.8%
	30%	87.5%	100.0%
	40%	100.0%	-
Ni 1 to Ni 4	10%	-	-
	15%	50.0%	75.0%
	20%	75.0%	100.0%
	25%	100.0%	-

TABLE 11

COMPARISON BETWEEN EXPERIMENTAL VALUES OF C_{sf} AND r AND CALCULATED VALUES USING THE MODIFIED ROHSENOW CORRELATION (Eq. 49) FOR COPPER PLATED SURFACES

Run No.	Grain Ratio $G = \frac{\text{grains/inch}}{600}$	Experimental Values		Calculated Values	
		C_{sf}	r	C_{sf}	r
Cu 12	2.797	0.0175	0.350	0.0175	0.351
13	2.583	0.0168	0.340	0.0171	0.342
11	2.408	0.0174	0.335	0.0168	0.334
14	2.027	0.0161	0.324	0.0161	0.317
15	1.592	0.0150	0.289	0.0154	0.298
9	1.217	0.0139	0.294	0.0147	0.282
*2	1.033	0.0134	0.273	0.0144	0.273
10	0.973	0.0143	0.250	0.0143	0.271
6	0.853	0.0138	0.283	0.0140	0.266
7	0.667	0.0137	0.255	0.0137	0.257
8	0.243	0.0136	0.236	0.0130	0.239

* Original unplated copper surface

TABLE 12

PROPERTIES OF WATER

Temperature ^{o}F	200	212	220
Specific Heat, Btu/lb_m-^{o}F	1.004	1.00697	1.007
Viscosity, lb_m/ft.hr.	0.7400	0.6876	0.6500
Density of Saturated Liquid, lb_m/cu.ft.	60.13	59.81	59.63
Density of Saturated Vapour, lb_m/cu.ft.		0.0373	
Thermal Conductivity of Saturated Liquid, Btu/hr.ft.^{o}F	0.392	0.393	0.395
Surface Tension of Saturated Liquid, lb_f/ft.		0.0042	
Latent Heat of Vaporization, Btu/lb_m		970.6	

TABLE 13

PROPERTIES OF AIR AT ATMOSPHERIC PRESSURE

Temperature, ^{o}F	100	150	200
Viscosity, lb_m/ft.hr.	0.0459	0.0484	0.0519
Thermal Conductivity, Btu/hr.ft.^{o}F	0.0157	0.0167	0.0181
Specific Heat, Btu/lb_m-^{o}F	0.240	0.241	0.241

TABLE 14

ABSOLUTE INTERFACE FREE ENERGIES IN ERGS/CM^2 *

Metal	Investigator	Value G	Temperature Range
Copper Grain Boundary	Bailey and Watkins	640	800-900°C
	Sears	860	800°C
	Fullman	490	945°C
	Van Vlack	595	1000°C
	Mean	646	
Copper Metal	Hutting	1650	32.5°C
	Udin,Shlaer,Wulff	1650	1000°C

Ratio of interface free energies $\frac{646}{1650} \simeq \frac{1}{3}$

The surface tension or interfacial tension is identical numerically to the surface free energy if expressed in the same type of units.**

Ratio of interfacial tensions for copper grain boundary and copper solid metal, $\frac{G^b}{G^{sv}} = \frac{\sigma_b}{\sigma_{sv}} \simeq \frac{1}{3}$

* McLean, D., Grain Boundaries in Metals, Oxford at the Clarendon Press, 1957, pp. 76-80.

** Swalin, R.A., Thermodynamics of Solids, John Wiley and Sons Inc., New York, 1962, p. 181, 204.

APPENDIX II

SAMPLE CALCULATIONS

A. Calculation of Heat Loss

Following the method of W.H. Murray (M_7) and using the temperature measurements t_{13} and t_{14} of the stainless steel fin given in Table 6, an equation was developed to estimate the heat loss from the fin at various heat inputs as illustrated below:

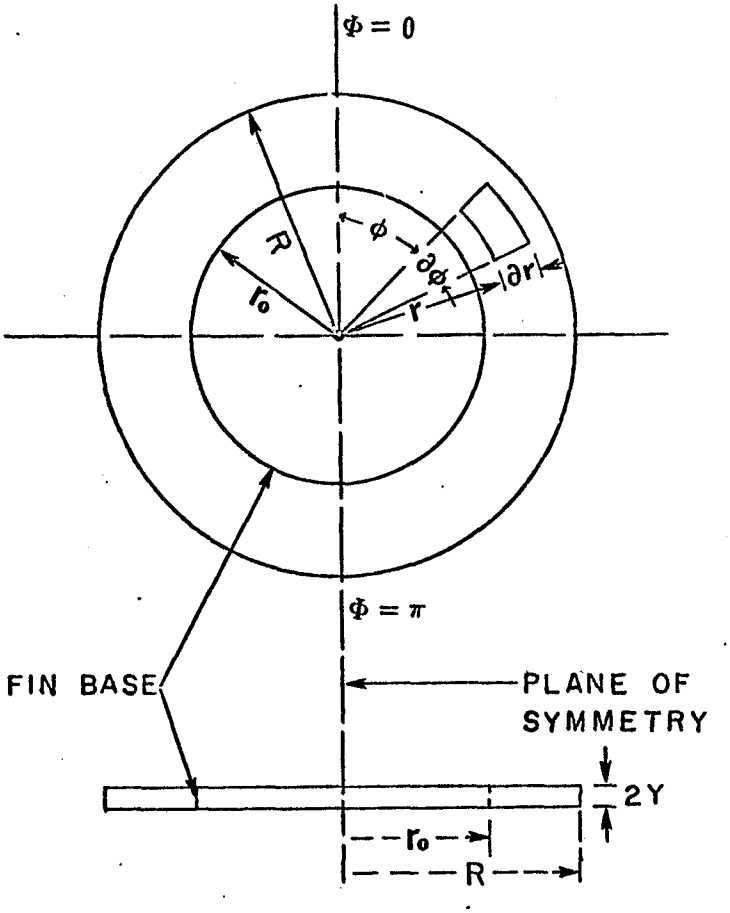

FIG·42 DIAGRAM OF THE CIRCULAR FIN OF UNIFORM THICKNESS

The stainless steel fin is considered as receiving heat through one edge whose temperature is known and transmitting to the surrounding medium through the exposed surfaces. A differential equation of heat flow can be set up by making a heat balance on the elemental particle as illustrated in the figure (Fig. 42) which yields

$$\frac{\partial^2\theta}{\partial r^2} + \frac{1}{r}\frac{\partial\theta}{\partial r} + \frac{1}{r^2}\frac{\partial^2\theta}{\partial\phi^2} = \frac{h}{ky}\theta \qquad (52)$$

The solution of the above equation for θ, the temperature at any point on the fin, is an infinite series involving modified Bessel Functions of the first and second kind and may be written as

$$\theta = \sum_{n=1}^{n=\infty}(A_n \cos\mu_n\phi + B_n \sin\mu_n\phi)[I_{\mu n}(mr) + C_n K_{\mu n}(mr)] \qquad (53)$$

where $m = \sqrt{\frac{h}{ky}}$ and A_n, B_n, C_n, μ_n are four arbitrary constants whose values are evaluated using proper boundary conditions. This results in a rather complicated expression for the temperature θ as given in the original paper (M_7).

The equation for heat transfer Q_f through the fin is then expressed as $Q_f = \int h\theta dA$, which for the special case of uniform temperature around the inner edge of the fin reduces, after substituting the expression for θ, to a simpler form:

$$Q_f = 4\pi\theta_o r_o \sqrt{hky} \times \xi \qquad (54)$$

where

$$\xi = \frac{I_1(mR)\, K_1(mr_o) - K_1(mR)\, I_1(mr_o)}{I_1(mR)\, K_o(mr_o) + K_1(mR)\, I_o(mr_o)} \qquad (55)$$

B. Application of Equation (54) to Compute Heat Loss

From Table 6, at total heat input of 39063 Btu

$t_{13} = 227.28^{\circ}F$ and $t_{14} = 214.90^{\circ}F$

The temperature θ_o of the inner edge of the fin was calculated by linear extrapolation along the fin radius and could be assumed to be uniform around the edge without any serious error.

θ_o computed $= 229.44^{\circ}F$

The heat loss from the fin consisted of the heat transfer by convection from its top surface to water at near boiling temperature and the heat transfer by convection from its bottom surface to air at room temperature. These two parts were computed separately and added together to arrive at the total heat loss as shown below.

1. Heat Loss from Fin to Water on One Side

The convection heat transfer coefficient h_{cw} was calculated using the following correlation of Fishenden and Sanders (M_1):

$$h_{cw} = C_1 \frac{k}{L} \left(\frac{g\beta_f \Delta t L^3 \rho^2 C_l}{\mu k}\right)^{\frac{1}{3}}$$

$$= C_1 \frac{k}{L} (aL^3\Delta t)^{\frac{1}{3}} \qquad (56)$$

where $NGr_f \times N_{pr_f} = aL^3\Delta t \qquad (57)$

L = diameter of fin = 10 inches

$C_1 = 0.14$ for heated surfaces facing upward

and Δt = temperature difference between the mean temperature of the surface and the temperature of the ambient fluid.

$= 221.12 - 211.34 = 9.78^{\circ}F$

The physical properties C_ℓ, k, ρ, μ and β_f of the fluid were evaluated at a film temperature halfway between the mean temperature of the surface and the temperature of the ambient fluid. At the film temperature of $\frac{221.12 + 211.34}{2} = 216.23^{o}F$, the physical properties of water were evaluated from Table 12 and substituted in Equation (56) to obtain a $h_{cw} = 150 \frac{Btu}{hr.ft^{2o}F}$. From Equation (54),

$$Q_{lw} \text{ or } Q \text{ loss to water} = 2\pi\theta_o r_o x \sqrt{h_{cw} ky} \times \xi \qquad (58)$$

To evaluate ξ, $m_w = \sqrt{\frac{h_{cw}}{ky}}$

$$= \sqrt{\frac{150.6}{10.1 \times 12 \times 1/8}}$$

$$= 3.153 \text{ inch}^{-1} \text{ units}$$

$m_w r_o = 3.153 \times 3 = 9.46$

$m_w R = 3.153 \times 5 = 15.77$

Substituting the corresponding values of the modified Bessel function (W_7) in Equation (55) yields a value very close to unity for ξ.

Therefore from Equation (58), $Q_{lw} = 1503.5$ Btu/hr.

2. Heat Loss from Fin to Air

The heat transfer coefficient h_{ca} was calculated as before using the following correlation which is applicable for cooled plates facing downwards in the laminar range (M_1).

$$h_{ca} = 0.27 \left[\frac{L^3 \rho^2 g \beta_f \Delta t}{\mu^2} \left(\frac{C_\ell \mu}{k}\right)_f\right]^{0.25} \qquad (59)$$

The film temperature of air $\simeq \frac{221.12 + 74}{2} = 147.56^{o}F$. Substituting the physical properties of air evaluated from Table 13 at the above film

temperature in Equation (59),

$$h_{ca} = 1.285$$

$$m_a = \sqrt{\frac{h_{ca}}{ky}} = \sqrt{\frac{1.285}{10.1 \times 12 \times 1/8}} = 0.2912 \text{ inch}^{-1}$$

$$m_a r_o = 0.2912 \times 3 = 0.8736$$

$$m_a R = 0.2912 \times 5 = 11.456$$

From Equation (55) using proper values of modified Bessel functions, ξ was calculated to be 0.6773.

$$Q_{la} \text{ or Q loss to air} = 2\pi\theta_o r_o \sqrt{h_{ca} ky} \times \xi$$
$$= 87.5 \text{ Btu/hr.}$$

Total heat loss at a heat input of 39063 Btu is then equal to the sum of Q loss to water and Q loss to air.

$$\text{i.e. Q total loss} = Q_{lw} + Q_{la} = 1503.5 + 87.5$$
$$= 1591 \text{ Btu/hr.}$$

Similar heat loss calculations were made at other power inputs and the results obtained were tabulated in Table 6. A linear best fit of the above results yielded an equation of the form,

$$Q \text{ loss} = 0.01406 * Q \text{ input} + 1047.5 \qquad (60)$$

with a coefficient of correlation of better than 0.98. In all the subsequent experimental runs, Equation (60) was utilized to calculate the total heat losses through the stainless steel fin and these are recorded in Table 6.

3. Heat Loss Check

Run Cu. 11

Total heat input = 44514 Btu/hr.

Condenser water inlet temperature, ^{o}F = $38.1^{o}F$

Condenser water outlet temperature, ^{o}F = $72.1^{o}F$

Water flow rate = 20.95 lbs/minute

= 1257 lbs/hr.

Heat transferred from steam to cooling water

$$1257 \times 1 \times (72.1 - 38.1) = 42738 \text{ Btu/hr.}$$

Heat unaccounted,

$$Q_{loss\ 2} = 44514 - 42738$$

$$= 1776 \text{ Btu/hr.}$$

Heat loss through the fin as calculated previously (Table 6),

$$Q_{loss\ 1} = 1673 \text{ Btu/hr.}$$

$$\frac{Q\ loss\ 2}{Q\ loss\ 1} = \frac{1776}{1673} = 1.06$$

4. Calculation of Surface Temperatures

Run No. Cu. 11

Total heat input = 44514 But/hr
(Table 6)

Temperatures indicated by thermocouples in ^{o}F:

$t_1 = 253.71$	$t_4 = 270.00$	$t_7 = 283.11$
$t_2 = 297.22$	$t_5 = 313.36$	$t_8 = 327.35$
$t_3 = 328.79$	$t_6 = 369.35$	$t_9 = 391.00$

Thermocouple positions from the top surface (Table 2) in inches:

$t_1 = 0.217$ $t_4 = 0.217$ $t_7 = 0.217$

$t_2 = 0.765$ $t_5 = 0.774$ $t_8 = 0.767$

$t_3 = 1.302$ $t_6 = 1.324$ $t_9 = 1.314$

Simple linear extrapolation gave the corresponding temperatures of the surface as shown below (Table 5):

$T_{s1} = 240.53^{\circ}F$ $T_{s2} = 248.33^{\circ}F$ $T_{s3} = 258.96^{\circ}F$

The coefficient of correlation of the above linear best fits were 0.996, 0.997, 0.994 respectively.

5. Calculation of ΔT_m

Saturation temperature T_l corresponding to the local pressure $= 211.07^{\circ}F$

$\Delta T_1 = T_{s1} - T_l = 29.33^{\circ}F$

$\Delta T_2 = T_{s2} - T_l = 37.13^{\circ}F$

$\Delta T_3 = T_{s3} - T_l = 47.76^{\circ}F$

ΔT_4, the corresponding temperature difference of the top edge of the copper plate was obtained from Table 4, i.e. $\Delta T_4 = 44.61^{\circ}F$.

The above ΔT values were plotted against $(\frac{r}{r_o})^2$ as shown in Fig. 9. Using a computer programme, numerical integration was performed for values of $(\frac{r}{r_o})^2$ from 0 to 1 to obtain a ΔT_m of $43.29^{\circ}F$. Values of ΔT_m were obtained as above for other power inputs and tabulated against corrected heat flux Q/A in Table 7.

C. Application of Rohsenow's Correlation to the Data

Rohsenow's correlation is (Equation (48)),

$$\frac{C_\ell \Delta T_m}{h_{fg}} = C_{sf} \left(\frac{Q/A}{\mu_\ell h_{fg}} \sqrt{\frac{g_o \sigma}{g(\rho_\ell - \rho_v)}}\right)^r \left(\frac{C_\ell \mu_\ell}{k_\ell}\right)^s$$

For water the prandtl number exponent s = 1. Rearranging the above equation and taking logarithms on both sides,

$$\text{Log}\left[\frac{C_\ell \Delta T_m}{h_{fg}} \frac{1}{N_{Pr}}\right] = \text{Log } C_{sf} + r \text{ Log } \left[\frac{Q/A}{\mu_\ell h_{fg}} \sqrt{\frac{g_o \sigma}{g(\rho_\ell - \rho_v)}}\right] \qquad (61)$$

The above expression takes the form of a linear fit on log-log paper.

The physical properties of water were obtained at the average saturation temperature corresponding to the local pressure readings during a run. Typical values of these at standard conditions are given in Table 12 and corrections were applied for deviations from standard conditions encountered in the actual runs.

Example: Run Cu. 11

Average saturation temperature $t_\ell = 211.20^\circ F$

$C_\ell = 1.00688$ Btu/lb$_m$,$^\circ$F

$\mu_\ell = 0.690$ lb$_m$/ft.hr.

$k_\ell = 0.393$ Btu/hr.ft.$^\circ$F

$h_{fg} = 970.86$ Btu/lb$_m$

$\rho_\ell = 59.84$ lb$_m$/cu.ft.

$\rho_v = 0.03675$ lb$_m$/cu.ft.

$\sigma = 0.0042$ lb$_f$/ft.

From Table 7 values of Q/A and ΔT_m were substituted in Equation (61) and by the least square method the best values of the slope r and the intercept Log C_{sf} were evaluated.

Slope r = 0.3348

Log C_{sf} = -1.7593

hence,

C_{sf} = 0.0174 (Table 9)

APPENDIX III

ERROR ANALYSIS

The following are the possible sources of error in the present experimental measurements:

1. Errors in measuring the power input.
2. Errors in computing the heat losses.
3. Errors in measuring and extrapolating the thermocouple readings.
4. Errors in the grain size determination.

1. Errors in Measuring the Power Input

The ammeter and voltmeter used in power measurements were calibrated, periodically checked against standard instruments and proper corrections were applied to the readings. Possible errors due to parallax in reading meters were as follows:

Weston A.C. Voltmeter	0 - 75v	±0.25v
	75 - 150v	±0.25v
	150 - 300v	±0.50v
Weston A.C. Ammeter	0 - 10A	±0.05A
	10 - 20A	±0.05A
	20 - 50A	±0.10A

Errors in measured power inputs on account of the above parallax errors are,

High flux (190v, 25A, in each phase) 0.75%

Low flux (50v, 6A, in each phase) 1.50%

The power loss (I^2R loss) in the wiring between the meters and the cartridge heaters was computed from the size, length and resistance of the copper conductors used. This quantity was very small (maximum of 0.25%) and was subtracted from the meter readings to obtain the corrected power inputs.

2. Errors in Computing the Heat Losses

There are three possible sources of heat loss:

(a) heat lost from the top surface of the stainless steel fin to water.

(b) heat lost from the bottom surface of the stainless steel fin to the thermobestos insulation.

(c) heat lost from the heater unit itself to the thermobestos block insulation.

The heat lost through the stainless steel fin has been computed and appears in Appendix II. This was subtracted from the total heat flux to obtain the corrected heat flux in Table 7. However the fin equation used incorporates some assumptions and an approximate estimate of the errors introduced due to these will be $\pm 5\%$ of the computed loss.

In the above calculations the bottom surface of the fin was assumed to lose heat to atmospheric air whereas it actually transferred heat to the asbestos insulation packed underneath. It will be presently shown that the heat loss through modes (b) and (c) when added together is numerically equal to the heat loss from fin to atmospheric air and therefore no significant error is introduced by the above assumption.

The surface of the heater unit was approximately at 400°F at the higher ranges of heat flux and the outer surface of the insulation was at 100°F. From the information booklet on thermobestos insulation,

Surface		Insulation		
Diameter	Temp.	Thickness	Temp.	Heat loss/ft.
10"	400°F	4"	100°F	110 Btu/hr.

For a 9" length of insulation, heat loss is 110 x 0.75 = 82.5 Btu/hr.

Heat loss from the fin to insulation,

$$Q_{loss}^{F-I} = kA\Delta T_{mean}$$

$$= 0.105\pi \left[\left(\frac{5}{12}\right)^2 - \left(\frac{3}{12}\right)^2\right] \times 116$$

$$\simeq 5 \text{ Btu/hr.}$$

Total heat loss to insulation, (b) + (c) = 87.5 Btu/hr, which is equal to the heat loss from the fin to atmospheric air as calculated in Appendix II. A probable error of ±10% was assigned to the above calculations.

3. Errors in Measuring and Extrapolating Thermocouple Readings

The thermocouples used were periodically calibrated in an oil bath. They were pressed against the surface of contact and held in position with springs. Great care was taken to insulate the junctions of thermocouples, lead wires and connecting points on the switches. After carefully following the aforesaid procedure, one can assume that the errors in temperature readings because of the above factors are likely to be very small. The millivolt potentiometer had a dial which can be read to ±0.002 mv. This might have introduced an error of ±0.1°F in the

temperature measurements.

Another source of error is due to the extrapolation of the thermocouple readings to obtain the surface temperatures. The thermocouples were embedded at typical locations which were representative of the whole area of the heat transfer surface. A single value of the extrapolated surface temperature was estimated to have an error of $\pm 0.5^{\circ}F$. Assuming an error of $0.1^{\circ}F$ in the saturation temperature of the liquid, a total error of $\pm 0.7^{\circ}F$ in the calculated ΔT values is probable. This error when expressed in percentage amounts to about $\pm 5\%$ at ΔT of $15^{\circ}F$ and $\pm 2\%$ at a ΔT of $40^{\circ}F$.

4. Errors in the Grain Size Determination

During each run three representative spots were selected and polished on the surface. At each spot, six counts were made by rotating the eyepiece of the microscope and counting the number of the grains bisected by the 0.01 inch long reticle line. A typical grain count as measured in Run Cu 12 is given below:

Spot 1		Spot 2		Spot 3	
No. of grains	Deviation from Mean	No. of grains	Deviation from Mean	No. of grains	Deviation from Mean
16	0.78	17	0.22	17	0.22
15	1.78	17	0.22	19	2.22
16	0.78	18	1.22	17	0.22
15	1.78	17	0.22	17	0.22
16	0.78	18	1.22	18	1.22
16	0.78	17	0.22	16	0.78

Average number of grain = 16.78 per 0.01 inch

= 1678 per inch.

Average relative deviation from mean = 14.88/18 = 0.8267

percent deviation from mean = $\frac{0.8267 \times 100}{16.78} \simeq 5\%$

Calculation of total error

High heat flux:

		Fraction error
Total flux	$Q \simeq 47500$ Btu/hr.	$f = 0.0075$
Fin and	$Q_1 \simeq 1600$ Btu/hr.	$f_1 = 0.05$
Body Losses	$Q_2 \simeq 100$ Btu/hr.	$f_2 = 0.1$
Wire Loss	$Q_3 \simeq 160$ Btu/hr.	$f_3 =$ negligible

$$\text{Total error} = \frac{Qf + Q_1f_1 + Q_2f_2 + Q_3f_3}{Q - (Q_1+Q_2+Q_3)} \times 100 \simeq 1\%$$

Low heat flux:

		Fraction error
Total flux	$Q \simeq 3075$ Btu/hr.	$f = 0.015$
Fin and	$Q_1 \simeq 1000$ Btu/hr.	$f_1 = 0.05$
Body Loss	$Q_2 \simeq 70$ Btu/hr.	$f_2 = 0.1$
Wire Loss	$Q_3 \simeq 10$ Btu/hr.	$f_3 =$ negligible

Total error $\simeq 5\%$

The free convection heat transfer mechanism probably starts to influence at low heat fluxes; hence the greater error is at the lower end of the boiling curve. The errors will lie between the above two extremes at other values of heat flux.

A summary of the estimated errors in the present investigation is as follows:

	Q/A	ΔT_m	Grain count
High heat flux (250000 Btu/hr.ft^2 $\Delta T \simeq 40^\circ$F)	$\pm 1\%$	$\pm 2\%$	$\pm 5\%$
Low heat flux (11000 Btu/hr.ft^2 $\Delta T \simeq 15^\circ$F)	$\pm 5\%$	$\pm 5\%$	$\pm 5\%$

BIBLIOGRAPHY

A_1 Addoms, J.N., Heat Transfer at High Rates to Water Boiling Outside Cylinders, D.Sc. Thesis, Massachusetts Institute of Technology(1948).

A_2 Agarwal, A.L., M.Sc. Thesis, Mechanical Engineering Department, University of Wisconsin (1961).

B_1 Bankoff, S.G., J. Phys. Chem. 60, 952 (1956).

B_2 Bankoff, S.G., A.I. Ch.E.J. 4, 24 (1958).

B_3 Bankoff, S.G., Chem. Eng. Progr. Sym. Series 55, No. 29, 87 (1959).

B_4 Bankoff, S.G., Diffusion-Controlled Bubble Growth, in Advances in Chem. Eng., Vol. 6, Academic Press, New York (1966).

B_5 Bankoff, S.G., and R.D. Mikesell, Chem. Eng. Progr., Symp. Series 55, No. 29, 76-86 (1959).

B_6 Berenson, P.J., Intern. J. Heat Mass Transfer 5, 985 (1962).

B_7 Blum, M., and C. Kasper, Trans. Faraday Soc., 31, 1203 (1935).

B_8 Bonilla, C.F., and C.W. Perry, Trans. A.I.Ch.E. 37, 685 (1941).

B_9 Brenner, A., Electro-deposition of Alloys, Academic Press, New York, Vol. 1, p. 187 (1963).

B_{10} Bruijn, F.J., Physica 26, 326 (1960).

B_{11} Butts, A., and V. DeNora, Trans. Am. Electrochem. Soc., 79, 163 (1941).

B_{12} Buehler Metallurgical Apparatus Ltd., Evanston, Illinois, Instruction for Operating A B Portamet Spot Polisher.

C_1 Cichelli, M.T., and C.F. Bonilla, Trans. A.I.Ch.E. 41, 755 (1945).

C_2 Clark, H.B., P.S. Strenge and J.W. Westwater, Chem. Eng. Progr., Symp. Series 55, No. 29 (1959).

C_3 Corty, C., and A.S. Foust, Chem. Eng. Prog., Symp. Series 51, No.17 (1955).

D_1 Dergarabedian, J. Appl. Mech., 20, 537 (1953).

D_2 Dougherty, D.E., and H.H. Rubin, Proc. Heat Transfer and Fluid Mech. Inst., Stanford Univ. Press, Stanford, California, p. 222 (1963).

E_1 Ellion, M.E., Jet Propulsion Laboratory Memo 20-88, Cal. Inst. Tech. (1958).

F_1 Farber, E.A., and R.L. Scorah, Trans. A.S.M.E., 70, 369 (1948).

F_2 Forster, K., and R. Greif, Trans. A.S.M.E., Series C, J.Heat Transfer, 81, 43 (1959).

F_3 Forster, H.K., and N. Zuber, A.I.Ch.E. Journal, 1, 531 (1955).

F_4 Fritz, W., Phys. Zeit., 36, 379 (1935).

G_1 Gaertner, R.F. and J.W. Westwater, Chem. Eng. Progr., Symp. Series No. 30, Vol. 56, (1959).

G_2 Gauvin, W., and C.A. Winkler, Canadian Journal of Research, A 21; 37 (1934)

G_3 Griffith, P., and J.D. Wallis, Chem. Eng. Progr., Symp. Series 30, 56, 49 (1960).

G_4 Gunther, F.C., and F. Kreith, Jet Propulsion Lab., Cal. Inst. Tech., Progr. Rept. No.4, 120 (1950).

H_1 Hamburger, L.G., Int. J. Heat Mass Transfer, Vol. 8, 1369 (1965).

H_2 Han, C.Y., and P. Griffith, Int. J. Heat Mass Transfer, Vol. 8, 887 (1965).

H_3 Harrison, W.B., and Z. Levine, A.I.Ch.E. - A.S.M.E. Joint Heat Trans. Conf. paper 57-HT-27, State College, Pennsylvania (1957).

H_4 Hess, J.B., Metal Interfaces, Am.Soc. Metals, p. 148 (1951).

H_5 Hsu, S.T., Engineering Heat Transfer, Van Nostrand Co., Princeton, New Jersey (1963).

H_6 Hsu, Y.Y., and R.W. Graham, NASA-TN-D-594 (1961).

I_1 Ishigai, S., Inoue, K., Kiwaki, Z., and T. Inai, Int. Heat Transf. Conf., Boulder, Colorado, paper 26 (1962).

J_1 Jakob, M., Heat Transfer,Vol. 1, Chpt. 29, John Wiley, New York, (1949).

J_2 Johnson, M.A., Javier De La Pena and R.B. Mesler, A.I.Ch.E. Journal, 12, No.2, 344 (1966).

K_1 Kazakova, E.A., The Engineer's Digest, 12, No.3, 81 (1951).

K_2 Kehl, G.L., Principles of Metallographic Laboratory Practice, McGraw-Hill, New York (1949).

K_3 Kreith, F., and Sommerfield, F., Proc. Heat Transfer and Fluid Mech. Inst., Stanford University, p. 127 (1949).

K_4 Kurihara, H.M., Fundamental Factors Affecting Boiling Coeffcients, Ph.D. Thesis, Purdue University, (1956).

K_5 Kutateladze, S.S., Fundamentals of Heat Transfer, Translated from Russian by Scripta Technica, Inc., Edited by R.D. Cess, 2nd Edition, E. Arnold, London (1963).

L_1 Leidenfrost, J.G., On the Fixation of Water in Diverse Fire, Transl. from German by Wares, C., Int.J. Heat Mass Trans., Vol. 9, No. 11, 1153 (1966).

L_2 Leppert, G., and C.C. Pitts, Boiling, in Advances in Heat Transfer, Vol 1, Academic Press, New York, (1964).

L_3 Levy, S., Trans. ASME., Series C, J. Heat Transfer, 81, 43 (1959).

L_4 Lowenheim, F.A., Modern Electroplating, John Wiley, New York (1963).

M_1 McAdams, W.H., Heat Transmission, 3rd Ed., McGraw-Hill, New York (1945).

M_2 McAdmas, W.H., J.N. Addoms, P.M. Rinaldo, and R.S. Day, Chem. Eng. Progr. 44, 639 (1948).

M_3 McLean, D., Grain Boundaries in Metals, Oxford at the Clarendon Press (1957).

M_4 Mead, B.R., F.E. Romie, and A.G. Guibert, Proc. Heat Trans. and Fluid Mech. Inst., Stanford University, California (1951).

M_5 Merte, J., and J.A. Clark, University of Michigan, Report No. 2646-21-T, Tech. Rept. No. 3, Nov. (1959).

M_6 Moore, F.D., and R.B. Mesler, A.I.Ch.E. Journal, 7, No.4, 620 (1961).

M_7 Murray, W.M., J. Appl. Mech., A-78, June (1938).

N_1 Nukiyama, S., J.Soc. Mech. Engrs. (Japan), 37, 367 (1934).

N_2 Nickelson, R.L., and G.W. Preckshot, J.Chem.Eng. Data, 5, 310 (1960).

P_1 Plesset, M.S., and S.A. Zwick, J. Appl. Phys., 23, 95 (1952).

P_2 Plesset, M.S., and S.A. Zwick, J. Appl. Phys., 25, 493 (1954).

P_3 Pramuk, F.S., and J.W. Westwater, Chem. Eng. Progr., Symp. Series, 17, 51, 41 (1955).

P_4 Preckshot, G.W., and V.E. Denny, Can. J. Chem. Eng., 45, No. 4, 241, (1967).

R_1 Read, W.T., and W. Shockley, Imperfections in Nearly Perfect Crystals, John Wiley, New York p. 369 (1952).

R_2 Reiss, H., Ind. Eng. Chem., 44, 1284 (1952).

R_3 Reiss, H., J. Chem. Phys., 20, 1216 (1952).

R_4 Rogers, T.F., and R.B. Mesler, A.I.Ch.E. Journal, 10, No. 5, 656 (1964).

R_5 Rohsenow, W.M., and H. Choi, Heat, Mass and Momentum Transfer, Prentice-Hall, New Jersey (1961).

R_6 Rohsenow, W.M., Heat Transfer with Boiling, in Developments in Heat Transfer, M.I.T. Press, Cambridge, Massachusetts (1964).

R_7 Rohsenow, W.M., and J.A. Clark, Proc. Heat Transfer and Fluid Mechanics Inst., Stanford University, p. 193 (1951).

R_8 Roshenow, W.M., Trans. A.S.M.E., 74, 969 (1952).

S_1 Scriven, L.E., Chem. Eng. Sci., 10, 1 (1959).

S_2 Scriven, L.E., Chem. Eng. Sci., 17, 55 (1962).

S_3 Seigel, R., and C. Usiskin, J. Heat Transfer, 81, 3 (1959).

S_4 Sinnott, M.J., The Solid State for Engineers, Chapter 12, John Wiley, New York (1958).

S_5 Skinner, L.A. and S.G. Bankoff, Phys. Fluids, 7, 1 (1964).

S_6 Strenge, P.H., A. Orell and J.W. Westwater, A.I. Ch. E. Journal, 7, 578, (1961).

S_7 Swalin, R.A., Thermodynamics of Solids, Chapter 12, John Wiley, New York, (1962).

T_1 Tong, L.S., Boiling Heat Transfer and Two-Phase Flow, John Wiley, New York, (1965).

V_1 Vachon, R.I., and et. al, paper No. 67-HT 34, A.S.M.E.-A.I.Ch.E., Heat Transfer Conference, Seattle, Washington, August (1967).

V_2 Vachon, R.I., and et al., paper No. 67-HT 33, A.S.M.E. - A.I.Che.E. Heat Transfer Conference, Seattle, Washington, August (1967).

V_3 Van Stralen, S.J.D., Int. J. Heat Mass Transfer, 9, pp. 995, 1021 (1966).

V_4 Van Wijk, W.R., A.S. Vos and S.J.D. Van Stralen, Chem. Eng. Sci., 5, 68 (1956).

V_5 Van Wijk, W.R., and S.J.D. Van Stralen, Physica 28, 150 (1962).

V_6 Volmer, M., Kinetik der Phasenbildung, Steinkoff, Dresden and Leipzig (1939).

W_1 Wark, J.W., J. Phys. Chem., 37, 623 (1933).

W_2 Westwater, J.W., Things We Don't Know about Boiling Heat Transfer, in Theory and Fundamental Research in Heat Transfer, Ed. J.A. Clark, Macmillan Co., New York (1963).

W_3 Westwater, J.W., Boiling of Liquids, in Advances in Chemical Engineering, Vol. 1, Academic Press, New York, (1956).

W_4 Westwater, J.W., and D.B. Kirby, A.I.Ch.E. Preprint 14, 6th National Heat Transfer Conference, Boston (1963).

W_5 Westwater, J.W., and J.G. Santangelo, Ind. and Eng. Chemistry, 47, No. 8, 1605 (1955).

W_6 Williams, D.D. and R.B. Mesler, A.I.Ch.E. Journal, 13, No.5, 1020 (1967).

W_7 Watson, G.N., Theory of Bessel Functions, Table II, p 699, Cambridge University Press (1958).

Y_1 Young, R.K., and R.L. Hummel, Chem. Eng. Progr. 60, 7, 53 (1964).

VITA AUCTORIS

Name of the author:	Ramanathan Nagarajan
Place and date of birth:	Poosalangudi, Thanjavur Dist., Tamil Nad, India. January 15, 1939
Schools attended (with dates):	Viraraghava High School, Thanjavur, India 1943-54
	Loyola College, Madras, India 1954-56
Universities attended (with degrees obtained and dates):	Annamalai University, Chidambaram, Tamil Nad, India
	Bachelor of Engineering (Chemical) 1956-60
	Indian Institute of Technology, Kharagpur, West Bengal, India
	Master of Technology 1960-61
	University of New Brunswick, Fredericton, N.B., Canada
	Master of Science 1961-63
	University of Windsor, Windsor, Ontario, Canada
	Candidate for the degree of Doctor of Philosophy 1963-68
Publication:	"Liquid Diffusivities for the System Methanol-Toluene" by L.W. Shemilt and R.Nagarajan, Canadian Journal of Chemistry, 45, 1143-48 (1967).